Nitrogen-Doped Carbon Nanotubes and their Composites as Oxygen Reduction Reaction Electrocatalysts for Low Temperature Fuel Cells

by

Drew Higgins

A thesis
presented to the University of Waterloo
in fulfillment of the
thesis requirement for the degree of
Master of Applied Science
in
Chemical Engineering

Waterloo, Ontario, Canada, 2011

Author's declaration:

I hereby declare that I am the sole author of this thesis. This is a true copy of the thesis, including any required final revisions, as accepted by my examiners.

I understand that my thesis may be made electronically available to the public.

Abstract:

Currently the main challenges still facing the commercialization of low temperature fuel cells is the high system cost of these devices, along with limited operational stability and power output. At the root of all these causes in the catalyst layer, containing expensive Pt based catalysts required to facilitate the hydrogen oxidation reaction (HOR) occurring at the anode and the oxygen reduction reaction (ORR) occurring at the cathode. In this project, alternative ORR catalyst materials are investigated in order to reduce the Pt dependency and decrease the excessive costs associated with this noble metal, while simultaneously improving the catalytic activity.

The ORR kinetics are inherently very sluggish and often times are considered the limiting factor facing the performance of fuel cell devices. In order to generate power at an acceptable rate for real world applications, a significant amount of Pt catalyst is required. This is traditionally in the form of Pt nanoparticles evenly distributed on a porous carbon support material (Pt/C) due to the high electrochemically active surface area that can be obtained in this configuration. Pt is an extremely expensive noble metal however, with very limited natural abundance. Thus, a significant reduction or elimination of the Pt dependence at the cathode of fuel cells is an urgent necessity in order to reduce the overall system cost to the levels required for commercialization. Moreover, the operational stability of Pt/C is still very low and suffers deactivation by Pt dissolution and/or agglomeration, and corrosion of the carbon support due to the harsh conditions present at the site of the cathode. Thus, a challenging task presents itself to the scientific community where the development of highly active ORR electrocatalysts is required, while simultaneously decreasing the overall Pt dependence and increasing the operational stability of these materials.

Common strategies employed to improve the ORR activity and operational stability of Pt-based electrocatalyst materials involve either: i) combining Pt with other metals to produce alloy compounds, ii) developing catalysts with different configurations, i.e. nanowires, nanotubes, thin films, etc., or iii) development and use of novel support materials in order to enhance the catalyst-support interactions and improve mass transport and electronic properties. Moreover, the development of non-precious metal (i.e. Fe, Co) containing electrocatalysts, or even metal free catalyst materials with high ORR activity and operational stabilities would provide immense economical benefits to promote the commercialization of low temperature fuel cells. Promising performance has been reported for these materials, however the operational activity and stability of non-precious metal catalysts are still not at the level required for fuel cell applications. Metal-free carbon-nitrogen based catalysts are the most

recently emerging field of ORR electroctalysis due to the environmental benefits they possess when compared with metal-based catalyst materials. Work in this field is still primitive; however preliminary reports have indicated the feasibility of catalytically active ORR materials developed in the absence of metal species.

In the present work, the unique structural and electronic properties of nitrogen doped carbon nanotubes (N-CNTs) will be exploited towards fuel cell applications. This report contains four project contributions, all of which revolve around investigation of the electrochemical activity of N-CNTs or their composites towards the ORR. Detailed structural analysis is also provided to supplement the electrochemical investigations in order to elucidate the exact factors affecting the catalytic activity observed and provide insight into the behavior and applicability of N-CNTs towards ORR electrocatalysis for fuel cell devices.

The first study investigates N-CNTs as Pt nanoparticle supports as ORR electrocatalysts for PEMFC applications. Due to the distinct electronic properties and surface functional groups present on the surface of N-CNTs, improved Pt nanoparticle dispersion and uniformity were obtained using N-CNTs with higher surface nitrogen contents. The inherent advantages arising from nitrogen incorporation were clearly demonstrated with comparison made between N-CNTs synthesized from two different precursor solutions along with undoped CNTs. It was found that a 16.9% increase in the peak power density of a fuel cell setup was obtained when using N-CNTs as supports, compared with CNTs.

The second study is directed at the use of N-CNTs synthesized from aliphatic diamine precursor solutions with varying carbon chain lengths for use as ORR electrocatalysts in AFCs. It was found that using a precursor solution with higher nitrogen to carbon contents (i.e. shorter chain length) would result in N-CNTs with improved nitrogen incorporation along with enhanced ORR activity and product selectivity. This study elucidated the importance of using nitrogen rich precursor materials and provided insight into the nature of the ORR occurring on the surface of N-CNTs, where it was demonstrated that using ethylediamine as a nitrogen rich precursor solution could result in a five-fold improvement in kinetic current densities obtained through half-cell testing at a electrode potential of -0.2 V vs Ag/AgCl compared with precursors with reduced nitrogen contents.

The third study involved fabrication of a thin, free standing film composed of highly active N-CNT materials developed in the second study. This thin film was utilized as a stand-alone, ionomer free cathode catalyst in an alkaline anion exchange membrane fuel cell setup. The performance of this thin

film in a single membrane electrode assembly (MEA) was found to be superior to that of commercial Pt/C catalyst. The improved performance was attributed to the high inherent ORR activity of the N-CNTs, along with the high surface aspect ratios of the N-CNTs and the porous structure of the thin film, enabling reactant access.

The fourth study investigates CNTs post-treated with cyanamide in the absence of any metal species (CNT-cy). After high temperature pyrolysis, the ORR activity of CNT-cy was found to improve, along with significantly higher product selectivities when compared with untreated CNTs. The improved performance was attributed to the deposition of a thin surface layer containing catalytically active site structures observed following pyrolysis by TEM. At higher cyanamide loadings in the precursor, deposition of a more uniform film with a higher degree of surface coverage was favoured and found to result in improved ORR performance.

All of the studies presented in this work involve the development and application of N-CNTs or their composites towards the electrocatalysis of ORR for low temperature fuel cell devices. Insight into the applicability of N-CNTs towards ORR electrocatalysis is made readily available, supplemented by detailed structural characterization techniques. This work will provide details regarding the specific factors influencing ORR activity and will elucidate the benefits and ORR activity resulting from the inherent surface functional groups present on N-CNTs. This work will provide a fundamental basis for future investigations focused around the application of N-CNT in electrochemical devices, along with the development of novel nanomaterials for fuel cell applications.

Acknowledgements:

The work reported herein was financially supported by the Natural Sciences and Engineering Research Council of Canada and the University of Waterloo.

Special thanks goes to my supervisor, Dr. Zhongwei Chen and several of my colleagues including Ryan Hsu, Clark (Zhu) Chen, Ja-Yeon Choi, Wenmu Li, Doralice Meza Calderon, Bing Li, Shaomin Zhu, Jason Wu, Raihan Ahmed and Hadis Zarrin for their assistance and support.

Moreover I would like to acknowledge support from my reviewers, including Dr. Yuning Li, Dr. Michael Fowler and Dr. Zhongwei Chen.

Table of Contents

List of Figures

List of Tables

List of Abbreviations, Symbols and Nomenclature

AEM	anion exchange membrane
AEMFC	alkaline anion exchange membrane fuel cell
AFC	alkaline fuel cell
CNT	carbon nanotube
CV	cyclic voltammetry
DAB	1, 4 diaminobutane
DAP	1, 3 diaminopropane
DAB-CNTs	1, 4 diaminobutane based nitrogen doped carbon nanotubes
DAP-CNTs	1, 3 diaminopropane
DOE	United States Department of Energy
DWNT	double walled carbon nanotube
E^o	standard reversible redox potential
e^-	electron
ECSA	electrochemically active surface area
ED	ethylenediamine
ED-CNTs	ethylenediamine based nitrogen doped carbon nanotubes
FeAc	iron acetate
GDL	gas diffusion layer
HOR	hydrogen oxidation reaction
MEA	membrane electrode assembly
MWNT	multiwalled carbon nanotube

N-CNT	nitrogen doped carbon nanotube
NC_x	nitrogen doped carbon nanostructures
ORR	oxygen reduction reaction
PEM	proton exchange membrane of polymer electrolyte membrane
PEMFC	proton exchange membrane or polymer electrolyte membrane fuel cell
Pt/C	carbon supported platinum nanoparticles
Pt/CNT	carbon nanotube supported platinum nanoparticles
Pt/N-CNT	nitrogen doped carbon supported platinum nanoparticles
PTFE	polytetrafluoroethylene (teflon)
RHE	reversible hydrogen electrode
RRDE	rotating ring disc electrode
SEM	scanning electron microscopy
SWNT	single walled carbon nanotube
TEM	transmission electron microscopy
TGA	thermogravimetric analysis
XRD	x-ray diffraction
XPS	x-ray photoelectron spectroscopy

1.0 Introduction

With increasing environmental awareness and ever depleting fossil fuel supplies, the demand for environmentally friendly, sustainable energy technologies is at the forefront of modern day research and development. With the amount of yearly crude oil discoveries in 2020 expected to be half the amount in 2000 [1], low temperature fuel cells are considered promising replacements to traditional combustion engines as they provide efficient chemical to electrical energy conversion, producing only environmentally benign byproducts in the form of water and heat [2]. Low temperature fuel cells rely on continuous reactant feeds simultaneously to the anode and cathode electrodes, where electrochemical oxidation and reduction will occur, respectively. The anode and cathode are separated by an insulating membrane and thus a current will be drawn through an external circuit that can be used to power electrical devices. The anode feed stream consists of an oxidant, generally hydrogen, that if produced by renewable technologies can significantly reduce and even eliminate the dependence on natural resources and provide immense environmental and economic benefits. Other oxidants used can include methanol, ethanol or even hydrogen storing compounds (i.e. sodium borohydride or ammonia) [3], however in the present thesis the main focus will be on proton exchange membrane fuel cells (PEMFCs) and alkaline fuel cells (AFCs) operating on hydrogen. Low temperature fuel cells and most significantly the PEMFC are considered ideal for stationary, mobile and even transportation applications, due to their low operation temperature ($< 120^{o}C$), quick start up time and transient response capabilities [2].

Despite intensive research focused on the development of fuel cell technologies, significant challenges still face the widespread commercialization of these devices. Specifically, the high system cost and limited stability of low temperature fuel cells are two issues that must be overcome and in most cases, the two of these issues are intertwined. A majority of the high system cost stems from the electrodes, consisting of the expensive catalyst layer (due to its significant Pt content, especially at the cathode, where the sluggish oxygen reduction reaction (ORR) occurs) and the gas diffusion layers. Stability issues generally stem from degradation of the catalyst layers and the membrane electrolyte materials, with significant work being done in recent years directed at understanding the exact causes, effects and mechanism of fuel cell performance loss [2, 4-6]. With the catalyst layers contributing significantly to the overall system cost and performance degradation of low temperature fuel cells, the development of novel nanomaterials with high catalytic activity, operational stability and low cost would provide immense progress towards fuel cell commercialization. Thus, the present thesis is directed at research in this field.

The report is structured so that the reader will be presented with a more specific background on PEMFCs and AFCs, along with their associated technical challenges with a focus on catalytic materials. The work discussed hereafter consists of ORR catalyst materials developed for utilization in PEMFC and AFC cathodes derived from nitrogen doped carbon nanotubes (N-CNTs), so understanding on their exact nature and properties will also be presented. Subsequently, physical and electrochemical characterization techniques utilized will be summarized, followed by full reports including an introduction, results and discussion and conclusions relating to four seperate investigations carried out. These involve:

i. N-CNTs as supports for Pt nanoparticles in acidic conditions (similar to those present in PEMFC). This chapter is based on reference [7].
ii. N-CNTs synthesized from various aliphatic diamines. This chapter is based on reference [8].
iii. Thin, free standing N-CNT film as standalone cathode catalyst in an alkaline anion exchange membrane fuel cell setup. This chapter is based on reference [9].
iv. Metal free N-CNTs synthesized by a post treatment method

The latter three investigations focus on the performance of N-CNT complexes under alkaline conditions, similar to those encountered in AFCs.

1.1 Proton Exchange Membrane Fuel Cells

The first PEMFC was developed in the 1960s and provided versatility when compared with previously developed solid oxide fuel cells due to their small size and low operating temperatures. PEMFCs were initially used in the NASA Gemini projects of the 1960s. Ultimately however, limited stability (ca. 500 h of operation) and water management issues led to their replacement by AFCs for the infamous Apollo missions [3]. Around this time, PEMFCs fell out of favour due to CO poisoning issues and high system costs [10], requiring up to 28 $mgcm^{-2}$ of Pt on the electrodes [3], several orders of magnitude over the present requirements. In the late 1980s and early 1990s government and military energy requirements sparked newfound interest in PEMFC development directed at cost reduction and performance improvements [10]. Since then, immense progress has been made in this field and the PEMFC has emerged as a promising energy conversion device for mobile and stationary applications. Moreover, the use of PEMFCs in automobiles has been envisioned for several years as replacements to traditional combustion engines which would provide immense environmental benefits due to zero green

house gas emissions during operation. Drawing off the advantages of high power densities, low operating temperatures, rapid start up times and amenability to varying load requirements [11], steady progress is being made towards their commercialization. Challenges hindering commercialization and widespread use still remain however, deriving from the high system cost and limited operational stability of PEMFCs [12], along with the demand for a hydrogen fuel infrastructure and economy [13].

1.1.1 Operational Principles

In its most simplistic form, a PEMFC stack consists of several unit cells configured together in a setup depicted in Figure 1. Each unit cell is typically comprised of two bipolar plates, two seals and a single membrane electrode assembly (MEA). Hydrogen as the fuel and air/oxygen as the oxidant are fed to the anode and cathode electrodes in isolation, respectively, where they undergo the necessary electrochemical reactions.

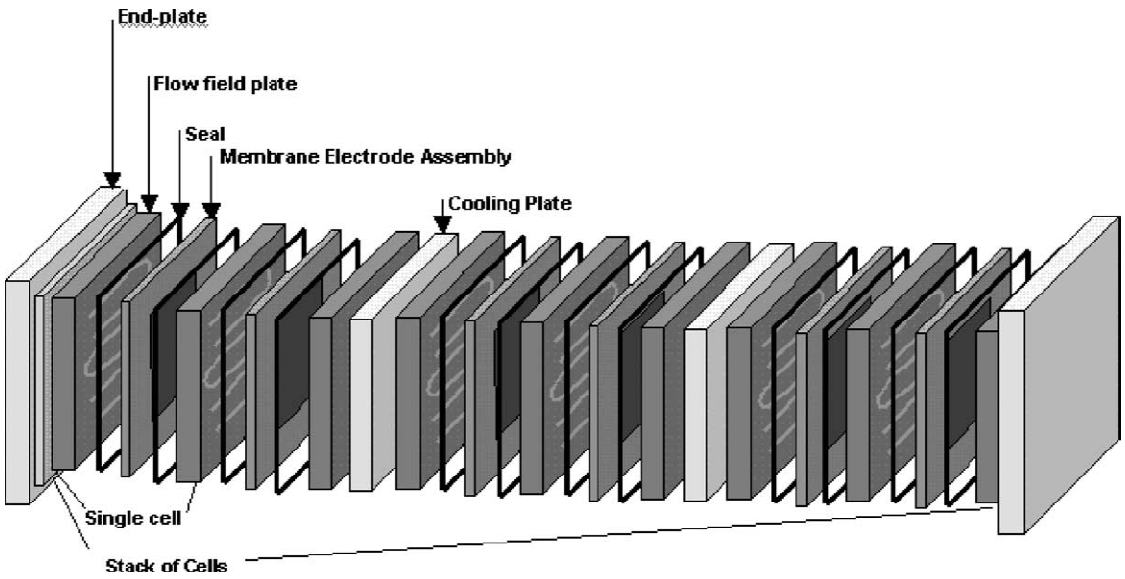

Figure 1: Hardware of a PEMFC stack, Reprinted from [11], Copyright 2003 with permission from Elsevier.

Hydrogen as a fuel, often times generated from fossil fuel reforming, bioprocesses and other renewable sources is directly fed to the anode, where it will undergo hydrogen oxidation according to Equation 1:

$$H_2 \rightarrow 2H^+ + 2e^- \qquad E^o = 0 \text{ V vs RHE} \qquad (1)$$

The protons then migrate through the polymer membrane and the electrons are directed through the external circuit to the site of the cathode. At the cathode, oxygen (or air) is continuously fed which reacts with available protons and electrons in the ORR mechanisms provided in Equation 2:

$$O_2 + 4H^+ + 4e^- \rightarrow 2H_2O \qquad E^o = 1.229 \text{ V vs RHE} \qquad (2)$$

Catalysts with a high selectivity for the ORR occurring by Equation 2 are favourable, however the ORR can proceed by an indirect pathway, forming H_2O_2 intermediates following Equation (3):

$$O_2 + 2H^+ + 2e^- \rightarrow H_2O_2 \qquad E^o = 0.7 \text{ V vs RHE} \qquad (3)$$

These hydrogen peroxide species can either be released into the system, or become further reduced to form water by Equation (4):

$$H_2O_2 + 2H^+ + 2e^- \rightarrow 2H_2O \qquad E^o = 1.76 \text{ V vs RHE} \qquad (4)$$

H_2O_2 formation will lower the performance of fuel cell systems, as it requires two separate $2e^-$ reduction processes. Moreover, H_2O_2 byproducts can have detrimental effects on the fuel cell component materials, specifically the polymer membrane [2]. Thus, increased selectivity towards the more efficient direct $4e^-$ process is extremely important when screening catalyst materials. The overall PEM fuel cell reaction can be summarized as equation (5):

$$H_2 + {}^1/_2O_2 \rightarrow H_2O \qquad (5)$$

The bipolar plates separating the individual MEAs have four primary duties [11]. These include: i) distribution of the fuel and oxidant feed streams, employing flow fields of various geometries to improve mass transfer and reactant access to the electrode surfaces, ii) current collection to carry electrons from the anode, through the external circuit to the site of the cathode, iii) water and thermal management, where they are designed in order to effectively remove water and heat byproducts to avoid catalyst flooding and overheating, respectively, and iv) as cell seperators and for mechanical stability. Bipolar plates typically consist of graphite, coated metals or both materials complexed together. Cost, corrosion resistance, chemical compatibility, density, thermal properties and electronic conductivity are the main considerations when designing these materials [11].

The individual MEAs (Figure 2) are comprised of a proton conducting membrane electrolyte separating the anode, and cathode electrodes. The membrane electrolyte serves a very important purpose, separating the two half-cell reactions and transporting protons from the anode to cathode in order to carry out the overall reaction. Moreover, the membrane electrolyte in an insulator material,

inhibiting the flow of electrons through its cross section to avoid creating a short circuit. The electrons are then forced through the external circuit in the form of electrical energy. The membrane electrolyte generally utilized is a perfluorosulfonic acid (PFSA) material (typically Nafion) [2, 11], with a backbone structure similar to that of commercial Teflon. This backbone structure is functionalized with negatively charged sulfonic acid groups, which facilitate proton transport. The anode and cathode electrodes consist of a catalyst layer deposited onto a porous gas diffusion layer (GDL) in a manner depicted in Figure 3. Porous carbon cloth or carbon paper is the traditional material utilized as a GDL, with its primary purposes to facilitate even reactant distribution to the catalyst layer, conduct electrons to the bipolar plate and effectively transport water byproducts. In order to drive the necessary oxidation and reduction reactions at a practical rate for fuel cell operation, Pt nanoparticles supported on a porous carbon black support material (Pt/C) is the catalyst of choice as hitherto, it has demonstrated the highest combined catalytic activity and operational stability. The current Pt requirement at the site of the cathode is significantly higher (ca. 0.4 $mgcm^{-2}_{electrode}$) [14] than at the site of the anode (< 0.2 $mgcm^{-2}_{electrode}$)[15], due to the extremely sluggish kinetics of the ORR compared to the hydrogen oxidation reaction (HOR).

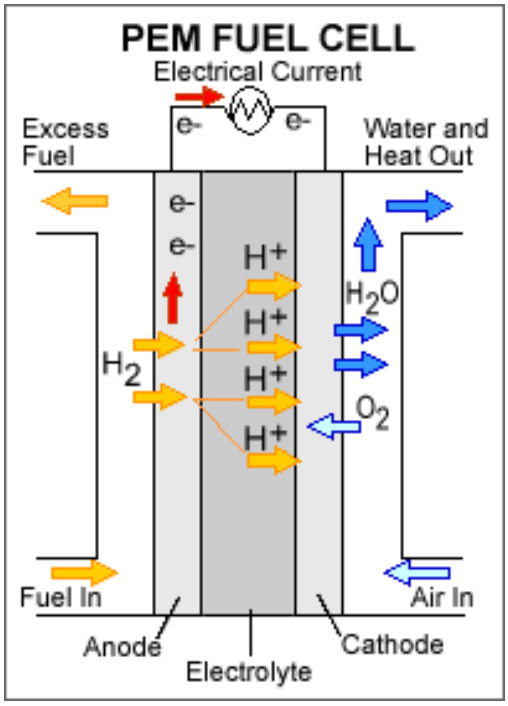

Figure 2: Single cell arrangement for PEMFC, taken from [16].

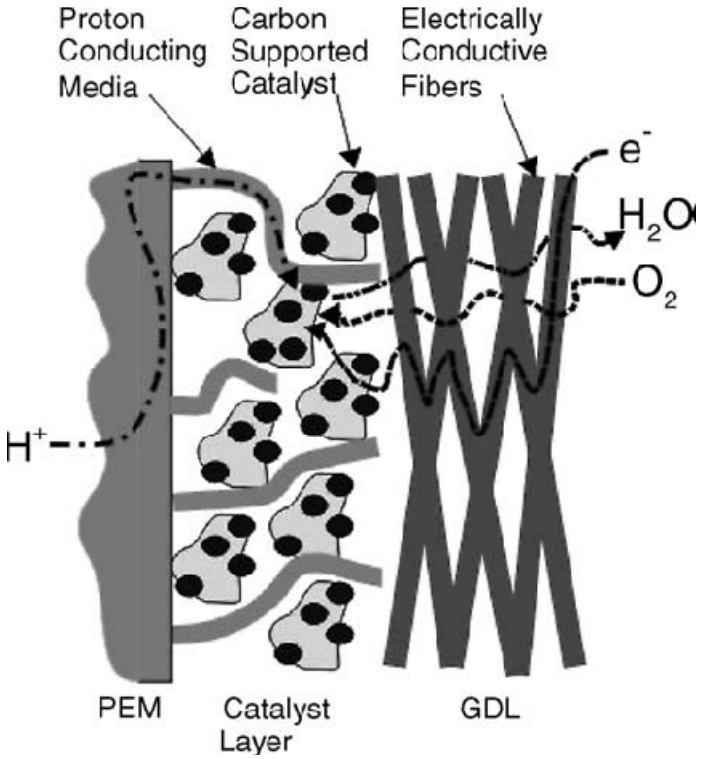

Figure 3: Schematic of catalyst layer coated onto porous GDL, reprinted from [17], Copyright 2004 with permission from Elsevier.

PEMFCs typically operate between 50-100^{o}C [18]. Increasing the operation temperature of PEMFCs is ideal in terms of high power output of these devices. This is at the expense of stability, where system components including the polymer membrane and catalyst layers will be accelerated at elevated temperatures [2]. Each unit cell operates at a voltage of approximately 0.7 V [3], thus in order to draw reasonable power from these devices they are generally connected in series in a bipolar arrangement. Operating PEMFCs on pressurized feed streams can be beneficial in terms of system performance and power output, however requires increased system complexity and the associated costs therein.

1.1.2 Technical Challenges

High cost and limited operational stability are the two major challenges that need to be overcome in order to realize the sustainable commercialization of PEMFCs. By 2015, the United States Department of Energy (DOE) has issued technical targets of 15 dollars per kW of power output and 5000 h of operational stability with limited performance loss [19]. At the root of both cost and stability issues is the catalyst layers utilized at the site of the anode and the cathode, consisting of expensive Pt based materials. According to a study completed for the DOE in 2007, it was reported that approximately 55%

of the overall fuel cell cost stems from the Pt based catalyst layers [20]. The kinetics of the ORR occurring at the cathode are inherently much more sluggish than the HOR occurring at the anode, and this is often times considered the primary factor limiting the overall PEMFC performance. This results in extensive reliance on high Pt-loading catalyst materials in order to facilitate the ORR at a reasonable rate.

Traditionally, high surface area Pt/C has been the catalyst of choice, consisting of uniformly dispersed Pt nanoparticles (diameters ca. 2-4 nm) on a porous carbon support with a TEM image of these materials displayed in Figure 4. This dispersive arrangement can effectively increase the Pt utilization and catalytically active surface areas. Unfortunately, the high surface energy of zero dimensional nanoparticles render these materials highly susceptible to several forms of degradation. The harsh conditions (i.e. high potential and acidic environment) present at the site of the cathode can effectively lead to Pt nanoparticle dissolution, particle agglomeration, Ostwald ripening and even Pt poisoning by contaminants present in the reactant feed streams [2, 4, 21]. All of these degradation mechanisms will result in significant performance loss of the fuel cell stack due to decreased rates of reactions and ECSA. Moreover, corrosion of the carbon support is a significant degradation issue affecting the catalyst layers. This phenomena has been extensively investigated [4, 22, 23] and is known to occur following equation (6):

$$C + 2H_2O \rightarrow CO_2 + 4H^+ + 4e^- \qquad E^o = 0.207 \text{ V vs RHE} \qquad (6)$$

This reaction is known to have a reversible potential of 0.207 V vs RHE, which is well below the potential values encountered at the cathode. This indicates that at normal operating conditions, corrosion of the carbon support is thermodynamically favourable. While electrode potential is considered the main parameter governing the rate of carbon corrosion, other factors including higher temperatures, reduced humidity and fuel starvation can accelerate the degradation [2]. Pt will also serve as a catalyst for carbon oxidation, so higher contact between Pt and the carbon support will increase the rate of this reaction [24]. Attempts to improve the stability of Pt-based catalyst materials include alloying with other metals [2, 25, 26], modifying the distinct nanostructure of Pt into different configurations (i.e. 1D nanowires/nanotube [27, 28] or 2D thin layers [29] and investigating novel catalyst support materials [30, 31]. These attempts have been met with some success, however the performance targets set by the DOE [19] have still not been obtained.

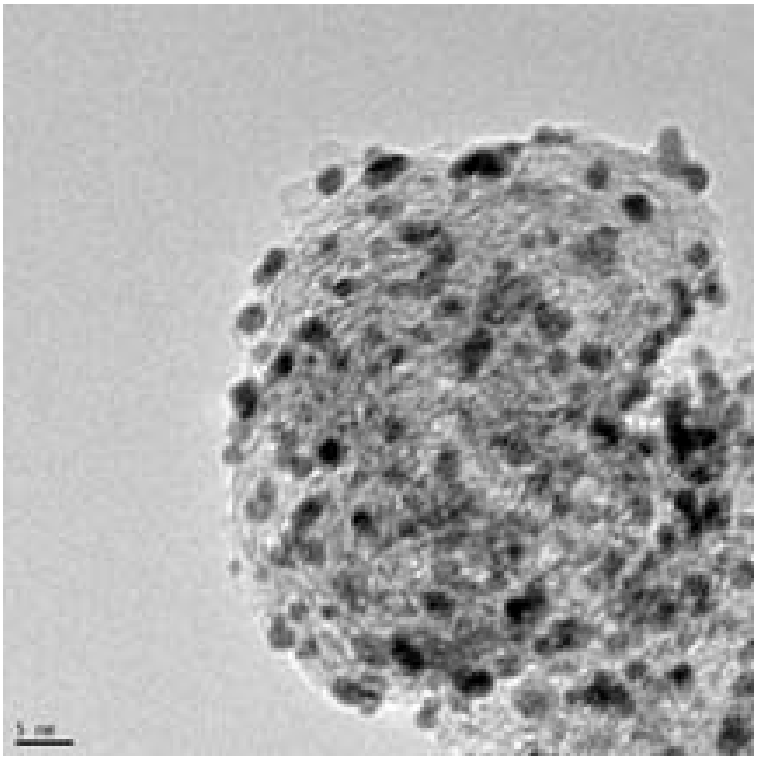

Figure 4: TEM image of commercial Pt/C catalyst.

Improving the Pt mass based activity of ORR electrocatalyst materials is an urgent necessity, in order to lower the Pt loading and improve fuel cell performance. This would effectively reduce the overall system cost and would alleviate the significant reliance on this noble metal with limited natural supplies. Attempts to improve the ORR activity generally involve modification of the distinct electronic and structural properties of the catalyst materials, along with enhancing the catalyst-support interactions. Alloying Pt with other non-noble transition metals (i.e. Fe, Co, Ni, etc.) has been demonstrated to provide distinct Pt mass based performance increments, attributed to d-band shifts, Pt lattice contraction and modified surface reactivities [32-37]. Development of materials with distinct nanostructures in order to increase Pt utilization has involved the development of thin nanowires with high surface aspect ratios [38, 39], nanotubes [27] and even monolayer Pt catalysts [40-42] so that effectively all Pt atoms have exposure to reactants. Simultaneously improving Pt-mass based activities without sacrificing catalyst stability is a significant challenge. Further work is required in order to increase the overall power density of PEMFCs to 0.8-0.9 Wcm^{-2}_{MEA} at cell voltages above 0.65 V while effectively reducing the overall Pt loading to 0.15 $mgcm^{-2}_{MEA}$ and maintaining operational stability. Reaching these targets would make PEMFC usage for large-scale automotive applications a reality [15].

The performance and stability of other component materials must be taken into account when looking at fuel cell systems as a whole. Numerous efforts have been focused on improving the performance of the polymer membranes, which are also prone to time dependent performance drift resulting from structural, chemical and thermal degradation [2]. While these issues cannot be overlooked, the focus of the present work is on the cathode catalyst materials utilized in fuel cells and a thorough discussion of other component materials is not necessary.

1.2 Alkaline Fuel Cells

AFCs have been conceptualized since the early 1900s [3] and have been in existence dating back to the 1950s as a power source for a farm tractor [43]. Since then, these devices have been utilized for extensive transportation applications and even as power supply for the NASA lunar missions in the 1960s [3]. The promising performance towards these applications popularized AFCs and motivated significant research efforts on their development in the 1970s and 1980s. Relatively recently, emergence of PEMFCs has eclipsed efforts on the development of AFCs and they have fallen out of favour with the scientific community. Despite this, research and development of AFCs has not been forgotten, as they provide numerous advantages that still render them promising devices. Most significantly, the ORR overpotential occurring at the cathode under alkaline conditions is significantly lower than under acidic conditions such as those encountered in a PEMFC [3, 43, 44]. This allows operation at higher voltages with fewer activation losses and provides opportunity for the utilization of non-precious catalyst materials (however Pt usage has not been completely dismissed) [3, 43]. AFCs also provide many cost benefits over PEMFCs deriving from the aforementioned reduction/elimination of Pt based catalysts due to more facile reaction kinetics, along with cheaper electrolytes and simplistic system designs [3]. Alkaline environments further offer less corrosive operating environments which can reduce component degradation resulting in stability improvements [45-47]. Low power densities and electrolyte contamination are the two most significant issues facing the development of AFCs, although cost reduction is of relative importance in order to improve the economic feasibility of AFC commercialization.

1.2.1 Operational principles

Alkaline fuel cells traditionally operate on hydrogen feeds to the anode and oxygen (or air) to the cathode in a configuration illustrated in Figure 5. Other fuels have been investigated as alternatives to hydrogen, including methanol or ethanol, however hydrogen still remains the fuel of choice. Under alkaline conditions, the overall fuel cell reaction given in Equation (5). The exact reaction mechanisms of the two half cells slightly differ however. At the site of the cathode, oxygen that is continuously fed will undergo ORR to form hydroxide anions. This can proceed by two pathways, the first of which is the more efficient, direct 4e- transfer following Equation (7):

$$O_2 + 4e^- + 2H_2O \rightarrow 4OH^- \qquad E^o = 0.401 \text{ V vs RHE} \qquad (7)$$

In alkaline media, the ORR can also occur by a more indirect process. First, the oxygen molecules will undergo a 2e- reduction, forming HO_2^- hydrogen peroxide species, either as an intermediate or a final byproduct [48]. This reaction follows Equation (8):

$$O_2 + 2e^- + H_2O \rightarrow OH^- + HO_2^- \qquad E^o = -0.07 \text{ V vs RHE} \qquad (8)$$

These species can either be released into the system as detrimental byproducts [REF], chemically decompose forming a single O2 molecule and hydroxide anion [48], or ideally be further reduced by another 2e- reduction process (overall 4e-) following Equation (9):

$$HO_2^- + 2e^- + H_2O \rightarrow 3OH^- \qquad E^o = 0.87 \text{ V vs RHE} \qquad (9)$$

Following these reactions, formed hydroxide anions will be transported through the electrolyte to the anode, where they will take part in the HOR following Equation (10):

$$2H_2 + 4OH^- \rightarrow 4H_2O + 4e^- \qquad E^o = -0.83 \text{ V vs RHE} \qquad (10)$$

Similar to the PEMFC, the alkaline electrolyte must be impervious to electron flow directing them through an external circuit.

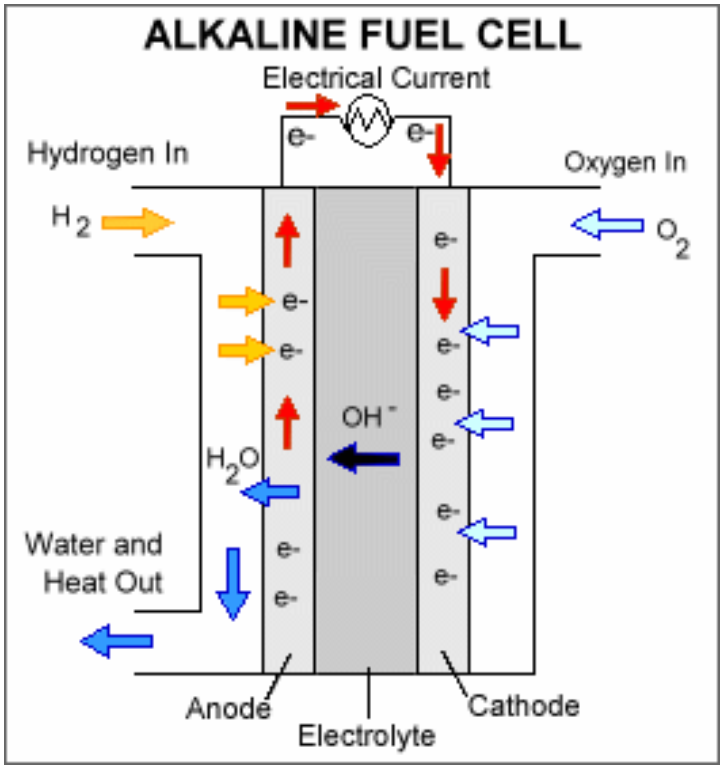

Figure 5: Single cell arrangement for AFC, taken from [16].

AFCs have the potential to operate in the absence of Pt due to the much more facile ORR kinetics occurring in alkaline conditions, a phenomena well documented, however not well understood [48]. In this regard, common electrode configurations have consisted of porous three dimensional Ni or Ag structures. Early work utilized porous nickel electrodes fabricated from sintered Ni powders [49]. This later evolved toward the use of Raney metals electrodes. These materials were produced by fabrication of a composite material consisting of an active metal such as Ni or Ag, and an inactive metal such as aluminum. After synthesis of this composite, the aluminum component could be effectively dissolved out, forming three dimensional porous structures with high surface area and electronic conductivity. Numerous arrangements have been employed utilizing electrodes of this structure comprised of Ni at the anode and Ag at the cathode [50]. In later years, the use of rolled electrodes was presented. These would consist of catalyst materials mixed with polytetrafluoroethylene (PTFE) and rolled onto a porous Ni substrate [51]. The catalyst materials utilized often consist of high surface area carbon supported catalytic materials, including Pt or non-noble components such as manganese oxides [3]. It should be noted that utilizing Pt can alleviate the requirement for complex metal based electrode structures, however bears with it high cost and limited availability.

AFCs generally rely on the use of liquid electrolyte materials, most specifically solutions of potassium hydroxide (KOH). Due to the significant issue of electrolyte contamination, various electrolyte configurations have been investigated including circulating liquid electrolytes [52], liquid electrolyte immobilized in a porous matrix material [53] and most recently anion exchange membranes (AEMs) [54-56]. All of these configurations have their respective advantages and drawbacks which will be discussed further in the technical challenges section. Increasing the pressure of reactant gases in AFCs can result in improved performance, although a significant amount of investigations on AFCs have generally focused on ambient condition operation (i.e. atmospheric pressure). This has caused some discrepancy when comparing the performance of AFCs with that of pressurized PEMFCs [43], however, it should be noted that investigations involving the use of pressurized reactants results in promising AFC performance that is comparable to PEMFCs. Above ambient operating temperatures are generally used, where increases in the cell temperature can significantly improve fuel cell performance due to the reduction in activation overpotentials for the electrochemical half cell reactions [3]. It has been reported that minimum operation temperature of 60^{o}C can be utilized [3], however these devices are generally operated at temperatures between 90-100^{o}C [18] in order to provide a compromise between cell performance and stability issues. Bipolar plates are not generally utilized in AFCs, mainly due to the high inherent conductivity of the metal electrodes and the insulating properties of PTFE utilized in rolled electrodes. Thus, electrode edge connections are possible providing simpler and lighter cell designs, while reducing system costs due to elimination of the bipolar plates. It should be noted however that many different stack setups have been investigated over the years and an optimal configuration has not been exclusively confirmed.

1.2.2 Technical Challenges

While cost and performance improvements are two issues that consistently need to be addressed, the primary challenge facing AFC technologies relates to electrolyte poisoning due to the presence of CO_2 impurities in the reactant feeds [43, 51]. CO_2 impurities will react with hydroxide anions in the electrolyte solution following either Equation (11) or (12):

$$CO_2 + 2OH^- \rightarrow CO_2^{-3} + H_2O \qquad (11)$$

$$CO_2 + 2KOH \rightarrow K_2CO_3 + H_2O \qquad (12)$$

Significant performance losses can be attributed to these reactions. Specifically, each reaction reduces the hydroxide anion concentration in the electrolyte solution and the solubility of carbonate species. This will serve to reduce the anionic conductivity of the electrolyte, reduce the pH and limit hydroxide anion accessibility to the anode, resulting in diminished HOR rates and power output [3, 43]. Carbonate precipitation will also have several detrimental effects, including: i) blocking of catalyst pores, resulting in reactant access and water management issues [43], ii) increased viscosity of electrolyte solutions hindering mass transport [3] iii) increased volume and vapour pressure of the electrolyte [43] and iv) electrode and component damaging resulting from solid formation [3]. Overall, it is indicated that CO_2 poisoning is the main challenge limiting the commercialization of AFC usage. In order to overcome these challenges it is suggested that AFCs need to be run on pure reactant feeds, require on-board scrubbers or require adequate electrolyte configurations. Investigations into the latter have included circulating electrolytes, intermittent electrolyte replacement, or most recently the development of AEMs [54-56]. Each of these options possesses several advantages and disadvantages that will not be discussed in detail. However, the use of AEMs in fuel cell setups is very promising and will be utilized in one of the studies reported herein. Thus, the subsequent discussions related to AFC technologies will have more of a specific focus on anion exchange membrane fuel cells (AEMFCs).

Improving the performance of AFCs is extremely important in order to increase the practicability of these devices and drive the technology further towards commercialization. Low performance generally stems from the AEM and the catalyst layers utilized. With respect to the former, low anionic conductivity and thermal stability are two issues that still require further improvement [56]. In the case of the latter, development of highly active electrocatalyst materials will serve to improve the overall performance of AFCs. The design and synthesis of novel nanostructured electrocatalyst materials with improved performance is important and a focus should be on improving surface aspect rations, active site densities and utilization. When utilizing non-precious metal or metal-free catalyst materials, hydrogen peroxide byproduct formation is also a significant challenge facing catalyst performance [2]. ORR following the $2e^-$ reduction mechanism resulting in hydrogen peroxide formation will lower the overall efficiency and produce these corrosive byproducts that can be detrimental to component stability. Thus, when investigating new catalyst materials, the selectivity towards the more efficient $4e^-$ ORR mechanism must not be overlooked.

Reducing the overall system cost will also significantly improve the economic feasibility of successfully commercializing these devices. Despite diminished reliance on Pt based catalysts compared

with PEMFCs, there is still a significant dependence on metal based catalyst materials (i.e. Fe, Co, Ni, Au). Not only are there significant costs associated with the mining, extraction, recycling and disposal of metal components, there are significant environmental impacts involved with each of these processes. Research and development efforts need to be directed at the production of inexpensive catalyst materials with a significantly reduced, or even eliminated metal dependence, while maintain high ORR activity and operational stability.

1.3 Nitrogen doped carbon nanotubes

The attention of the scientific community was first drawn to CNTs in 1991 [57] and steady research efforts on their properties and potential applications has since ensued. CNTs are versatile nanomaterials that consist of graphene sheets rolled up in a tubular formation as depicted in Figure 6. CNTs can consist either of a single (SWNT), double (DWNT) or multiple (MWNT) graphene sheets which can drastically alter their overall properties [58]. They can have diameters as small as 1 nanometer [59] and as large as several hundreds of nanometers, with varying lengths up to several micrometers. Thus, generally CNTs are considered one dimensional nanomaterials and possess numerous advantages associated with their anisotropic nature. The main advantages of CNTs lie in their distinct structural and electronic properties. Firstly, their mechanical properties are unrivaled, displaying extremely high structural strength despite being extremely lightweight [59, 60]. Graphitic carbon is also mechanically and chemically more stable than disordered carbonaceous species, leading to a higher degree of structural integrity of the CNT walls. Second, their high surface aspect ratios and capillary like nature deriving from their hollow structure can render them ideal for many applications including catalysis and energy storage [59]. Third, they possess attractive thermal properties, including stability at extremely high temperatures and exception thermal conductivity [60]. Finally, their unique, tunable electronic properties are fascinating and are so immense they have been the focus of entire review papers [59]. CNTs can have either metallic or semiconductor electronic properties with tunable band gaps, properties that have led to their investigation towards applications including energy conversion and storage, conductive high strength composites, field emission devices and many more [58-60].

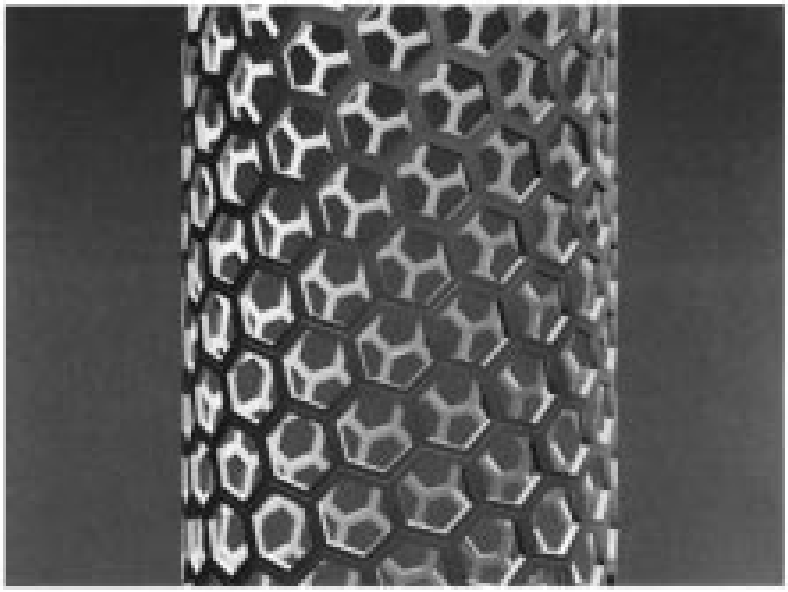

Figure 6: Schematic of basic CNT structure, reprinted in part with permission from [61], Copyright 1999 American Chemical Society.

Heterogeneous chemical doping of CNTs, specifically nitrogen atoms incorporated into N-CNTs can significantly alter the distinct physical properties of these materials making them amenable and more applicable to numerous applications. The incorporation of nitrogen into CNTs was first reported in 1994 [62], where researchers utilized arc-discharge methods to fabricate CNTs substitutionally doped with nitrogen and boron atoms. Since then, N-CNTs have been synthesized by several different methods, resulting in N-CNTs with varying nitrogen contents, structural and electronic properties. High temperature synthesis methods can be utilized, which include arc-discharge or laser ablation. These methods involve the rapid evaporation of precursor targets and subsequent N-CNT growth and deposition on substrate materials. Relatively low temperature growth methods such as CVD are also commonly applied and generally consist of injecting precursor solutions into a tube furnace, where nanotube growth occurs under an inert environmental. These two methods are *in situ* nitrogen doping procedures and can be very versatile, requiring relatively simple precursor materials consisting of only carbon and nitrogen in the presence of a growth catalyst (i.e. Fe, Co, or Ni). As previously mentioned, the physical properties of the as grown N-CNTs depend significantly on the synthesis methods, but also rely on the type of precursor materials utilized as well. Nitrogen contents ranging anywhere from minimal incorporation (< 1 at. %) up to ca. 20 at. % have been reported [63]. Post treatment of CNTs has also been mentioned in the literature, however not extensively investigated.

Resulting from dopant atoms, N-CNTs exhibit higher degrees of crystalline disorder compared with their undoped counterparts [64]. Nitrogen atoms serve to induce localized defects and structural disorder that render N-CNTs with lower structural stabilities and distinct surface properties, including chemical reactivity originating from these sites [63]. This can provide many benefits, where reactive surface groups can act as focal points for chemical functionalization [65, 66] or as anchors for metal particle or ion adosorption [30, 67]. Dependent on the type of catalyst materials utilized and the inherent nitrogen content, the structure of N-CNTs often consists of long chains of bamboo-like compartments, with a TEM image depicting this structure displayed in Figure 7. The possible nitrogen configurations in the graphitic walls of N-CNTs have been extensively investigated and four primary geometries have been proposed. These include pyridinic, pyrollic, quaternary and oxidized nitrogen species (Figure 8), each possessing distinct localized physical properties. Generally speaking, the incorporation of dopant nitrogen atoms will result in enhanced electronic properties of the N-CNTs. Due to the extra valence electron provided by nitrogen atoms into the graphitic lattice of CNTs, these materials can be considered n-type semiconductors [68]. Dopant atoms induce localized electronic features and enhance the number of electronic states in the valence and conduction bands and can result in improved electronic conductivity compared with undoped CNTs [63, 64].

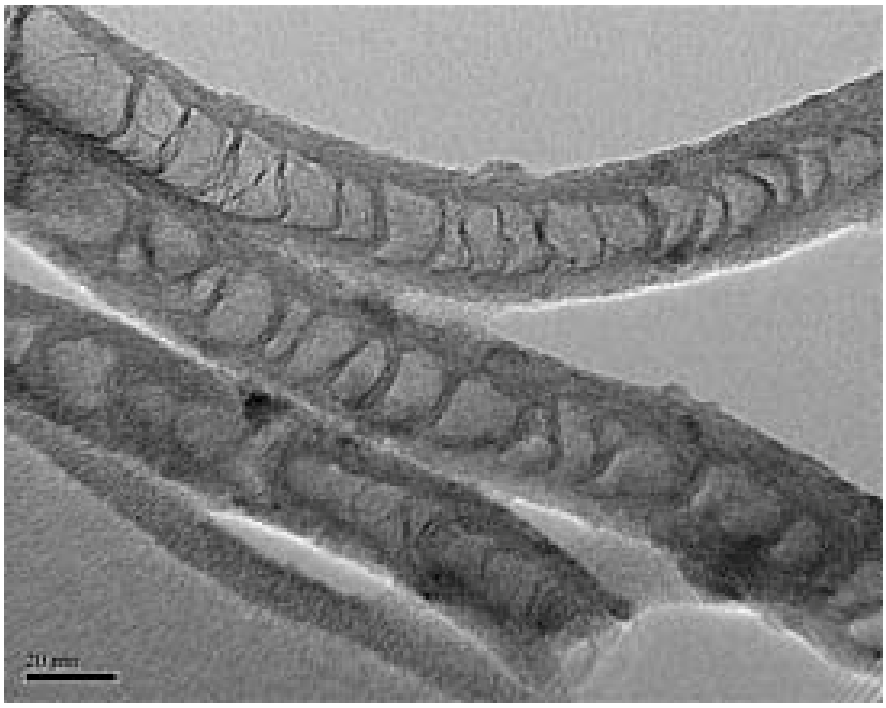

Figure 7: TEM image illustrating the bamboo-like morphology of N-CNTs.

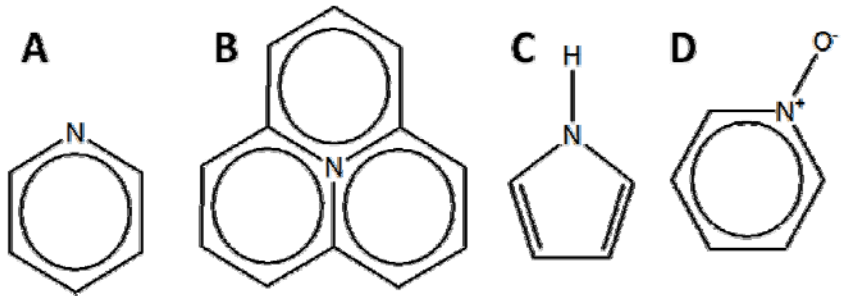

Figure 8: Nitrogen configurations in the graphitic structure of N-CNTs. A) pyridinic, B) quaternary, C) pyrollic and D) oxidized nitrogen species.

1.4 Project scope and objectives

The main focus of the projects presented here will be to capitalize on the distinct electronic and structural properties of N-CNTs described above. Through careful design and investigation, N-CNTs will be utilized either as Pt nanoparticle catalyst supports, or as standalone electrocatalyst materials. The overall objective will be utilizing N-CNTs in the cathode catalyst layers of PEMFCs and AFCs in an attempt to overcome the technical challenges facing the commercialization of low temperature fuel cells as highlighted in previous sections. Detailed characterization of these materials will be done in order to provide further insight and understanding regarding the nature and applicability of N-CNTs as ORR electrocatalyst materials or catalyst supports. This work will further provide a basis of knowledge for the future design and synthesis of highly active, stable ORR electrocatalyst materials.

2.0 Structural and electrochemical characterization techniques

In order to develop a fundamental understanding regarding the specific structures and morphology of the materials synthesized in this work, several physical characterization techniques must be utilized. Electrochemical characterization techniques will also be employed in order to determine ORR kinetics and activity of the catalyst materials. Moreover, to further probe the nature of the ORR activity of electrocatalyst materials and provide an indication of catalytically active site geometries, electrochemical characterization must be effectively coupled with detailed surface characterization techniques. This section will provide experimental details regarding the structural and electrochemical characterization techniques utilized throughout this work along with the basic theoretical principles associated with each technique.

2.1 Scanning electron microscopy

Scanning electron microscopy (SEM) utilized an extremely versatile electron microscope, commonly used by scientists and researches worldwide to investigate the surphace morphology, atomic compositions, crystallography and even electrical conductivities of a wide range of materials. Insight into these factors is drawn by irradiating the area to be investigated by a focused beamed of electrons in a rasting pattern (i.e. line by line, progressively). The electron beam will interact with the samples, emitting signals in the form of secondary electrons, backscattered electrons, characteristic x-rays and photons [69]. The images commonly seen in science journals, on websites or in the news are obtained by processing of the secondary and backscattered electrons, which are a direct product of the interactions occurring between the focused electron beam and the surface of the sample under investigation [69]. These images can obtain a resolution similar to the size of the focused electron beam and can be in the range from several nanometers to the micrometer scale. SEM devices can also be equipped in order to collect and process emitted x-ray signals, which can provide information regarding the bulk atomic composition of the sample being investigated. In this work, SEM will be utilized mainly for investigation of the distinct microstructure and morphology of the catalyst materials being developed.

2.2 Transmission electron microscopy

Transmission electron microscopes (TEMs) are devices used to obtain high resolution images of nanomaterials with precision approaching the atomic scale. TEMs operate by irradiating a sample with an electron beam of constant current density. This electron beam is produced either by means of field emission, Schottky or thermionic processes, where it is further passed through several condensers in order to provide illumination of a very small area of interest [70]. The emitted electrons will interact with the atoms of the sample being investigated by either inelastic or elastic scattering. These electron signals are then collected and processed using dynamic theories of electron diffraction [70], resulting in an image that is magnified, focused and projected for easy viewing. TEM devices allow imaging on the nanometer scale, and with high resolutions they can obtain, enable imaging of the crystal defects, atomic rows and crystalline structures of sample materials.

2.3 X-ray diffraction

X-ray diffraction (XRD) is a common technique used to provide structural characterization of a sample material utilizing x-ray beams. It can be used to identify materials with known diffraction patterns or to determine the structure of newly developed materials. Diffraction occurs when irradiation by electromagnetic waves interact with a regular array of scattering centers that have a spacing similar in size to the wavelength of the radiation [71]. Thus, X-rays with wavelengths similar to the spacing of atoms (the scattering centers) in a crystalline sample will provide diffraction patterns useful for interpretation of the specific atomic arrangement present in the samples being irradiated. X-ray radiation emitted onto these samples will be diffracted in a pattern characteristic of the distinct geometrical arrangements of the atoms. For example, Figure 9 depicts a typical XRD pattern of in-lab developed Pt/C. 2θ represents the diffraction angle of the scattered radiation and the peaks observed are related to the increased intensity of radiation scattered at these specific angles. This is due to the crystalline planes present in the material, with each peak displayed in this figure characteristic of the face centered cubic structure of Pt, correlated to a specific crystalline plane [71] (i.e. peak observed at ca. 67^{o} attributed to Pt(220) phase) [72]. During diffraction studies, x-ray beams are emitted by x-ray tubes, with a wavelength specific to the type of source material utilized. In the present work, an Al Kα x-ray source was utilized with a wavelength of 1.54 Angstroms. The main purpose for collecting XRD patterns in our samples is to identify and confirm the diffraction patterns of the materials we are investigating match the expected crystalline structures that should be present. Furthermore, with Pt

nanoparticles dispersed over a support material, such as N-CNTs in this work, the average diameter of these nanoparticles can be estimated by Equation (13), the Scherrer equation [73, 74]:

$$d = \frac{0.9\lambda_{K\alpha 1}}{B_{(2\theta)}cos\theta_{max}} \qquad (13)$$

Where d is the average particle diameter, $\lambda_{K\alpha 1}$ is the x-ray wavelength (in our case 1.54 Angstroms), $B_{(2\theta)}$ is the half-peak width in radians and θ_{max} is the maximum angle of the peak. For the materials developed and investigated in this work, average Pt nanoparticle diameters were estimated using the Pt(220) peak located at ca. 67.75 degrees as there was no interference between this peak and the characteristic peaks of the graphitic support materials.

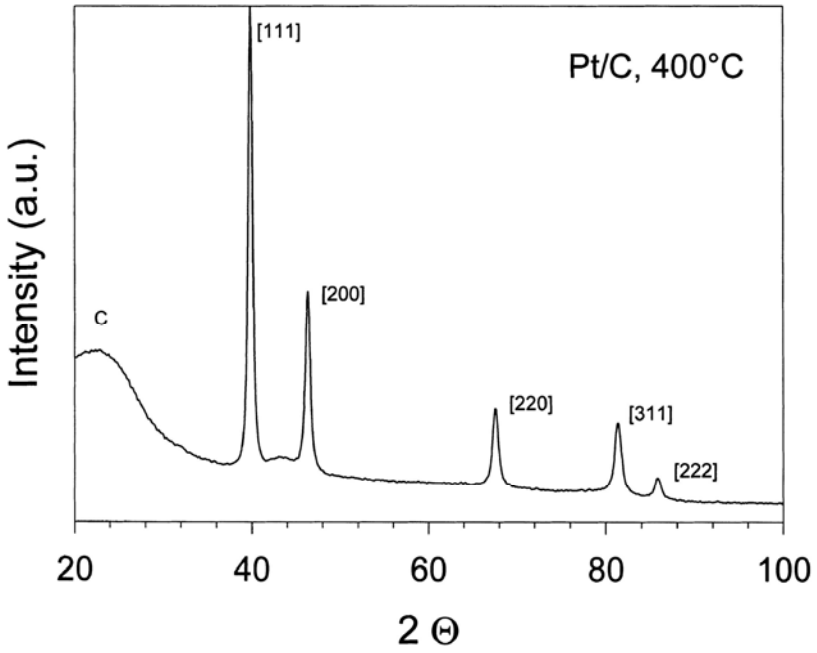

Figure 9: Typical XRD pattern for in-lab developed Pt/C displaying characteristic fcc Pt diffraction patterns, reprinted from [72], Copyright 2001 with permission from Elsevier.

2.4 Raman spectroscopy

Raman spectroscopy is a powerful characterization tool that will provide information about the vibration states of a material, a property that is characteristic of the chemical bonds and molecular symmetries present. The sample material is illuminated with monochromatic light, usually in the form of a laser. The projected photons will interact with the electron clouds and molecular bonds, causing the molecules to shift to a more energetic vibration state. Upon relaxation, the molecules will return to an energy level slightly higher than in their initial state and in doing so will emit a photon with a frequency shift characteristic of this vibration state change. Thus, processing the emitted photons will provide a

spectrum that can be used to characterize materials based on their distinct molecular configurations. In the present study, Raman spectroscopy will be used for characterization of CNT and N-CNT samples. This technique has been well established to provide detailed information about the vibrations present in CNT based materials [75]. Specifically, first order Raman spectra will be obtained and analyzed based on two peaks observed with CNT materials, referred to as the G-band, located at ca. 1550-1605 cm^{-1} and the D-band located at ca. 1350cm^{-1} [68, 76]. The G band is due to the E_{2g} optical mode present in the two dimensional graphitic structure of CNTs [68, 77, 78] and is very similar to the vibrations that are intrinsic in all sp^2 bonded carbon species [76]. The D-band is considered disorder induced [68, 78] and is attributed to Raman scattering occurring from sp^2 carbons containing either vacancies, impurities or other symmetry breaking defects [76]. The intensity of the D band to the G band, namely the I_D/I_G ratio, can be considered a quantitative measure of the degree of defects present in the CNT samples. In the case of N-CNTs, higher I_D/I_G ratios can provide indication of structural disorder and edge plane exposure arising from heterogeneous atomic doping, an indication of successful nitrogen incorporation [48, 79-81].

2.5 X-ray photoelectron spectroscopy

X-ray photoelectron spectroscopy (XPS) is a surface characterization technique used to determine chemical states, electronic states and ultimately the composition and arrangement of atoms in the top 0.5 to 5 nm [71] of a sample, with the possibility for higher probing depths. The sample material is exposed to incident x-ray photons with a known energy, represented by Equation (14):

$$E_{photon} = hv \qquad (14)$$

Where h is the Planck constant and v is the frequency of the x-ray photon. The x-rays will interact with the surface of the sample material and a measurement device is utilized in order to determine the number and kinetic energies of the electrons emitted. From these measurements, the binding energy of the emitted electrons can be determined by Equation (15):

$$E_{binding} = E_{photon} - E_{kinetic} - \phi \qquad (15)$$

Where $E_{kinetic}$ is the kinetic energy of the emitted electrons and ϕ is the work function of the measurement spectrometer. The binding energy of the electrons present in the surface of a material are characteristic of the atoms and surface chemistries present. XPS is a very important technique when dealing with surface catalysis, thus, in the present study, XPS will be carried out on N-CNT based catalyst

materials. This is in order to determine the nitrogen functional groups present on the surface of these catalysts, which will provide insight into the chemical nature and atomic configurations of the catalytically active sites.

Numerous studies have reported characterization of N-CNT materials using XPS. High resolution XPS carried out on the N1s peaks provide the most reliable indication of nitrogen functional groups present. Namely, the four functional groups mentioned previously (Figure 8) have electrons with previously determined binding energies. The specific binding energies are: i) 398.6 eV for pyridinic nitrogen species present on the edge plane of N-CNT materials [82-84], ii) 400.0-400.6 for pyrollic nitrogen species, iii) 401.1-401.7 eV for quaternary (or substituted graphitic like) nitrogen species and iv) 402.0-405.0 eV for oxidized nitrogen species [84]. Thus, high resolution N1s signals obtained from XPS analysis can be broken down into contributing peaks and the respective atomic contributions quantitatively determined by integrating these peaks.

2.6 Thermogravimetric analysis

Thermogravimetric analysis (TGA) is a characteristic tool that measures the weight change in a sample material as a result of changing temperatures. TGA is used to determine thermal stabilities, decomposition temperatures, along with moisture, and the content of metal or organic/inorganic species present. In the present work, the TGA device utilized consists of a sample holder that continuously monitors the weight of the material being investigated. Steady heating was carried out in a reaction chamber under a continuous flow of N_2/air (50/50), and heating was carried out from 60 to 900^{o}C at a rate of 20^{o}Cmin^{-1}.

2.7 Half cell electrochemical testing

Half-cell electrochemical testing will be carried out employing a rotating ring disc electrode (RRDE) setup. The system utilizes a RRDE tip (Figure 10), equipped with a glassy carbon disc electrode which is separated from a Pt ring electrode by a thin layer of Teflon. Catalyst materials are ultrasonically suspended in an ethanol/water mixture in order to prepare a well dispersed ink (concentration of 4 mg catalyst / 2 mL ethanol and water). 20 uL of this catalyst ink will subsequently be deposited on the glassy carbon disc electrode (area = 0.19635 cm^2). Catalyst adherence will then be ensured by coating the electrode with 10 uL of a 0.05 wt. % Nafion solution. The catalyst loaded RRDE tip will be fixed to an

electrode rotator and electronically connected to a potentiostat in order to measure and control electrode currents and voltages.

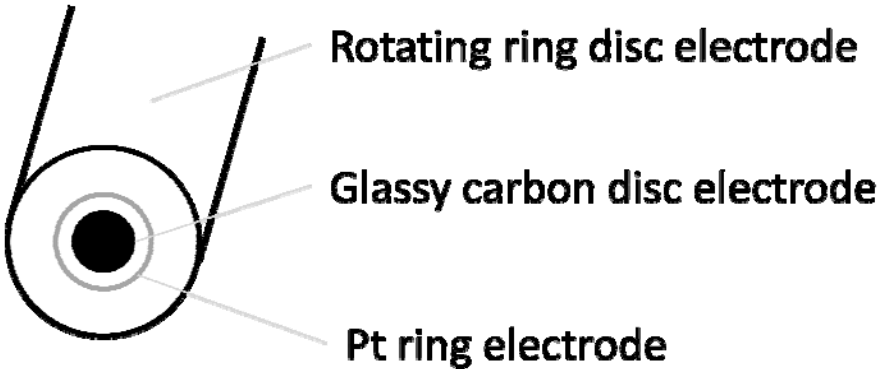

Figure 10: RRDE tip used during half-cell electrochemical testing.

This RRDE tip will then be immersed into an electrolyte solution of either 0.1 M $HClO_4$ or 0.1 M KOH for acidic and alkaline testing, respectively. The electrolyte will be contained in a glass cell containing an Ag/AgCl reference and Pt wire counter electrode. Linear potential sweeps will be obtained at ranges highlighted in the Specific Experimental Details section of the respective studies. These sweeps will be carried out under oxygen saturated conditions to obtain polarization curves which provide indication of the ORR kinetics occurring on the catalyst materials. Background currents will be obtained in nitrogen saturated electrolyte and removed in order to eliminate capacitative contributions. Various electrode rotation speeds will be employed (100, 400, 900 and 1600 rpm) and all testing carried out at room temperature (ca. 22^{o}C). A typical polarization curve for commercial Pt/C in alkaline electrolyte is provided in Figure 11 as an example. This figure encompasses the potential range that ORR will occur in resulting in generation of a current. At high potentials (Region A, Figure 11) the ORR is under electrochemical kinetic limitations. Optimal catalyst materials will shown minimal kinetic limitations and the ORR will occur at potentials as close to the reversible equilibrium potential of the ORR (i.e. minimal overpotential losses) as possible. As the electrode potential decreases (Region B, Figure 11), the ORR is under a mixed control regime, effected simultaneously by electrochemical kinetic limitations and mass transfer limitations. At much lower potentials (Region C, Figure 11), a diffusion limited current plateau is reached. At this point, the electrochemical kinetics of ORR are proceeding rapidly enough that the limiting factor facing the ORR is diffusion of O_2 species in the electrolyte to the surface of the catalyst materials. The higher diffusion limited currents observed at increasing rotation speeds result from the laminar hydrodynamic flow regimes caused by electrode rotation (Figure 12). At higher rotation speeds

the supply of O_2 saturated electrolyte available to the electrode will be increased and diffusion limiting effects will be reduced.

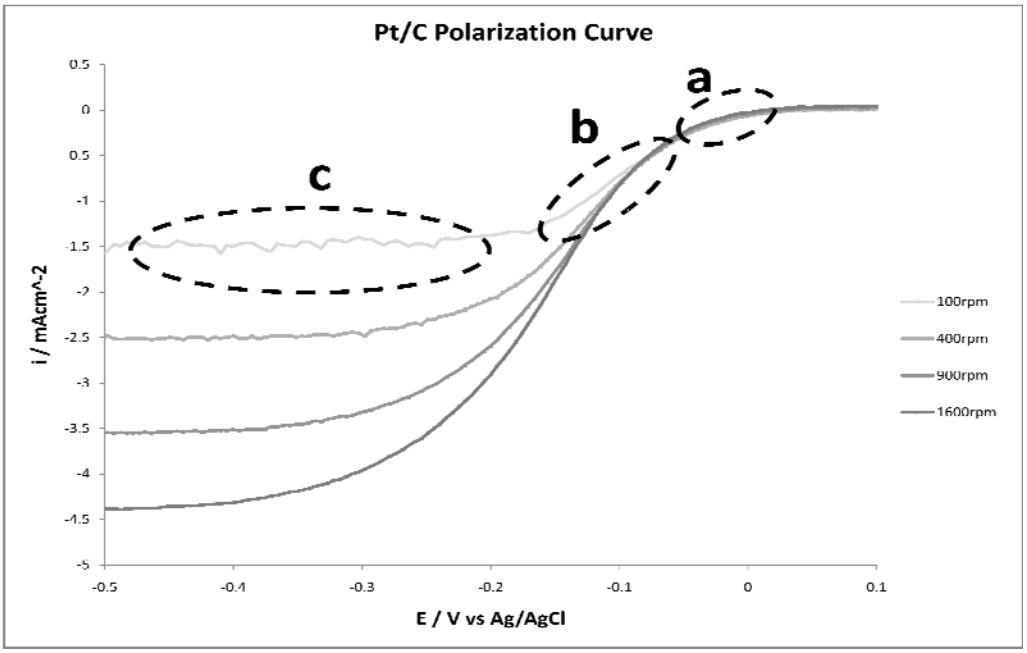

Figure 11: Typical half-cell polarization curve of commercial Pt/C, displaying different electrode rotation speeds and current control regimes.

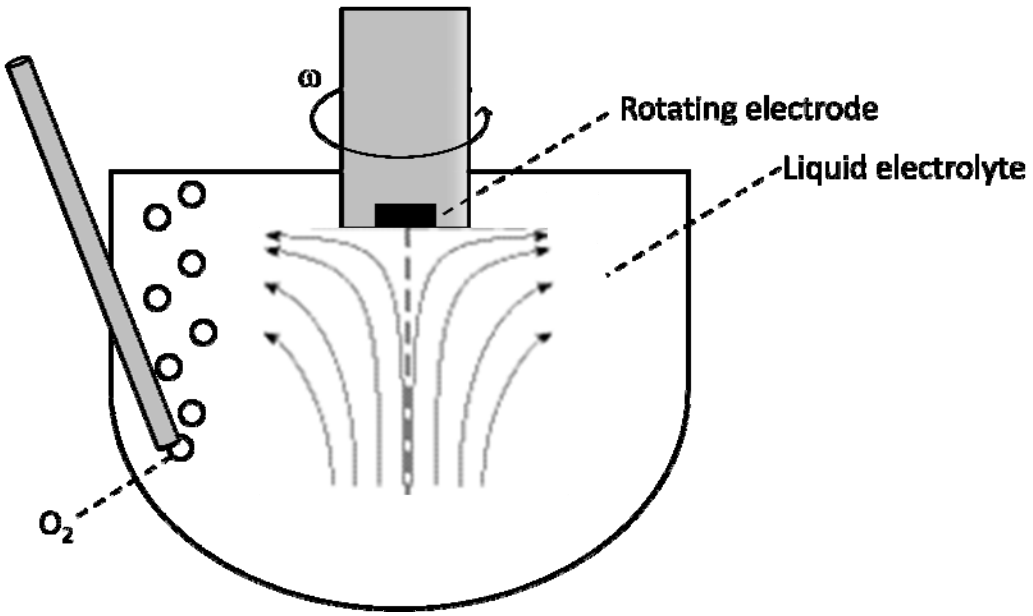

Figure 12: Laminar hydrodynamic flow patterns induced by electrode rotation which will be enhanced at higher electrode rotation speeds (ω).

The Koutecky-Levich equation can be used in order to investigate the electrochemical kinetics previously discussed using ORR polarization data obtained from half-cell testing. The overall observed current density can be broken down following Equation (16), the Koutecky-Levich equation:

$$\frac{1}{i} = \frac{1}{i_k} + \frac{1}{i_d} \qquad (17)$$

Where i is the overall observed current density, i_k is the kinetically limited current density, i_d is the diffusion limited current density and the effects of the Nafion coating are considered negligible. At high overpotentials, i_k will be very large and this term will become negligible, resulting in the current plateau observed in Range C of Figure 11, where $i = i_d$. i_d as previously mentioned depends on the electrode rotation speed (ω) and can be expressed mathematically by Equation (18):

$$i_d = 0.62nF[O_2]D_{O2}^{2/3}v^{-1/6}\omega^{1/2} \qquad (18)$$

Where n is the average number of electrons transferred in the reaction, F is Faraday's constant, $[O_2]$ is the concentration of oxygen in solution, D_{O2} is the diffusion coefficient of oxygen in solution and v is the viscosity of the solution. All of these, with the exception of ω are constant values and can be combined into a single constant B. Thus, equation (17) can be expressed as Equation (19):

$$\frac{1}{i} = \frac{1}{i_k} + \frac{1}{B\omega^{1/2}} \qquad (19)$$

A plot of i^{-1} versus $\omega^{-1/2}$ is then referred to as a Koutecky-Levich plot and should display linear behavior (assuming a first order reaction with respect to oxygen) with a y-intercept of i_k^{-1} and a slope of B^{-1}. This can be applied in order to determine the kinetically limited current density of catalyst materials at various potentials (eliminating the effects of diffusion) and if desired, the number of electrons transferred which will provide indication of the catalyst selectivity towards the more efficient 4 electron reduction process.

RRDE voltammetry is designed to provide inherent analysis of the reaction selectivity towards the 4 electron ORR instead of relying on complex calculations and data plotting techniques. With electrode rotation, the electrolyte will flow in a similar arrangement to Figure 12. Thus, while the ORR is occurring on the catalyst surface, reactants will continuously be swept away by hydrodynamic flow. This flow will traverse along the electrode surface, passing over the Pt ring electrode. The Pt ring electrode will be set at a voltage such that any hydrogen peroxide species produced by the catalyst materials will be oxidized. The electrode collection efficiency N, takes into account the efficiency of product transport and contact with the ring electrode. In the present study, N is equal to 0.26, or more specifically,

approximately 26% of all hydrogen peroxide species generated at the disc electrode will be oxidized at the ring electrode. Measuring the ring electrode current, I_R, the number of hydrogen peroxide species can be deduced and the selectivity of the catalyst material towards the more efficient 4 electron ORR process can be calculated by Equation (20):

$$\%Selectivity = \left[\frac{(I_D-(I_R/N))}{(I_D+(I_R/N))}\right] * 100\% \qquad (20)$$

Where I_D is the absolute value of the measured disc current. Furthermore, the average number of electrons transferred can be calculated by Equation (21):

$$n = \frac{4*I_D}{(I_D+\frac{I_R}{N})} \qquad (21)$$

Utilizing both equation (20) and (21) however is redundant and only one will be utilized for each study presented here. Product selectivities as close to 100% as possible (i.e. 100% of the O_2 molecules react to form H_2O) and average number of electrons as close as possible to 4 are ideal, indicating efficient ORR catalysis occurring on the catalyst materials. In the present work these calculations will be done for Pt-free catalyst materials in order to investigate their ORR mechanisms, kinetics and product selectivities. Ring currents will be collected in alkaline conditions while maintaining the Pt ring electrode potential at 0.5 V vs Ag/AgCl in order to effectively oxidize any hydrogen peroxide species reaching the surface.

Cyclic voltammetry (CV) analysis can be applied in order to determine the electrochemically active surface area (ECSA) of Pt-based catalyst materials in acidic electrolyte. CV involves cycling the potential of the catalyst coated electrode under nitrogen saturated conditions. Figure 13 illustrates a typical CV polarization curve obtained for commercial Pt/C. At lower electrode potentials (i.e. in the range below ca. 0.35 V vs RHE), two peaks are observed, Q' and Q'', attributed to the adsorption and desorption of hydrogen species, respectively. The shaded region indicated the capacitive current present on the surface of Pt/C. Upon integration of these two peaks, the charge transfer occurring during the adsorption of desorption of hydrogen species can be calculated. Based on the charge transfer occurring during these specific processes readily available in the literature and the assumption that the Pt surface is effectively covered by a monolayer of hydrogen species, the ECSA of the catalyst materials can be calculated. Generally, the average charge transfer occurring during these processes (Q) can be calculated by averaging Q' and Q''. Following that, the ECSA of the Pt-based catalyst can be calculated by Equation (22) [85, 86]:

$$ECSA = \frac{Q}{mc} \qquad (22)$$

Where m is the Pt loading ($mgcm^{-2}$) on the electrode surface and c is the charge required to oxidize a monolayer of hydrogen on the surface of Pt (0.21 mC per cm^2 of surface coverage).

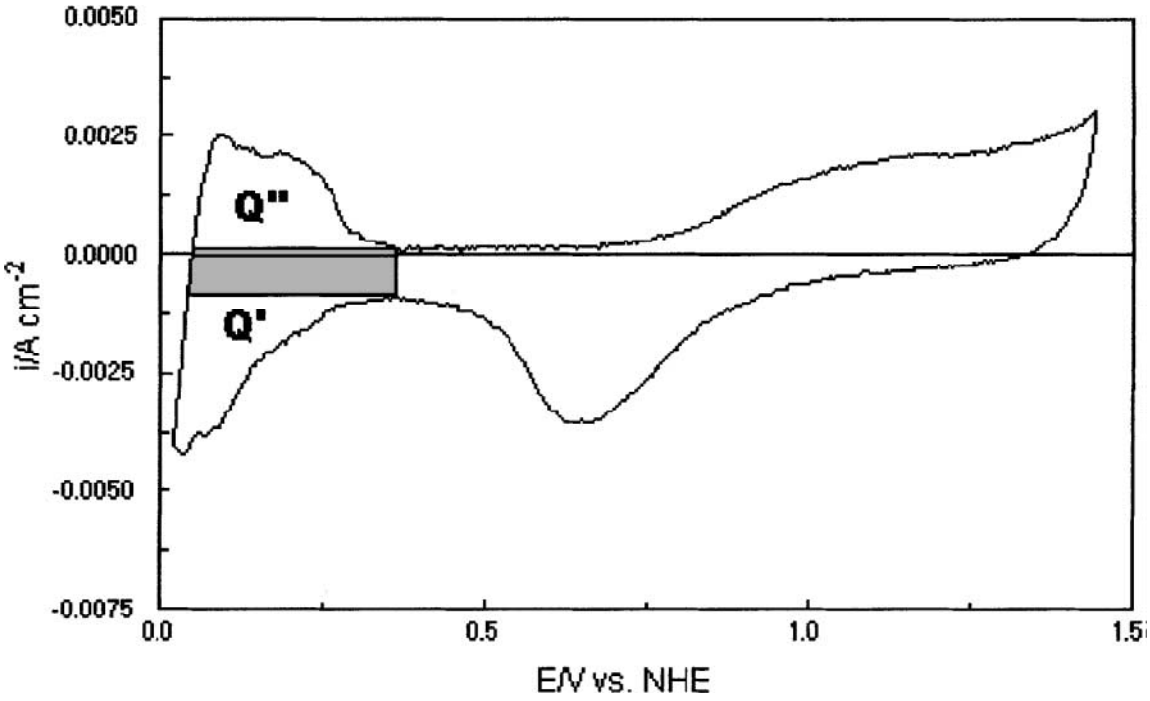

Figure 13: Typical CV curve for Pt/C displaying the typical hydrogen adsorption (Q') and desorption (Q'') regions, reprinted from [86], Copyright 2002 with permission from Elsevier.

2.8 Membrane electrode assembly testing

While electrochemical half cell testing provides valuable information regarding the kinetics of ORR occurring on the surface of the catalyst materials being investigated it does not provide detailed information regarding the potential performance of these materials in an actual fuel cell setup. In order to investigate this, single cell MEAs are fabricated. An MEA consists of a simple single fuel cell, with a PEM or AEM sandwiched between the anode and cathode electrodes and the whole system sealed on both ends with sealing gaskets. The catalyst layer is comprised of the electrocatalyst materials in direct contact with the current collecting GDL, which is generally carbon cloth or carbon paper. There are several methods of MEA fabrication utilized [87], with two primary approaches commonly followed. The first involves spray coating, painting or electrodepositing the catalyst material directly onto the two respective GDLs, followed by insertion of an electrolyte membrane between them and hot pressing the

whole assembly to ensure uniform contact and good adhesion. The second method involves coating of the catalyst materials directly onto each side of the polymer electrolyte followed by hot pressing. Sometimes, another approach is also used, referred to as the decal method. It involves coating a transfer film with the catalyst materials and then hot pressing it onto the polymer electrolyte [88]. With this method however it is more difficult to control the exact amount of catalyst loaded into the electrode structure. The exact method of electrode fabrication and MEA assembly used will have a significant impact on the output performance.

Generally the most promising electrocatalyst materials are utilized for MEA testing in order to investigate their applicability as catalyst layers in an actual fuel cell setup. Testing protocols for catalyst durability may vary, with some standard protocols issues by the DOE [19]. The actual performance tests consist of a single sweep of the cell potential, while constantly measuring the current produced. This will result in a MEA polarization curve, with a typical one provided in Figure 14. It is seen that even at open circuit conditions (no concentration being drawn), the actual cell potential is below the theoretical reversible cell potential, an unavoidable phenomena. When current is being drawn, three distinct regions are generally observed. The first region in which a rapid loss of voltage is observed when increased currents are being drawn is attributed to activation overpotentials. This is due to the slow electrochemical kinetics of the reactions occurring at the electrodes and the voltage is lost driving these reactions. The second region in which a constant cell voltage loss is occurring with increased current densities can be attributed to ohmic losses of the cell. This is due to the resistance to electron flow caused by the electrode materials, interconnections and wires. Resistance to ion transport in the polymer electrolyte will also contribute to this decrease in cell voltage. Finally, at high current densities the voltage drop ramps downwards as a result of mass transport and concentration losses. At high current densities, the reactants are being used up at a rate superior to diffusion of these species to the electrocatalyst surface. MEA polarization curves also often times include power density curves. These are calculated by simply multiplying the current density by the cell voltage in order to obtain power output. A common gauge of fuel cell performance is the maximum power output produced.

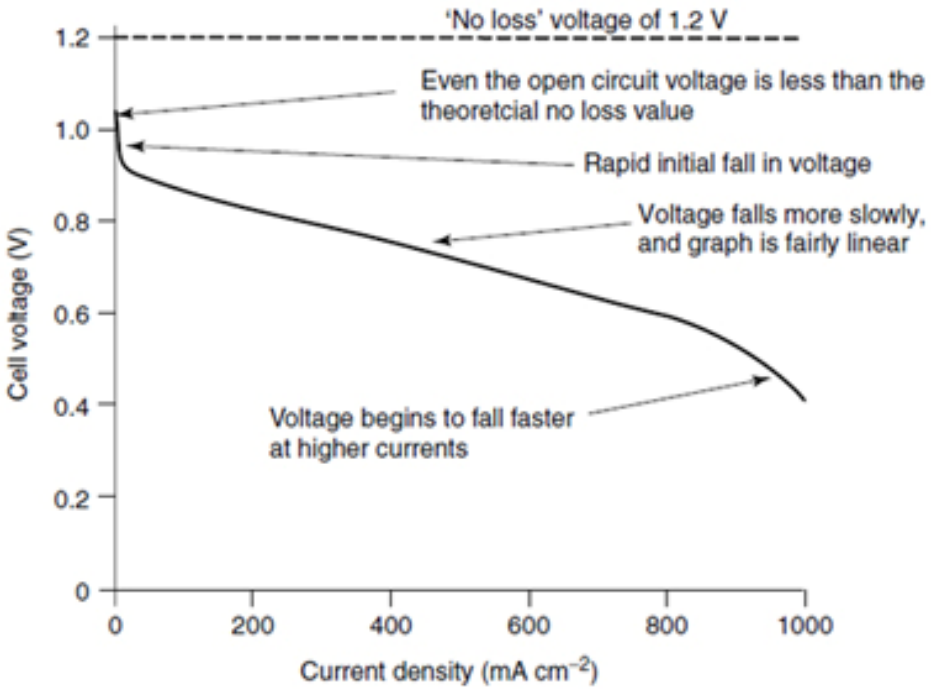

Figure 14: Typical fuel cell polarization curve showing voltage losses, with permission from [3], Copyright 2003, Wiley and Sons.

3.0 Effect of N-CNTs as Pt nanoparticle supports

Higgins, D., Meza, D., Chen, Z., "Nitrogen-Doped Carbon Nanotubes as Platinum Catalyst Supports for Oxygen Reduction Reaction in Proton Exchange Membrane Fuel Cells". Journal of Physical Chemistry C, 2010, pp. 21982-21988.

3.1 Introduction and purpose

Efforts to improve the performance and appeal of carbon supported Pt nanoparticle catalysts in the cathodic catalyst layer of fuel cells generally consists of attempts to improve the overall catalyst performance by either: i) improving Pt dispersion to increase the utilization of this noble metal, ii) improving the activity of the Pt species, or iii) improving the catalyst layer structure [89]. It has been found that the catalytic activity of Pt nanoparticles toward ORR is strongly related to the structural and electronic properties of the carbon support material [73, 90]. Currently, high surface area carbon blacks are the support material of choice, however further improvements to fuel cell performance can be achieved by investigations into alternative support materials. CNTs have been considered as Pt catalyst supports, where Pt/CNTs have consistently been found to display higher catalytic activity than traditional Pt/C due to their distinct electronic and structural properties[73, 91-98]; however, CNTs possess very low inherent catalytic activity toward the ORR. Nitrogen-doped carbon nanotubes (N-CNTs) have recently been reported to have significant catalytic activity toward ORR in alkaline conditions [99]. This ORR activity, along with the morphology and properties of the N-CNT materials is directly related to the type of nitrogen-carbon precursor and growth catalyst utilized [100, 101]. Furthermore, N-CNTs synthesized from pyridine [102], melamine [30], and acetonitrile [103] precursor solutions have been previously investigated as platinum catalyst support materials (Pt/N-CNTs), which have been shown to display high catalytic activity and durability toward ORR in acidic conditions. This enhanced electrocatalytic activity was attributed directly to the incorporation of nitrogen into the graphitic structure of CNTs, resulting in enhanced structural and electronic properties. However, the effect of the nitrogen-carbon precursor solution utilized for N-CNT synthesis on the ORR catalytic activity of Pt/N-CNT composite materials is still not clear.

In the present study, N-CNTs synthesized from ethylenediamine (ED-CNTs) and pyridine (Py-CNTs) were utilized as Pt nanoparticle support materials in order to elucidate the effect of N-CNT precursor solution on the morphology, nitrogen content, and resulting ORR electrocatalytic activity of Pt/NCNT composites. With comparison made to Pt/CNT materials, we demonstrate enhanced ORR

activity of Pt/N-CNTs materials, with ED-CNT displaying the highest activity, directly attributed to the significant nitrogen content obtained. These highly active Pt/ED-CNTs were then utilized as a cathode catalyst in a membrane electrode assembly (MEA) and shown to have significantly higher activity than nitrogen free CNT supported Pt (Pt/CNTs) catalysts.

3.2 Experimental

3.2.1 Synthesis methods

N-CNTs were synthesized using CVD. Ferrocene (2.5 wt. %) was utilized as the growth catalyst and was dissolved in either pyridine or ethylenediamine prior to the growth procedure. Synthesis was carried out in a tube furnace, heated to 800^{o}C under inert gas flow. The precursor solution was injected at a rate of 0.05 mLmin^{-1} by a syringe into the horizontal quartz tube reactor, where growth occurred on smaller quartz tube substrates. After the reaction was complete, the furnace was cooled down to 400^{o}C and opened to the atmosphere in order to oxidize any amorphous carbon species. Synthesized N-CNTs were collected by scraping off the small quartz tube growth substrates. These collected materials were then acid treated in 0.5 M H_2SO_4 at 90^{o}C for 1 hour in order to remove any residual iron particles present from the growth catalyst. Prefunctionalized CNT materials were purchased from Nanocyl.

Pt nanoparticle deposition was carried out by a well developed ethylene glycol reduction method. In this procedure, the catalyst support material (either N-CNTs or CNTs) were ultrasonically dispersed in ethylene glycol for several hours. Following this, chloroplatinic acid hexahydrate was added while stirring to obtain an overall Pt loading of 20 wt. %. NaOH was utilized to increase the solution pH above 13 and Pt nanoparticle reduction was carried out by refluxing the solution at 140^{o}C for 3 hours. After deposition the samples were filtered, washed and dried overnight.

3.2.2 Specific experimental details

In this study, all potentials were converted to the RHE scale for convenience. CV curves were obtained by sweeping the electrode potential between 0.05 and 1.25 V vs RHE at a scan rate of 50 mVs^{-1} under nitrogen saturated conditions, with no electrode rotation. ORR polarization curves were obtained in the same potential range at a scan rate of 10 mVs^{-1} under oxygen saturated conditions and various electrode rotation rates.

The performance of Pt/ED-CNTs and Pt/CNTs as cathode catalysts in a single MEA were evaluated. The MEA was constructed following a decal method [104]. This method involved blending the catalyst sample in an ink solution containing 5 wt. % Nafion for 1 hour. Following this, glycerol was added and the ink solution was stirred for 24 hours. This ink was then painted onto Teflon transfer substrates and allowed to dry in an oven. A Nafion 112 PEM was simultaneously prepared and in order to transfer the catalyst materials from the decal transfer templates to the membrane surface, they were hot pressed together at 210^{o}C and 110 lbscm^{-2} for 5 minutes. The decals were then removed and the MEA was assembled into the fuel cell test station for performance evaluation. Catalyst loadings utilized were 0.2 $mg_{Pt}cm^{-2}$ for the cathode (either Pt/ED-CNT or Pt/CNT) and anode (commercial Pt/C). Gas flow rates of 0.2 and 0.5 Lmin^{-1} were utilized for oxygen and hydrogen, respectively.

3.3 Results and discussion

The successful incorporation of nitrogen in the N-CNTs was confirmed by XPS analysis and determined to be 4.74 at. % and 2.35 at. % for ED-CNTs and Py-CNTs, respectively. C1s signals for ED-CNT, Py-CNT and CNT samples are displayed in Figure 15a. The C1s signal for CNTs displays a peak at a binding energy (BE) of 284.5 eV, very similar to the the expected value of 284.3 eV for graphitic materials [105]. The C1s signal for N-CNTs exhibits a slight shift to a higher BE of and 284.8 eV for ED-CNTs and 284.7 eV for Py-CNTs, while also displaying broadened, asymmetric behaviour. These are all traits which are commonly observed for N-CNT materials [68, 80, 106].

The N1s signal from the ED-CNTs and Py-CNTs was collected and displayed in Figure 15b. In order to determine the exact amounts of the various nitrogen functional groups present, the N1s signal was deconvoluted into three separate contributing peaks. Upon peak integration, the functional groups present and their respective amounts were obtained and are provided in Table 1. Of interest is the significantly higher pyridinic nitrogen content present in ED-CNTs (35.09 % of nitrogen atoms scanned) compared with Py-CNTs (14.83 % of nitrogen atoms scanned).. Mixed reports have attributed the catalytically active sites of N-CNTs to either the pyridinic nitrogen site itself, possessing a localized electron pair, or to the planar edges and defect sites caused by the presence of these species [105-107]. Regardless, it has been determined that the amount of pyridinic nitrogen observed in the catalyst sample provides indication of the amount of edge plane exposure. This increase in edge plane exposure has been directly linked to the ORR performance observed, attributed to the ability of edge plane sites to readily facilitate the adsorption of oxygen, which has been directly linked to the ORR performance

observed [48, 81, 106]. In our ED-CNT sample, pyridinic species accounted for 35.09 % of the nitrogen atoms scanned, whereas in Py-CNTs this species accounted for 14.83% of the nitrogen atoms scanned. This is consistent with previous results indicating that at higher overall nitrogen contents, the formation of pyridinic functionalities is favoured [108, 109], where ED-CNTs contain a significant higher overall nitrogen content compared with Py-CNTs. This increase in nitrogen content has been attributed to the higher nitrogen to carbon ratio present during synthesis due to the fact that each ethylenediamine precursor molecule has one nitrogen atom for each carbon, whereas pyridine has only one nitrogen atom for every five carbons.

Table 1: Nitrogen functional groups present in ED-CNT and Py-CNT and their atomic percent of nitrogen atoms scanned. Reprinted with permission from [7], Copyright 2010 American Chemical Society.

	ED-CNT	Py-CNT
functional group	N at %	N at %
oxidized N	19.00	16.96
pyrrolic/quaternary	45.91	68.20
pyridinic	35.09	14.83

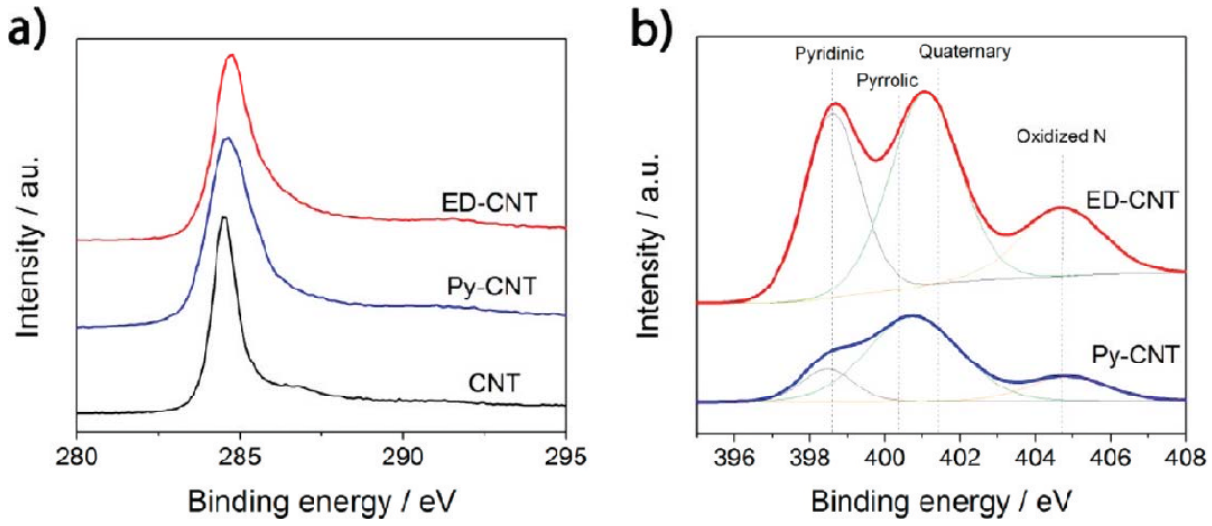

Figure 15: XPS images of (a) C1s signal displaying graphitic peaks for all samples and (b) N1s signal for ED-CNTs and Py-CNTs highlighting contributing nitrogen species. Reprinted with permission from [7], Copyright 2010 American Chemical Society.

Raman spectroscopy as displayed in Figure 16 was carried out in order to gauge the degree of structural deformations present in the ED-CNT, Py-CNT and CNT samples. ED-CNTs were found to have the highest I_D/I_G ratio of 2.07, slightly higher than 1.87 for Py-CNTs and significantly larger than 0.34 observed for CNTs. The larger I_D/I_G ratios observed for N-CNTs is a result of the structural defects and

edge plane exposure caused by heterogenous nitrogen atom incorporation into the graphite layers present on the walls of N-CNTs, consistent with XPS results.

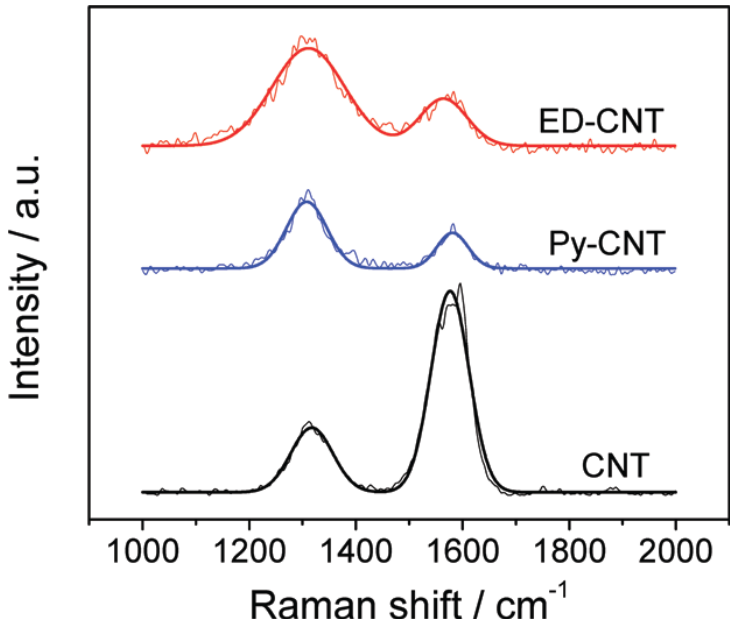

Figure 16: Raman spectroscopy for ED-CNTs, Py-CNTs, and CNTs displaying Raman first-order D and G bands. Reprinted with permission from [7], Copyright 2010 American Chemical Society.

Prior to Pt loading, the electrochemical activity of pristine ED-CNTs, Py-CNTs and CNTs towards the ORR was investigated in acidic conditions. Their respective polarization curves at 900rpm are displayed in Figure 17. Pristine N-CNTs displayed significant catalyst activity compared with the very limited activity observed for CNTs. This ORR activity was displayed at relatively high overpotentials as commonly observed with non-noble electrocatalyst materials [110]. The observed activity of the N-CNTs is directly attributed to the effect of nitrogen incorporation into the graphitic structure of CNTs. This has been shown to enhance the electronic and structural properties of the materials resulting in electron donor behaviour [111-114], and n-type semiconductance [68], factors that will serve to facilitate the ORR. Moreover, the performance of ED-CNTs was found to be superior to that of Py-CNTs. This can be attributed to the increase in nitrogen content, a parameter directly related to the effect of precursor solution utilized. It is proposed that the utilization of nitrogen rich ethylenediamine for N-CNT synthesis dictates the significant nitrogen incorporation observed for ED-CNTs. A higher presence of pyridinic nitrogen was confirmed by XPS analysis, providing reasonable explanation for the enhanced ORR activity observed [48, 81, 106, 115].

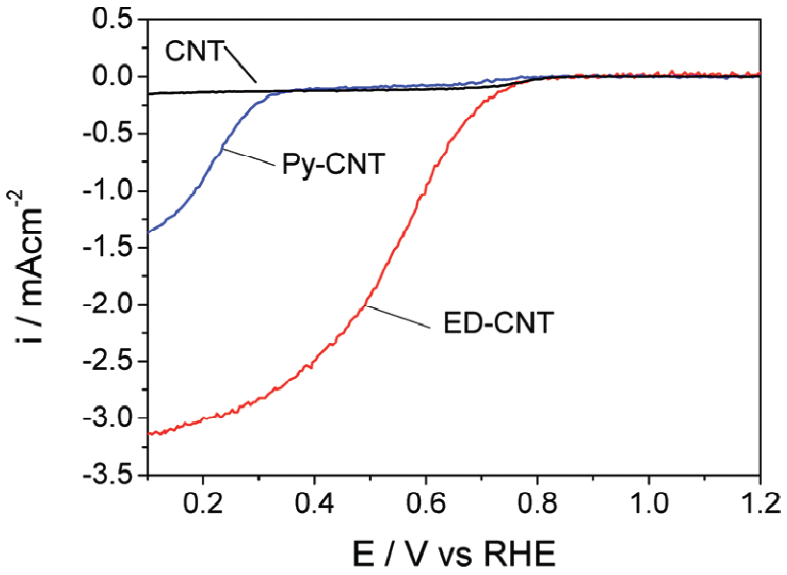

Figure 17: ORR polarization curves for pristine ED-CNTs, Py-CNTs, and CNTs in oxygen saturated 0.1 M HClO4, at a scan rate of 10 mV s-1 in the cathodic direction at a rotation speed of 900 rpm. Reprinted with permission from [7], Copyright 2010 American Chemical Society.

For N-CNT and CNT support materials, surface functional groups are required in order to anchor Pt nanoparticle deposition. Pt ions will interact with the functional group on the nanotube surfaces and will subsequently be reduced, forming nucleation sites that will facilitate nanoparticle growth [73, 116, 117]. The presence of inherent nitrogen functional groups in ED-CNTs and Py-CNTs provide anchoring sites for the adsorption of platinum ions and subsequent nanoparticle growth [118] with the steps and proposed mechanism [119] as depicted in Figure 18. It has been proposed that chemically reactive pyridinic and quaternary surface nitrogen species provide an affinity for metal deposition [120], resulting in successful metal particle attachment without requiring any surface functionalization procedure prior to deposition onto N-CNTs [114, 120]. On the other hand, CNTs require exposure to a surface functionalization procedure [121-123] which was carried out prior to purchase. This process is a necessity prior to platinum deposition, in order to provide anchoring sites for platinum ion adsorption on the relatively inert surface of CNTs [124]. After platinum deposition, TEM images were taken to investigate and confirm the loading of Pt nanoparticles onto the support materials.

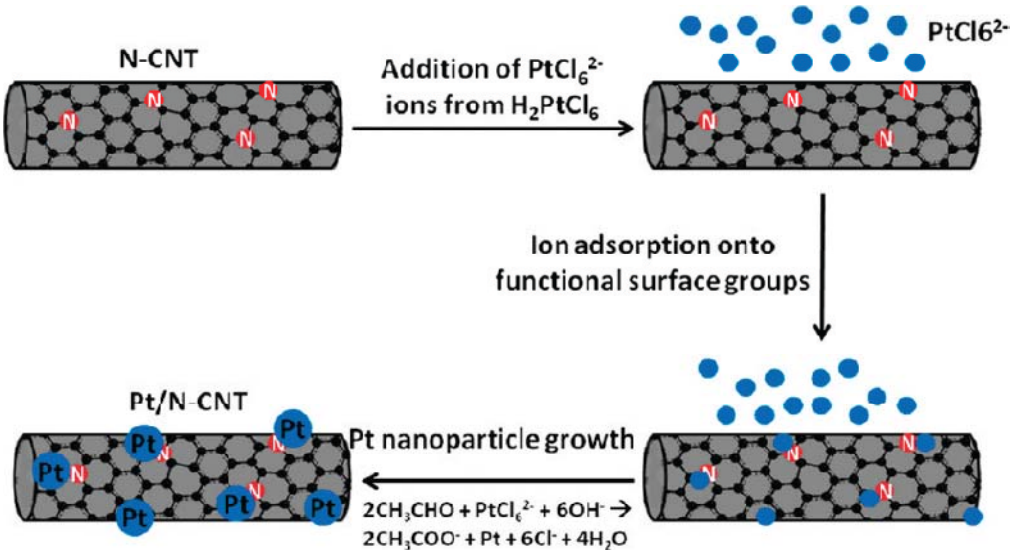

Figure 18: Schematic of ethylene glycol based platinum deposition on the surface of N-CNTs under alkaline conditions. Reprinted with permission from [7], Copyright 2010 American Chemical Society.

Figure 19 displays TEM images of Pt/ED-CNTs, Pt/Py-CNTs and Pt/CNTs (20 % wt. Pt) prior to and after platinum deposition, along with their respective particle size histograms. ED-CNTs and Py-CNTs clearly display a bamboo-like structure, consistently observed with N-CNTs due to the incorporation of nitrogen atoms into the graphitic structure of the materials [105, 109, 112, 125-127]. ED-CNTs (Figure 19a) display the highest degree of structural defects with smaller, rounder bamboo-like compartments, consistent with Raman analysis, whereas Py-CNTs (Figure 19c) display longer, more rectangular bamboo-like compartments. CNTs (Figure 19e) as expected, display a long, tubular morphology. After platinum deposition, Pt/ED-CNTs (Figure 19b) display the best dispersion of uniformly sized platinum nanoparticles. Pt/Py-CNTs (Figure 19d) display well dispersed platinum nanoparticles with a relatively higher degree of non-uniformity in the particle sizes observed. Pt/CNTs (Figure 19f) display the highest degree of non-uniform particle sizes compared with the other samples.

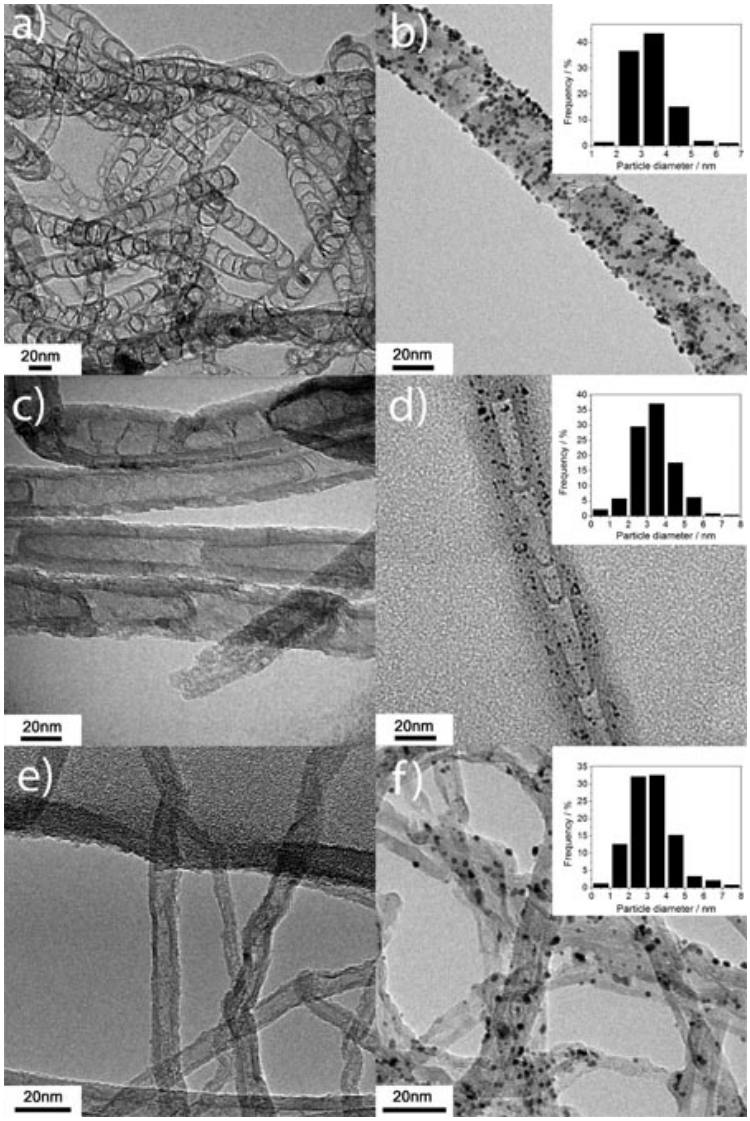

Figure 19: TEM images of (a) ED-CNTs, (b) Pt/ED-CNTs, (c) Py-CNTs, (d) Pt/Py-CNTs, (e) CNTs, and (f) Pt/CNTs along with the corresponding particle size histograms based on measurement of over 200 Pt nanoparticles. Reprinted with permission from [7], Copyright 2010 American Chemical Society.

XRD patterns of the Pt(220) peak are displayed for each sample in Figure 20. Average platinum nanoparticle sizes were calculated for each sample by applying the Scherrer equation [73, 116] and found to be 3.73 nm for Pt/ED-CNTs, 4.06 nm for Pt/Py-CNTs and 4.09 nm for Pt/CNTs. The difference in average platinum nanoparticle size was attributed to the number of functional sites available on the surface of the support material available for platinum anchorage and nanoparticle deposition. ED-CNTs, due to their high inherent nitrogen content possess a significant number of functional sites as confirmed by XPS analysis, leading to the reduced average platinum nanoparticle size. Relatively low nitrogen rich Py-CNTs and nitrogen free functionalized CNTs however possess a lower number of surface functional

groups, leading to an increase in the observed average platinum nanoparticle sizes. Clearly, N-CNTs can serve to improve the deposition of Pt nanoparticles in the absence of a costly and time consuming surface functionalization procedure that was carried out on the undoped CNTs prior to purchase. The magnitude of this improvement is directly related to the presence of inherent surface nitrogen functionalities prior to deposition.

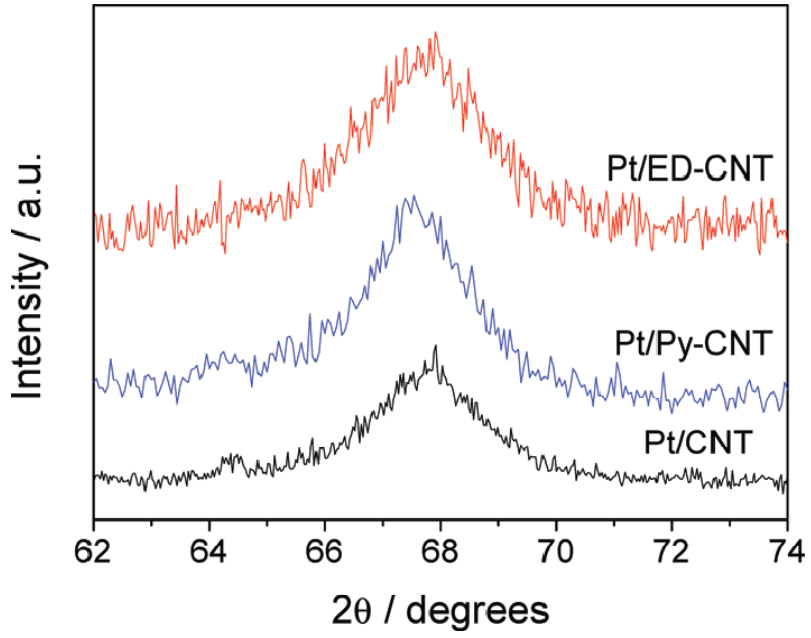

Figure 20: XRD patterns of the Pt(220) peak for Pt/ED-CNTs, Pt/Py-CNTs, and Pt/CNTs. Reprinted with permission from [7], Copyright 2010 American Chemical Society.

CV cycles displayed in Figure 21 were used to determine the ECSAs of Pt/ED-CNT, Pt/Py-CNT, and Pt/CNT catalyst samples based on the charge transfer for hydrogen desorption. The ECSA for Pt/ED-CNTs was calculated to be 67.5 $m^2 g^{-1}$, significantly higher than 38.7 and 37.7 $m^2 g^{-1}$ calculated for Pt/Py-CNTs and Pt/CNTs, respectively. The significant increase in ECSA for Pt/ED-CNTs can be attributed primarily to the smaller average platinum nanoparticle size and the uniform particle dispersion. The ECSA is a very important parameter when dealing with electrocatalyst materials; thus CV analysis indicated Pt/ED-CNTs offer superior performance as an ORR electrocatalyst when compared with Pt/Py-CNTs containing a relatively low nitrogen content, along with nitrogen free Pt/CNTs.

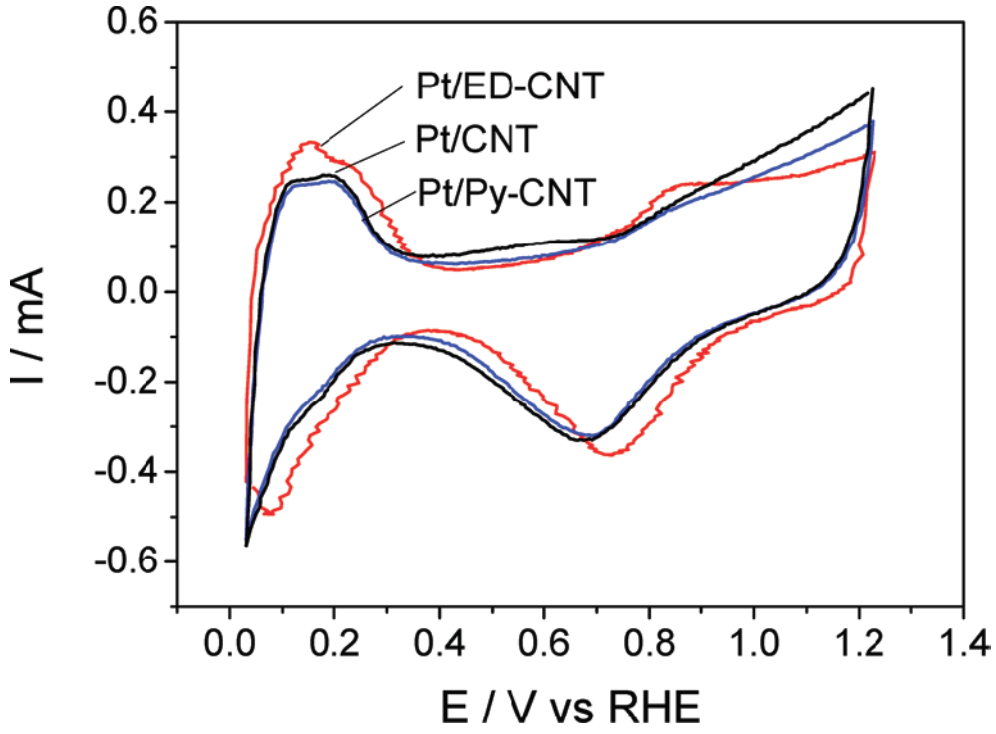

Figure 21: CV curves for Pt/ED-CNTs, Pt/Py-CNTs, and Pt/CNTs in nitrogen-saturated 0.1 M HClO4 at a scan rate of 50 mV s-1. Reprinted with permission from [7], Copyright 2010 American Chemical Society.

Steady state ORR polarization curves obtained for Pt/ED-CNT, Pt/Py-CNT and Pt/CNT catalyst samples by half cell testing in an acidic electrolyte are displayed in Figure 22a. All three samples displayed significant ORR activity along with well defined control regions (kinetic, mixed and diffusion limited) as expected with platinum containing materials. Pt/ED-CNTs displayed superior ORR activity compared with Pt/Py-CNTs and Pt/CNTs with respect to both half-wave potential and diffusion limited current densities. The half-wave potential was found to increase with nitrogen content of the support materials, where a half–wave potential of 0.74 V was observed for Pt/CNTs, 0.76 V for Pt/Py-CNTS and 0.79 V for Pt/ED-CNTs. The increase in ORR activity of the Pt loaded N-CNTs is not as significant in magnitude compared with the pristine samples displayed in Figure 17. The ORR activity of the pristine materials derives from catalytically active N-C sites as previously mentioned, whereas improvements of the ORR activity after Pt loading mainly result from the specific Pt-support interactions and properties. Thus, the increase in ORR activity of the Pt/N-CNT composites may be attributed to several factors. Well dispersed uniform sized platinum nanoparticles were observed through TEM analysis, with the effect on the observed ECSA of the samples previously mentioned, factors important for the ORR electrocatalysis. Improved electronic conductivity is also reported for N-CNT materials due to the n-type behaviour, which can serve to facilitate the facile transfer of electrons to reaction sites resulting in higher ORR

reactivity [68, 102, 112]. A synergistic effect may also be observed between the platinum nanoparticles and the support material, where the N-CNT supports possess inherent catalytic activity as previously discussed that can serve to electrochemically reduce ORR byproducts and intermediates, mainly hydrogen peroxide [48, 81]. Finally, it should be noted that an enhanced platinum-support bond is present due to the nitrogen functionalities on the surface of N-CNTs [102, 112]. This could be a result of the electron donor behaviour commonly reported for N-CNTs [111-114], or due to the stronger adsorption of platinum onto N-CNTs as indicated by a recent first-principles study [113] and confirmed by experimental analysis [128]. The exact nature of the enhanced platinum-support bond is not well understood, however the importance of nitrogen content in the support material is apparent. These results elucidate the effects of a high degree of nitrogen incorporation into the catalyst support material, reiterating the influence of the N-CNT precursor solution utilized on the activity of Pt/N-CNT composites. Nitrogen rich Pt/ED-CNTs displayed significantly higher ORR electrocatalytic activity than Pt/Py-CNTs containing relatively fewer nitrogen groups. Both Pt/N-CNT samples however outperformed nitrogen free Pt/CNTs.

Koutecky-Levich plots were generated for Pt/ED-CNTs, Pt/Py-CNTs and Pt/CNTs are displayed in Figure 22b-d. They represent the relationship of i^{-1} versus $\omega^{-0.5}$ and can be used to analyse the order of the ORR with respect to oxygen and to determine i_k values based on the intercepts. i_k values provide a good indication of the ORR kinetics on the surface of a catalyst, while eliminating the effects of reactant diffusion inside the electrochemical cell. All three plots display linear, parallel behaviour in the mixed control polarization region, indicating first order ORR kinetics with respect to oxygen [129]. i_k values for each sample were calculated at 0.7 V vs RHE and were found to be -16.53 $mAcm^{-2}$ for Pt/ED-CNTs, -13.59 $mAcm^{-2}$ for Pt/Py-CNTs and -6.58 $mAcm^{-2}$ for Pt/CNTs. This reiterates the importance of nitrogen content on the observed activity of the catalyst composite materials, where Pt/ED-CNTs were found to have the highest activity towards ORR after eliminating the effect of reactant diffusion.

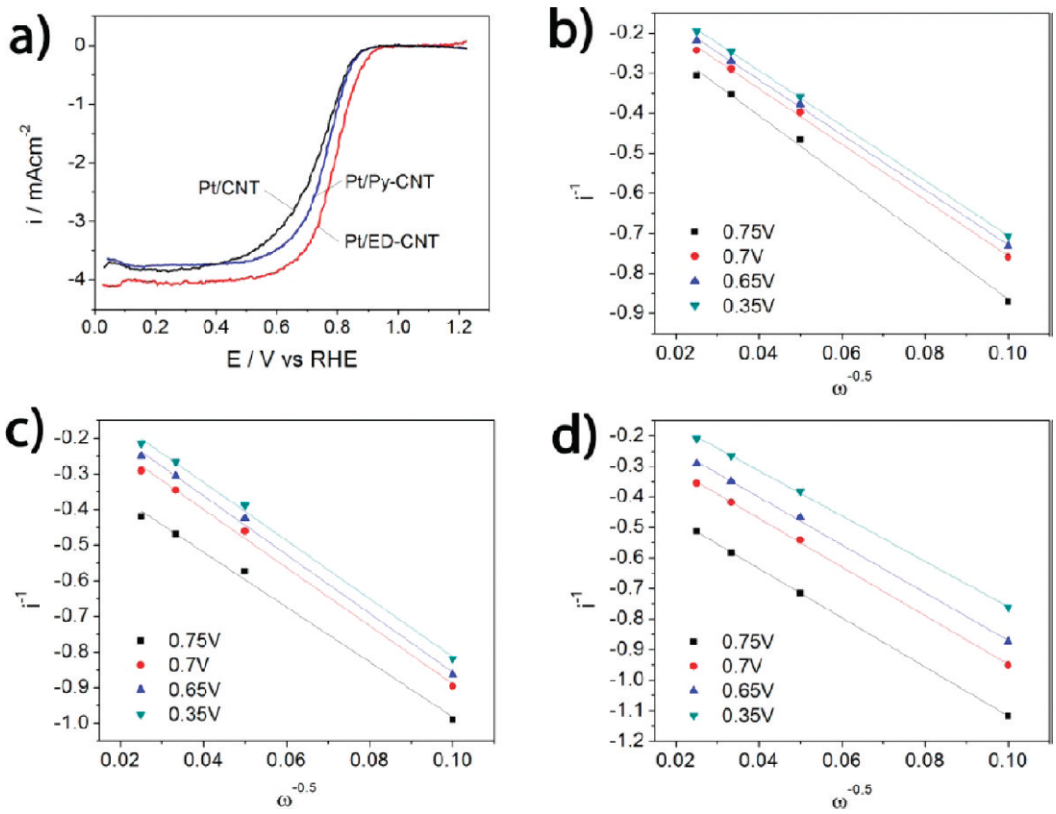

Figure 22: (a) ORR polarization curves for all samples in oxygen saturated 0.1 M HClO4 at a scan rate of 10 mV s-1 in the cathodic direction with a rotation speed of 900 rpm after stabilization. Corresponding Koutecky-Levich plots for (b) Pt/ED-CNTs, (c) Pt/Py-CNTs, and (d) Pt/CNTs. Reprinted with permission from [7], Copyright 2010 American Chemical Society.

Pt/ED-CNTs were selected as the optimal platinum loaded N-CNT support material due to the high observed nitrogen content leading to significant half cell activity and were subjected to testing in a MEA. Polarization and power density curves for Pt/ED-CNTs and Pt/CNTs in a single cell H_2/O_2 MEA system fabricated by a decal method are displayed in Figure 23. The peak power density for Pt/ED-CNTs was 1.04 Wcm^{-2}, an increase of approximately 16.9 % over that of Pt/CNTs (0.89 Wcm^{-2}). At a cell voltage of 0.6 V, Pt/ED-CNTs displayed a current density of 1.55 Acm^{-2}, approximately 24 % higher than Pt/CNTs (1.25 Acm^{-2}). Concurrent with half cell electrochemical testing and cyclic voltammetry analysis, Pt/ED-CNTs display improved ORR catalytic activity compared with Pt/CNTs under fuel cell conditions.

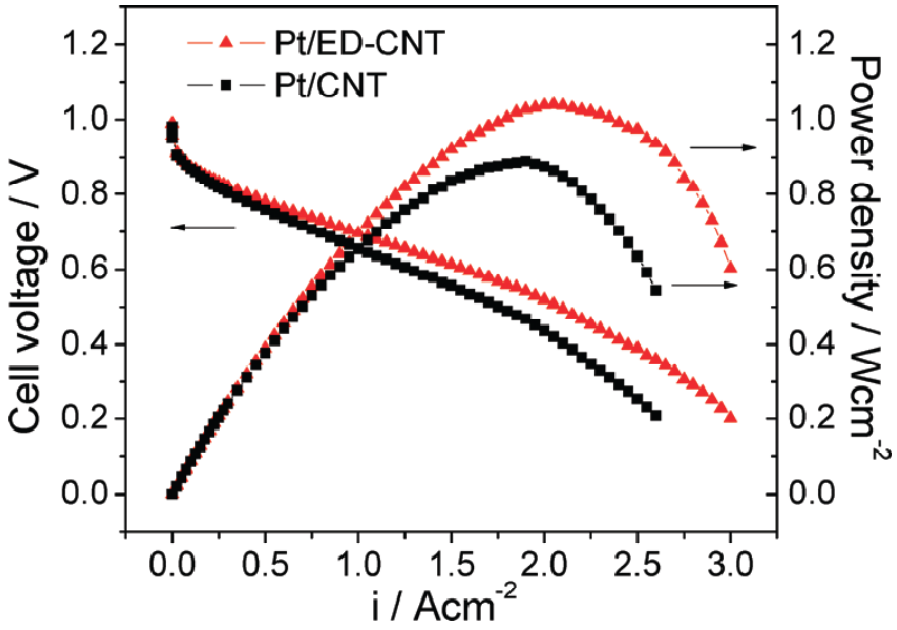

Figure 23: MEA polarization and power curves for 0.2 mgPt cm-2 Pt/ED-CNT and Pt/CNT cathodic catalyst loading, with 0.2 mgPt cm-2 commercial Pt/C as anodic catalyst in a single cell H2/O2 system with a Nafion 112 PEM. Reproduced with permission from [7]. Copyright 2010 American Chemical Society.

3.4 Conclusions

In summary, the importance of nitrogen precursor solution utilized for the growth of N-CNTs was elucidated for their application as platinum nanoparticle electrocatalyst support materials for the ORR. Utilizing nitrogen rich ethylenediamine as a precursor solution produced ED-CNTs with a relatively high nitrogen content (4.74 N at. %) as compared with pyridine based Py-CNTs (2.35 N at. %). This significant increase in nitrogen content led to facile deposition of well dispersed, uniformly sized platinum nanoparticles. A substantial increase in the ORR activity of these platinum composites was observed for Pt/ED-CNTs and Pt/Py-CNTs when compared with the nitrogen free Pt/CNTs. The observed half-wave potential was found to improve with increased nitrogen content in the support material. Pt/ED-CNTs were found to display a 16.9 % increase in peak power density and a 24% increase in current density at a cell potential of 0.6 V when tested in a MEA and compared with Pt/CNTs. N-CNTs are established as a potential alternative to replace traditional platinum support materials due to their distinct structural and electronic properties resulting in enhanced ORR performance. The present work highlights the importance of utilizing a nitrogen rich N-CNT precursor solution to a high degree of nitrogen incorporation in the electrocatalyst support materials.

4.0 Effect of precursor material on ORR activity of N-CNTs in alkaline conditions

Higgins, D., Chen, Z., Chen, Z., "Nitrogen doped carbon nanotubes synthesized from aliphatic diamines for the oxygen reduction reaction". Electrochimica Acta, 2011, pp. 1570-1575.

4.1 Introduction and purpose

With respect to the development of non-precious ORR electrocatalyst materials, investigations have taken several different approaches. Various materials investigated include transition metal chalcogenides [130, 131], carbon supported metal particles [132, 133], enzymatic compounds [134], and metal free nitrogen doped carbon materials [99, 135]. Specifically, several authors have reported enhanced ORR activity observed on nitrogen doped carbon materials formed at high temperatures, where there are mixed reviews attributing the increase in performance to either: i) active sites composed of metal-nitrogen ligand structures [133, 136-141], or ii) to the presence of nitrogen functional groups providing enhanced electron donor behavior and edge plane defects, facilitating the reduction of oxygen [48, 99, 106, 115, 135, 142, 143]. In the latter case, several reports have indicated that the primary function of the transition metal is not to function as an active site for the ORR, but to facilitate the stable incorporation of active nitrogen functionalities into graphitic carbons during high temperature synthesis [106, 115, 135, 143]. Specifically, metal-free N-CNTs have recently been found to display superior catalytic activity towards ORR in alkaline conditions when compared with traditional Pt/C, with their activity being attributed to the presence of pyridinic and pyrollic nitrogen species [99]. Since the increased performance is observed in the absence of metal containing compounds, nitrogen content is deemed an important factor when utilizing N-CNT catalysts. Chen et. al. [144] investigated the ORR activity of N-CNTs synthesized with varying pyridine-ethanol ratios. The resulting activity was investigated in alkaline conditions in order to determine the effects of increasing the presence of nitrogen during synthesis. It was found that a higher nitrogen content present during synthesis directly resulted in increased nitrogen incorporation into N-CNTs, along with improved ORR performance. The effect of nitrogen content was also previously investigated synthesizing N-CNTs from either ethylenediamine, or pyridine precursor solutions [145], where it was found that higher nitrogen contents in ethylenediamine based N-CNTs led to significant performance increase with respect to ORR compared with pyridine based N-CNTs.

It is well established that the properties of N-CNT materials are directly related to the type of precursor materials used during synthesis [144-150], with the amount of nitrogen present during growth

influencing the observed overall N-CNT nitrogen content. A significant amount of uncertainty however, still surrounds the exact effect that the nitrogen-carbon precursor solution has on the nitrogen content and ORR catalytic activity of synthesized N-CNTs. Thus, in the present work, three aliphatic diamine precursor solutions with similar structures were utilized for synthesis. These materials were selected because the only significant variation between their molecular structures is varying nitrogen-carbon ratios, resulting from differing carbon chain lengths. This provides a strategic basis in order to carry out a systematic investigation on the effect of the nitrogen-carbon ratio present during growth, on the resulting nitrogen content and catalytic activity of the as-synthesized N-CNTs. Ethylenediamine (ED), 1,3-diaminopropane (DAP) and 1,4-diaminobutane (DAB) were selected as the N-CNT growth precursor solutions. Detailed investigation into the nanostructure and atomic composition of synthesized N-CNT materials was completed, along with their ORR activity being investigated in alkaline solution.

4.2 Experimental

4.2.1 Synthesis methods

N-CNTs were produced by the method outlined in Section 3.2.1. Precursor solutions of ED, DAP and DAB with 2.5 wt. % ferrocene dissolved in as a growth catalysts were injected into the CVD quartz tube reactor.

4.2.2 Specific experimental details

For half-cell ORR electrochemical measurements performance in oxygen saturated 0.1 M KOH electrolyte, the disc potential was swept from 0.2 to -1.0 V vs Ag/AgCl at a scan rate of 10 mVs^{-1}. The ring electrode potential was kept constant at 0.5 V vs Ag/AgCl to ensure the further reduction of H_2O_2 species reaching the surface.

4.3 Results and discussion

In order to elucidate the effects of the precursor solution utilized for N-CNT synthesis, three nitrogen/carbon aliphatic diamine precursor solutions were investigated. As previously mentioned, ED, DAP and DAB were selected as they possess very similar structure, however provide varying nitrogen–

carbon atomic ratios as summarized in Figure 24. The elemental compositions of the synthesized products (ED-CNTs, DAP-CNTs and DAB-CNTs) were evaluated by XPS analysis with the results displayed in Table 2. This confirms the successful incorporation of nitrogen into all three N-CNT samples, where the amount of nitrogen doping was found to increase with the increasing nitrogen-carbon ratio present in the precursor solution. In this regard, ED-CNTs possessed the highest nitrogen incorporation (4.74 at. %) due to its nitrogen rich structure and thus a higher presence of nitrogen introduced to the growth environment. After N-CNT growth, the CVD furnace was exposed to ambient conditions at 400 ^{o}C in order to burn off any unstable amorphous carbon species, resulting in the observed oxygen content. The minimal iron content can be attributed to residual iron particles from the ferrocene growth catalyst remaining after acid leaching.

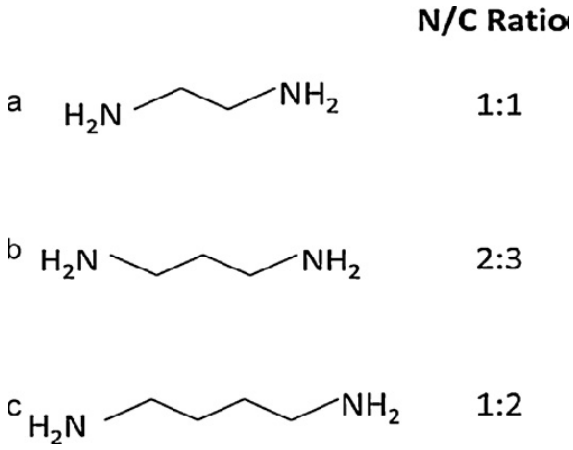

Figure 24: Molecular structure and corresponding nitrogen–carbon ratios for: (a) ED, (b) DAP and (c) DAB. Reprinted from [8], Copyright 2011, with permission from Elsevier.

Table 2: Overall atomic compositions determined by XPS analysis. Reprinted from [8], Copyright 2011, with permission from Elsevier.

Element	ED-CNT (at.%)	DAP-CNT (at.%)	DAB-CNT (at.%)
Carbon	91.50	92.77	94.66
Nitrogen	4.74	2.48	1.20
Oxygen	3.38	4.48	4.08
Iron	0.38	0.27	0.06

The C1s peaks for each sample are displayed in Figure 25a. The C1s peaks for each sample display a slight shift to a higher binding energy than values expected for for pure graphitic materials (284.3 eV) [151]. This is a commonly observed occurance for nitrogen doped graphitic materials [68, 80,

106, 142], where ED-CNTs displayed the most significant shift (284.8 eV) compared with DAP-CNTs (284.7 eV) and DAB-CNTs (284.6 eV), attributed to the varying nitrogen incorporation.

The N1s signal for each sample was broken down into three seperate peaks as displayed in Figure 25b in order to determine the nitrogen species present and their relative amounts. The first peak located at approximately 398.6 can be attributed primarly to pyridinic nitrogen [142, 151], present on the edge planes of the nanotube walls [106, 142, 151]. The second peak can be further deconvoluted into two contributing species: i) pyrollic nitrogen with a characteristic binding energy of 400.0-400.6 eV and ii) quaternatry nitrogen with a characteristic binding energy of 401.1-401.7 eV [151]. Thus, it was concluded that the peaks observed at approximately 401.0 eV indicated the presence of both these nitgrogen species with a shift in the peak location to a lower binding energy indicating more pyrollic nitrogen whereas on the contrary, a peak shift to a higher binding energy indicates more quaternary nitrogen. The final peak observed can be attributed primarily to oxidized nitrogen species with a characteristic binding energy of 402.0-405.0 eV [151]. The amount of contributing nitrogen species were calculated based on the areas of their respective peaks, with the results summarized in Table 3.

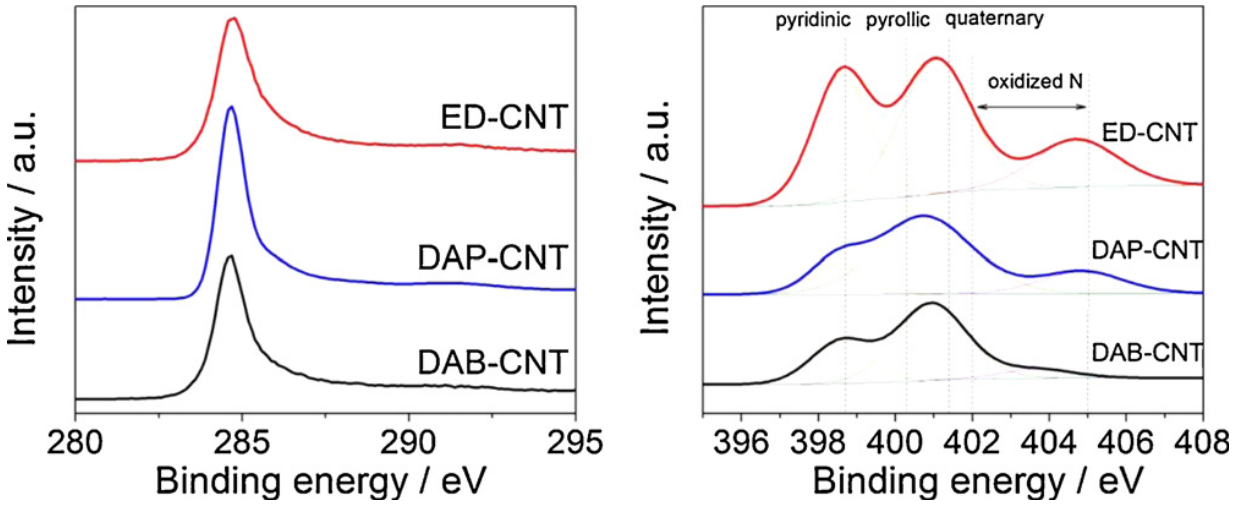

Figure 25: XPS of: (a) C 1s spectra and (b) N1s spectra for ED-CNTs, DAP-CNTs and DAB-CNTs. Reprinted from [8], Copyright 2011, with permission from Elsevier.

Table 3: Detailed breakdown of N1s spectra obtained from XPS analysis indicating peak positions and relative amounts of nitrogen species. Reprinted from [8], Copyright 2011, with permission from Elsevier.

Nitrogen species	ED-CNT		DAP-CNT		DAB-CNT	
	Peak position /eV	% N atoms scanned	Peak position /eV	% N atoms scanned	Peak position /eV	% N atoms scanned
Pyridinic	398.6	35.09	398.5	14.83	398.6	29.10
Pyrrolic/quaternary	401	45.91	400.8	68.21	400.9	63.37
Oxidized N	404.7	19.00	404.9	16.96	403.7	7.53

SEM images were obtained to investigate the morphology of synthesized samples as displayed in Figure 26. ED-CNTs, DAP-CNTs and DAB-CNTs all displayed similar structures, with a zigzag pattern observed. This zigzag pattern is a result of nitrogen incorporation which serves to reduce the linearity of synthesized CNTs [152].

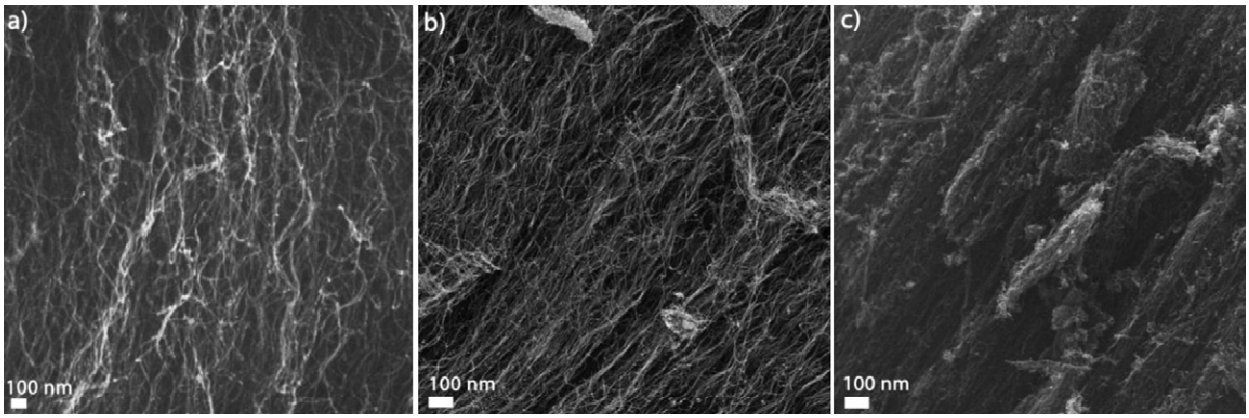

Figure 26: SEM images of: (a) ED-CNTs, (b) DAP-CNTs and (c) DAB-CNTs. Reprinted from [8], Copyright 2011, with permission from Elsevier.

TEM images displayed in Figure 27 were obtained in order to investigate the effect of nitrogen content on the morphology and nanostructure of the synthesized N-CNTs. All three samples displayed the characteristic bamboo-like morphology of N-CNTs commonly reported in literature [125, 126, 150, 153, 154], with some residual metallic iron particles observed on the surface. The formation of this bamboo-like nanostructure has been attributed to the incorporation of nitrogen dopant atoms, which lead to the energetically favored buckling of the graphitic nanotube walls [126, 155]. In direct agreement with this theory, ED-CNTs (Figure 27a) display the highest amount of structural deformations as a result of the significant nitrogen content. Small, round bamboo compartments are observed for ED-CNTs, whereas for DAP-CNTs (Figure 27b) and DAB-CNTs (Figure 27c), longer more rectangular compartments are observed. Furthermore, an increase in wall thickness was observed for N-CNTs with lower nitrogen contents consistent with a previous report [156]. An average wall thickness of 3.4, 7.2 and 10.1 nm was observed for ED-CNTs, DAP-CNTs and DAB-CNTs, respectively.

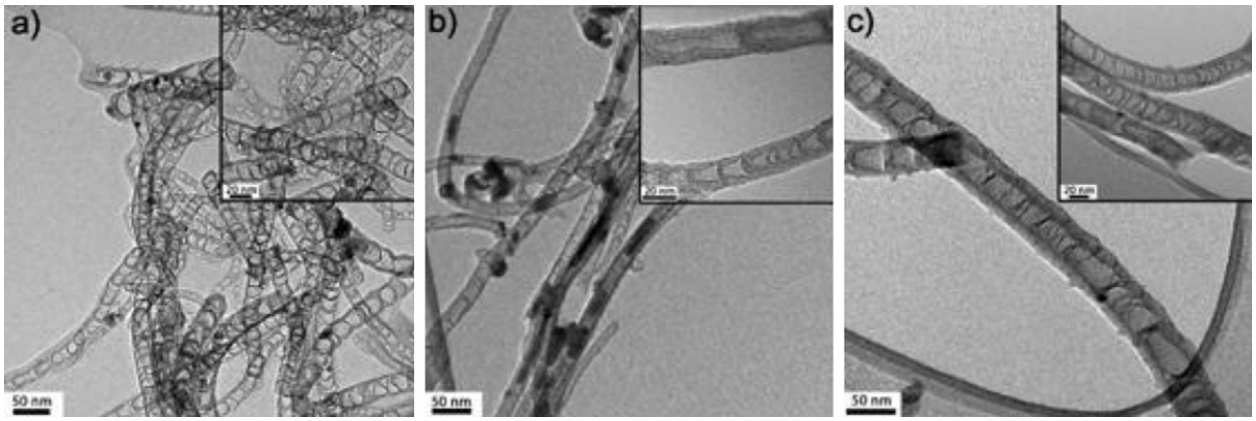

Figure 27: TEM images obtained displaying bamboo-like morphologies for: (a) ED-CNTs, (b) DAP-CNTs and (c) DAB-CNTs. Reprinted from [8], Copyright 2011, with permission from Elsevier.

The Raman spectrum of all three samples are displayed in Figure 28, displaying the commonly observed D and G bands that are characteristic of CNT materials [48, 157, 158]. The I_D/I_G ratios for ED-CNTs, DAP-CNTs and DAB-CNTs were determined to be 2.07, 1.41 and 1.35, respectively. These results are consistent with TEM analysis, where ED-CNTs displayed a significantly higher amount of structural defects compared with the other samples. From our materials, it is apparent that the I_D/I_G ratio increases as a direct result of nitrogen incorporation, which can be linked back to the choice of precursor solution utilized for N-CNT synthesis.

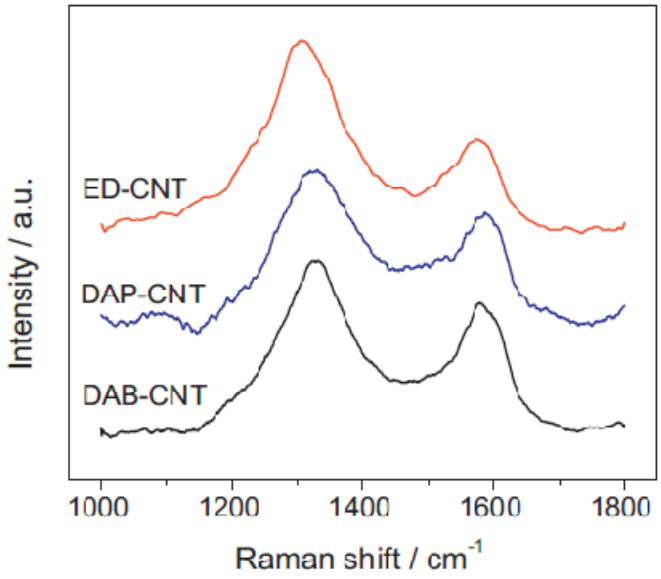

Figure 28: Raman spectroscopy of ED-CNTs, DAP-CNTs and DAB-CNTs displaying characteristic D and G band peaks. Reprinted from [8], Copyright 2011, with permission from Elsevier.

Polarization curves for ED-CNTs, DAP-CNTs and DAB-CNTs, along with their respective H_2O selectivities are displayed in Figure 29. H_2O selectivity values were determined in order to quantitatively gauge the preferential reduction of oxygen towards the more efficient 4 electron pathway, compared to the less efficient 2 electron pathway resulting in the formation of H_2O_2. A distinct trend is noticed for each of the samples, where increased ORR half cell activity (Figure 29a), along with higher H_2O selectivity (Figure 29b) was obtained for N-CNT samples with higher nitrogen contents. At a potential of -0.4 V vs Ag/AgCl and a electrode rotation speed of 900 rpm, ED-CNTs displayed a current density of 3.86 $mAcm^{-2}$, significantly higher than 2.30 $mAcm^{-2}$ and 1.75 $mAcm^{-2}$ obtained for DAP-CNTs and DAB-CNTs, respectively. Under the same operating conditions, ED-CNTs also displayed an H_2O selectivity of 87.0 %, a drastic improvment over 77.0 % displayed by DAP-CNTs and 61.6 % for DAB-CNTs.

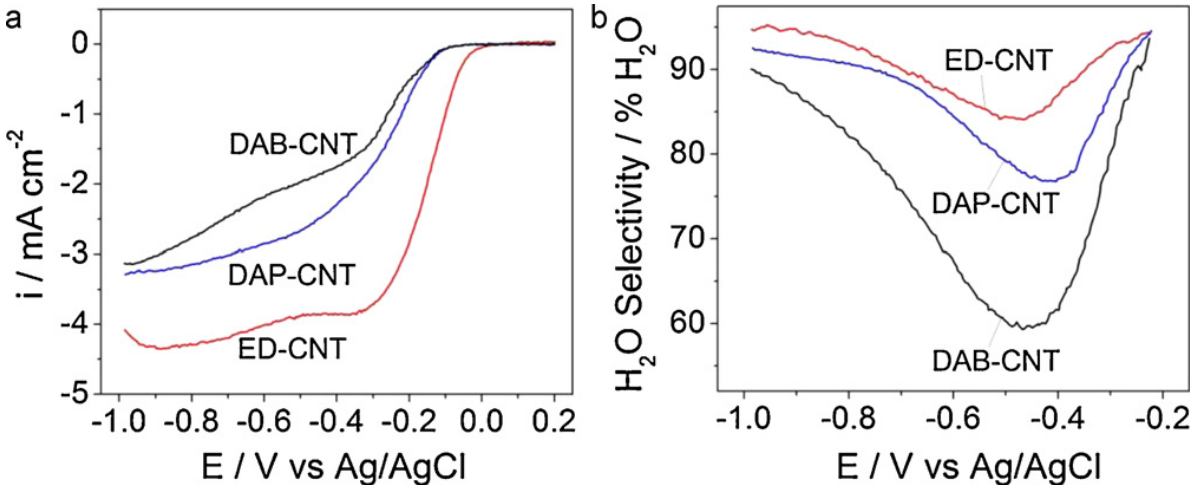

Figure 29: (a) ORR polarization curves and (b) H2O selectivities obtained in 0.1M KOH in the cathodic sweep direction at a scan rate of 10mVs−1 and electrode rotation rate of 900 rpm. Reprinted from [8], Copyright 2011, with permission from Elsevier.

The higher performance observed for ED-CNTs can be linked back to previous reports highlighting the importance of nitrogen groups on the ORR activity of nitrogen doped carbon materials. Pyridinic groups are commonly discussed and consist of a nitrogen atom hetereogenously bonded to two neighbouring carbon atoms, residing on the nanotube edge planes [106, 159, 160]. The increased density of these edge plane sites has been consistently shown to result in enhanced ORR activity [48, 106, 115, 135, 159, 160]. It should be noted however, that there is a degree of ambiguity surrounding this conclusion. There is uncertainty as to whether or not the pyridinic nitrogen atom itself provides the actual active site for promiting the ORR, or whether the reaction takes place on the edge plane defect sites. Regardless, the presence of pyridinic nitrogen provides indication of the amount of edge plane

exposure present on the nanotube walls and thus has been attributed to increased ORR activity. The nature of this peformance enhancement has been related to the increased electron density and electron donor properties present on the surface edge planes, a result of the extra valence electrons provided by the dopant pyridinic groups [48, 81, 160, 161]. As a result, these sites serve to faciliate the adsorption of oxygen, along with providing a synergistic effect by readily adsorbing and further reducing reaction intermediates, specifically hydrogen peroxide [48, 81, 160]. Through XPS analysis, ED-CNTs were found to possess a significant nitrogen content (4.74 at. %) along with a high degree of pyridinic species (1.66 total at. %). This provides a logical explanation for the increased ORR activity and H_2O selectivities observed. Diminished performance relative to ED-CNTs was observed for DAP-CNTs and DAB-CNTs. This aligns well with this hypothesis, with inferior performance attributed to lower pyridinic nitrogen contents (0.36 and 0.35 total at. % for DAP-CNTs and DAB-CNTs, respectively). It should be noted however, that the performance of DAB-CNTs was found to be significantly lower than DAP-CNTs, despite similar overall pyridinic nitrogen concentrations. This is attributed to the inferior overall nitrogen content (1.20 at. % versus 2.48 at. %), indicating the possibility of other active N-C functionalities [135], or changes to the bulk properties of N-CNTs induced by nitrogen incorporation, leading to increased electronic conductivities [68, 102, 112], electron donor behaviour [112, 114, 153, 162] and enhanced reactant and intermediate adsorption [48, 161, 163]. This illustrates the importance of the precursor solution utilized for N-CNT growth on the ORR activity of the samples observed in alkaline conditions. Higher nitrogen content containing N-CNTs, with some emphasis on pyridinic species will lead to significant improvements in the ORR activity. Furthermore, it has been found that at higher nitrogen contents (e.g. > 2 at. %) the formation of pyridinic nitrogen is preferred [156], reiterating the importance of using a nitrogen rich precursor solution such as ethylenediamine. It should be noted that the effect of the nominal iron presence in the N-CNT catalyst materials cannot be neglected. There is some uncertainty regarding the exact role of the iron species present, which could potentially be linked to ORR catalytically active pyridinic FeN_2/C_x species, low activity pyrollic FeN_4/C_x species [164], or inert iron and/or iron oxide particles. Regardless, the impact of nitrogen content with a focus on pyridinic (either Fe-coordinated or natural form) groups is apparent. To provide comparison, the polarization curves of ED-CNTs, DAP-CNTs and DAB-CNTs are provided alongside the performance of commercial Pt/C in Section 5.3. The ORR activity and H_2O selectivity of ED-CNTs was superior to even that of commercial Pt/C, a very promising result considering the economic and environmental benefits arising from the use of ED-CNTs as electrocatalyst materials.

KL plots were generated for ED-CNTs, DAP-CNTs and DAB-CNTs and are displayed in Figure 30. These plots display linear, relatively parallel behavior, an indication of first order kinetics with respect to oxygen [165]. Slight changes in the observed slopes are apparent, primarily in the case of DAB-CNTs. This could be a result of the deviation in number of electrons transferred as indicated by changing H_2O selectivity values (Figure 6b), or slight deviation from the proposed first order kinetics. Regardless, the intercept of KL plots can be used to calculate i_k values, which provide a good indication of the ORR kinetics on the catalyst surface, while eliminating the interfering effects of reactant diffusion. At an electrode voltage of -0.2 V vs Ag/AgCl, ED-CNTs displayed an i_k of -5.07 $mAcm^{-2}$, superior to -1.02 $mAcm^{-2}$ and -0.65 $mAcm^{-2}$ determined for DAP-CNTs and DAB-CNTs, respectively. This further confirms the enhanced performance of ED-CNTs after eliminating the effect of reactant diffusion due to the high nitrogen content and edge plane exposure.

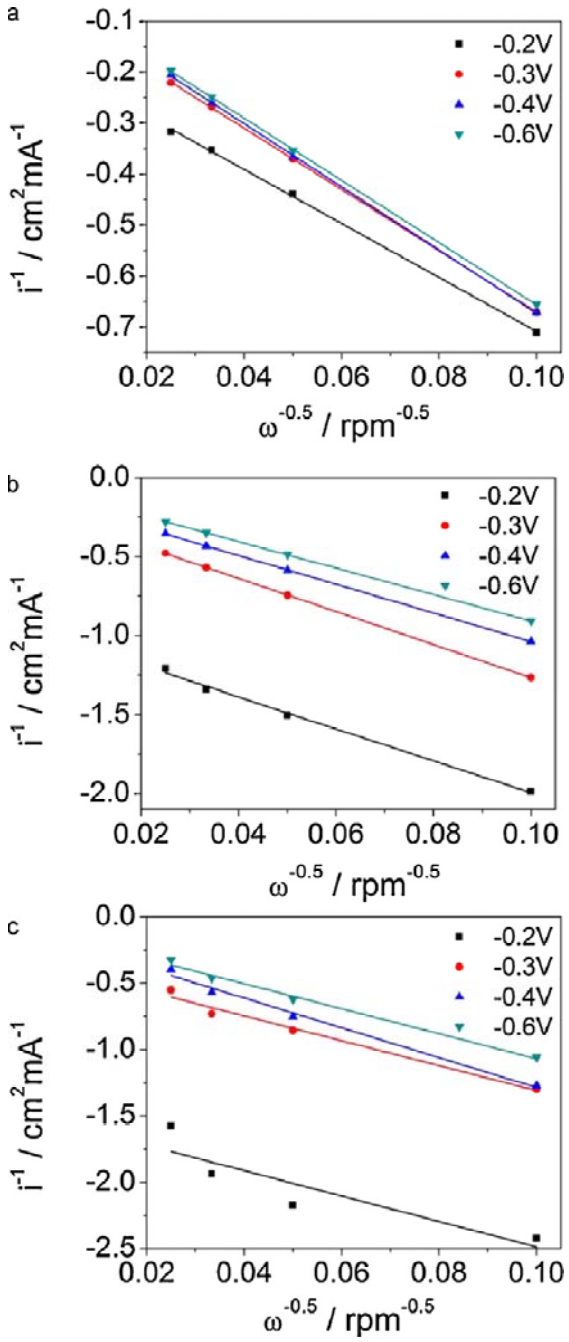

Figure 30: Koutecky–Levich plots for: (a) ED-CNTs, (b) DAP-CNTs and (c) DAB-CNTs in 0.1M KOH. Reprinted from [8], Copyright 2011, with permission from Elsevier.

4.4 Conclusions

Nitrogen rich N-CNTs are promising materials as ORR electrocatalysts in low temperature fuel cell applications, with the effect of various precursor materials illustrated in the present work. In

summary, N-CNTs were synthesized from three different aliphatic diamine precursor solutions with varying carbon chain lengths. It was concluded that using precursor solutions with higher nitrogen to carbon atomic ratios will result in N-CNTs with higher overall nitrogen content and enhanced ORR activity. ED-CNTs were found to contain 4.74 at. % nitrogen and were found to have superior ORR activity compared with DAP-CNTs (2.48 at. % nitrogen), which displayed higher activity than DAB-CNTs (1.20 at. % nitrogen). The increase in performance was attributed to the enhanced electronic, structural and chemical properties resulting from higher overall nitrogen contents, with some emphasis placed on pyridinic species indicating a higher degree of edge plane exposure.

5.0 Thin, free standing N-CNT film as cathode catalyst in alkaline anion exchange membrane fuel cells

Higgins, D., Chen, Z., "Nitrogen Doped Carbon Nanotube Thin Films as Efficient Oxygen Reduction Catalyst for Alkaline Anion Exchange Membrane Fuel Cell". ECS Transactions, 2010, pp. 63-68.

5.1 Introduction and purpose

As previously mentioned, AEMFCs offer a significant advantage over traditional AFCs in that the electrolyte membrane is not prone to poisoning by CO_2 that may be present in gas fuel streams [166, 167], leading to significantly higher durability. The ORR taking place on the cathode of AEMFC requires a highly active electrocatalyst most often consisting of expensive Pt or other noble metal (Au, Ag, etc.) based materials [166-169]. Developing an inexpensive, non-noble alternative to these materials without sacrificing performance or durability is essential for realizing AEMFC commercialization. Recently and herein, comparable ORR catalytic activity of N-CNTs in alkaline solution compared with traditional platinum loaded carbon black (Pt/C) has been reported [99, 170], however the performance of N-CNTs as a cathodic catalyst has not been investigated in an actual AAEMFC setup.

Drawing on the previous investigation (Section 4.0 of the present report), ED-CNTs with promising half cell electrochemical activity towards the ORR were fabricated into a thin, free standing film by a filtration method for use as a cathode for AEMFCs. The novelty of this work lies in the fabrication and testing of these thin films as an ionomer free cathode catalyst layer in an AEMFC. Utilizing N-CNT thin films as an cathode catalyst offers several advantages over commercial Pt/C towards AEMFC technologies: (i) N-CNT thin films are inexpensive and readily produced, while displaying high catalytic activity towards ORR, (ii) their porous nature allows for good oxygen diffusion, while their thin structure allows adequate hydroxide access, eliminating the requirement for an ionomer in the catalyst layer, (iii) N-CNT thin films are free standing and do not require any bonding agents that might interfere with catalytic performance, and (iv) N-CNTs have significant stability under operating conditions [99].

5.2 Experimental

5.2.1 Synthesis methods

Free standing ED-CNT films were fabricated by a filtration method. ED-CNTs were suspended in ethanol solvent and ultrasonicated to ensure adequate dispersion. The mixture was then filtered through an aluminum oxide membrane (Whatman, Anodisc 47, 0.02 mm) and annealed overnight at 100 °C. The filter membrane was immersed in 1 M sodium hydroxide solution for several minutes, after which the free standing thin ED-CNT film could be collected and was ready for use after drying.

5.2.3 Specific experimental details

MEAs with an active area of 5 cm^2 were prepared by pressing the anode, 70 µm thick FAA commercial AEM (Fuma-Tech GmbH) and cathode together. Catalyst ink was sprayed onto carbon paper in order to prepare the anode (0.5 $mg_{Pt}cm^{-2}$ Pt/C, E-TEK) electrode. The cathode electrode consisted of either the N-CNT thin film (0.2 $mgcm^{-2}$), or carbon paper sprayed with Pt/C (0.2 $mg_{Pt}cm^{-2}$) for comparison. The MEA cell temperature was kept constant at 80 °C and flow rates of 0.3 $Lmin^{-1}$ at a back pressure of 3 atm were utilized for both H_2 and O_2.

5.3 Results and discussion

Due to their high inherent ORR activity and significant nitrogen content, ED-CNTs were selected as ideal candidates for fabrication into thin films using a filtration method, followed by heat treatment. Their performance in comparison with Pt/C is displayed in Figure 31, along with DAB-CNTs and DAP-CNTs discussed in Section 4.0. An image of the thin film is displayed in Figure 32a, clearly demonstrating its free standing nature without any bonding agents. SEM images of the ED-CNT thin film were taken to investigate the microstructure of the material. A top view image is shown in Figure 32b displaying an interlaced mat of ED-CNTs with a highly porous bulk structure. The ED-CNTs are well dispersed creating a homogenous thin film.

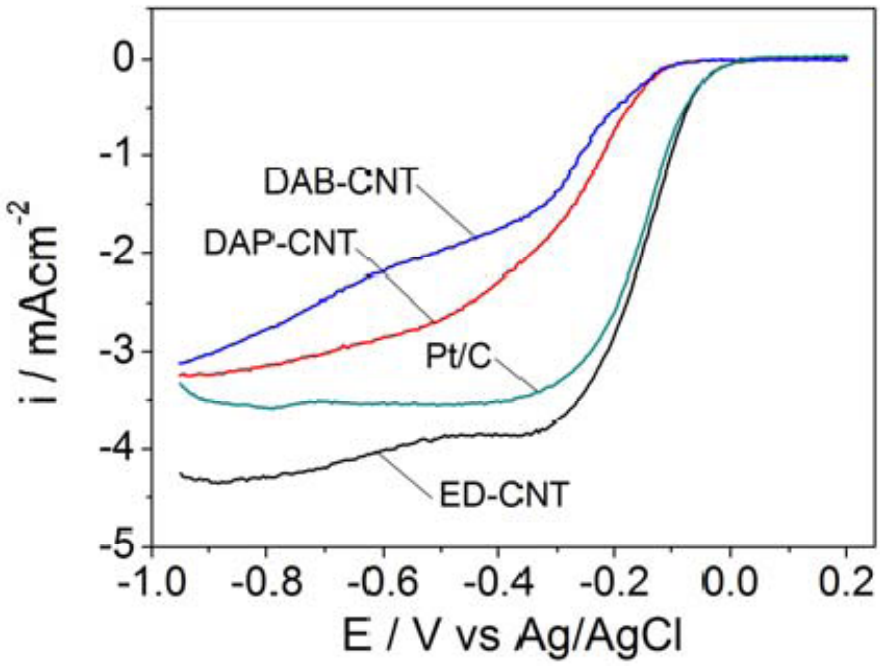

Figure 31: ORR polarization curves for N-CNT samples with Pt/C for comparison. Curves taken in 0.1M KOH at 900 rpm with a scan rate of 10 mVs-1 in the cathodic direction. Reproduced with permission from [9]. Copyright 2010, The Electrochemical Society.

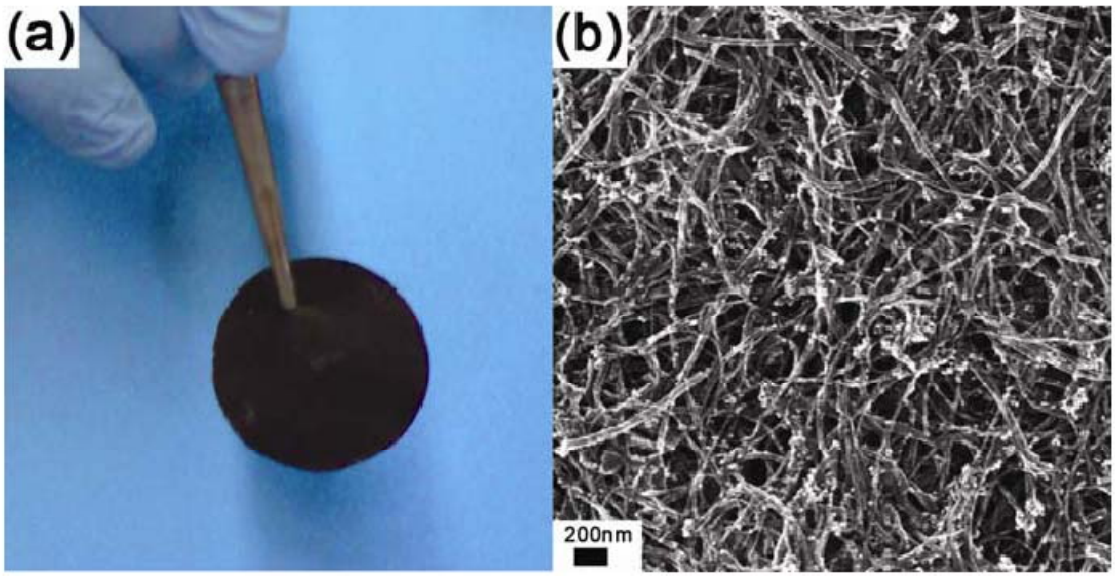

Figure 32: a) ED-CNT thin film displaying free standing nature and b) top view SEM image of ED-CNT thin film displaying homogeneous dispersion, resulting in highly porous, interlaced arrangement. Reproduced with permission from [9]. Copyright 2010, The Electrochemical Society.

The performance of an ED-CNT thin film was tested as an ORR cathode in an alkaline MEA setup and compared with the performance of commercial Pt/C catalyst under identical conditions. Results from MEA analysis are displayed in Figure 33. Maximum power densities of 25.5 $mWcm^{-2}$ and 19.1 $mWcm^{-2}$ were determined for the ED-CNT film and Pt/C, respectively, corresponding to a 34 % increase in performance for the ED-CNT film. At a cell potential of 0.6 V, current densities for the ED-CNT film and Pt/C were determined to be 37.5 $mAcm^{-2}$ and 27.5 $mAcm^{-2}$, respectively, a 36 % increase in performance for the ED-CNT film. These results indicate that ED-CNT thin films act as an efficient cathode in AEMFC MEAs, with performance superior to that of traditionally used Pt/C. The increase in performance observed for ED-CNTs can be attributed to their high inherent catalytic activity resulting from the significant nitrogen incorporation. Nitrogen doping has been shown to result in increased electronic conductivities [68, 102] and electron donor behavior [113, 171] of N-CNT materials. Moreover, high nitrogen concentrations have been reported to result in increased edge plane exposure resulting in active sites that serve to facilitate the adsorption and reduction of reactants and intermediates [48, 106]. Combined with ideal structural properties of the thin film, specifically a high surface aspect ratio and a highly porous structure, a logical explanation for the enhanced alkaline MEA performance is formulated. Thus, nitrogen rich N-CNT thin films are established as non-noble ORR electrocatalyst materials for use as a cathode layer in AEMFCs. They offer the distinct advantages of high inherent catalytic activity and a facile, relatively inexpensive synthesis procedure.

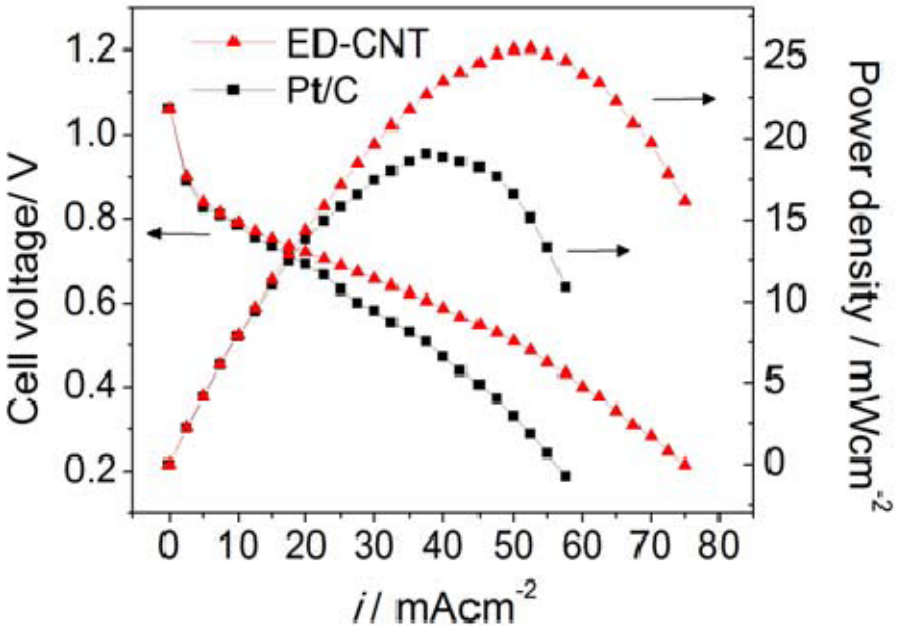

Figure 33: MEA performance displaying polarization curves (filled symbols) and power density curves (empty symbols) for 0.2 mgcm-2 ED-CNT thin film (red triangles) or 0.2 mgPtcm-2 commercial Pt/C (black squares) cathode catalysts, commercial FAA anion exchange membrane and 0.5 mgPtcm^{-2} commercial Pt/C anode catalyst. Reproduced with permission from [9], Copyright 2010 The Electrochemical Society.

5.4 Conclusions

In summary, thin, free standing ED-CNT films were synthesized and tested as an ORR cathode catalyst for use in AEMFCs. Electrochemical testing confirmed the catalytic activity of ED-CNTs prior to film fabrication, attributed to the presence of nitrogen atoms in the graphite lattice of the material. Using the ED-CNT thin film as a cathode catalyst in an AEMFC single MEA resulted in a significant increase in peak power density and current density under normal operating conditions (cell voltage of 0.6 V) compared with commercial Pt/C. This work confirms the potential of utilizing nitrogen right N-CNT thin films as cheap, effective ORR catalyst alternatives for use in AEMFCs.

6.0 N-CNTs synthesized from post treatment with cyanamide as metal free ORR catalysts in alkaline conditions

6.1 Introduction and purpose

While Pt based materials are undeniably the highest performing ORR electrocatalyst materials used for fuel cell applications, non-precious metal based materials are emerging as competitive replacements due to recent improvements with respect to their ORR activity and operational stability. As previously mentioned the use of readily available, non-noble metal based catalyst materials provides immense economical benefits and increases the feasibility of a sustainable fuel cell market. The most extensively studied non-precious catalysts to date generally consist of Fe and/or Co species, coordinated to nitrogen-carbon complexes [172]. The highest performing catalysts of this type are generally prepared by high temperature pyrolysis of a carbon support in the presence of transition metal species (usually inorganic salts [83, 173-175] or macrocycle complexes [176-178] and a nitrogen precursor. The latter generally consists of simple molecules, with the utilization of several nitrogen precursors including ethylenediamine [8, 101, 179, 180], 1,10 – phenanthroline [181-183], pyridine [100, 101, 184] and polyacrylonitrile [175, 185, 186] well documented, to name a few. More recently, several studies have focused on the utilization of cyanamide as a nitrogen source material as it has not been extensively investigated and is capable of forming favourable nitrogen-carbon configurations during pyrolysis treatments [187]. Studies by Chung et al. [188, 189] and Tian et al. [190] have indicated promising performance of high surface area carbons pyrolysed with an inorganic iron salt (FeAc or $FeSO_4$ salts) and cyanamide precursor. During high temperature treatment methods, the exact mechanism of active site formation and the role of the transition metal species are debatable. As previously discussed, the role of the transition metal species has been attributed to either: i) having a integral role in the active site moiety or ii) merely playing a role in the incorporation of nitrogen species into carbon supports forming catalytically active nitrogen-carbon species [191].

The reliance on the presence of non-precious metal species in ORR electrocatalysts still has several drawbacks [192]. Despite reduction in cost compared with noble metal species, these metals can by no means be considered inexpensive, with their supply depending exclusively on natural reserves. Moreover, the environmental impacts associated with mining, extraction and refining processes are immense, along with the recycling and disposal of catalyst residues and byproducts. Transition metal instabilities under the corrosive operating environments encountered at the cathode of fuel cells can

also lead to significant durability issues. Performance loss can result either from i) electrocatalyst poisoning by contaminants in the reactant feed streams, ii) demetallation of the active site structures [193], iii) leaching and subsequent contamination of system components (i.e. electrolyte membrane) by metal ions, or iv) decomposition of active site structures by H_2O_2 species formed due to poor catalyst selectivity [194]. The development of metal-free ORR electrocatalyst materials with high activity and operational stability would provide immense progress towards fuel cell commercialization, overcoming the issues and challenges associated with metal-based electrocatalysts.

On that note, metal-free CN_x ORR electrocatalysts are an emerging field of fuel cell research. This stems primarily from avoidance of the issues associated with metal-containing catalyst materials mentioned above and have been discussed in detail elsewhere [192]. Furthermore, their desirable properties including low cost, natural abundance, corrosion stability and unique, tailorable surface properties render them preferential candidates as ORR catalyst materials. Recent progress in this field has generally involved two approaches. The first involves synthesis of CN_x in the presence of metal catalyst materials, followed by purification by electrochemical or chemical methods [99, 195-198]. Through this approach however, the metal species can still play a significant role in the catalytically active site formation and the presence and influence of metal species on the ORR activity cannot be omitted entirely. Difficulties in the complete removal of strongly bonded metal species from CN_x nanostructures has also been reported [198]. The second approach involves synthesizing CN_x nanostructures in the absence of any metal species [199-204]. Research in the field of metal-free CN_x catalyst synthesis is still in its early stages of advancement, with some promising performances reported, indicating that transition metal species may not play a crucial role in active site formation. The ORR activity of metal-free CN_x catalysts however is still very low. Further work is essential in order to provide insight into the nature of metal-free catalytically active site formation mechanisms and atomic configurations. This will provide a valuable basis for the development of metal-free CN_x catalysts with improved ORR activity and operational stability.

In the present study, a simplistic post-doping method is employed utilizing cyanamide as the nitrogen source and functionalized CNTs as the carbon support. High temperature heat treatment is carried out on cyanamide coated CNTs in the absence of any metal additives and the resulting N-CNT materials are found to possess improved ORR activity and product selectivity in alkaline conditions. This provides indication that: i) metal species do not necessarily comprise the locale of ORR activity and ii) formation of catalytically active sites does not necessarily have to be facilitated by metal species.

Structural and spectroscopic characterization techniques are carried out in order to provide insight regarding the exact nature of the catalytically active sites. Due to the presence of oxygen, nitrogen and carbon species during high temperature pyrolysis it is very difficult to discern the specific catalytically active moiety. Regardless, improved ORR activity is attributed to increased surface coverage of the N-CNTs by a thin surface layer containing a variety of nitrogen, oxygen and carbon functional groups.

6.2 Experimental

6.2.1 Synthesis methods

Carboxylic acid (0.5 wt. %) functionalized CNTs were purchased for use in the present study. In order to: i) increase the surface reactivity, ii) increase the dispersion in ethanol solvents for processing purposes, and iii) ensure complete removal of surface metal impurities, the CNTs were further functionalized by refluxed in 6M HNO_3 for 6 hours. The resulting materials were filtered, washed thoroughly and dried before collection and processing. In order to coat the surface functionalized CNTs with cyanamide, 40 mg of CNTs were added to 40 mL of EtOH and sonicated to ensure adequate dispersion. Cyanamide was then added into the solution at CNT:cyanamide weight ratios 1:1, 1:2 and 1:4 (samples denoted CNT-cy1, CNT-cy2 and CNT-cy4, respectively). This solution was refluxed at 81 ^{o}C for 3 hours. The solvent was then allowed to evaporate completely and the collected solid was pyrolyzed under Ar for 1 hour at 900^{o}C.

6.2.3 Specific experimental details

For half-cell ORR electrochemical measurements performance in oxygen saturated 0.1 M KOH electrolyte, the disc potential was swept from 0.2 to -1.0 V vs Ag/AgCl at a scan rate of 10 mVs^{-1}. The ring electrode potential was kept constant at 0.5 V vs Ag/AgCl to ensure the further reduction of H_2O_2 species reaching the surface.

6.3 Results and discussion

After further purification and functionalization of the as received CNTs with HNO3 (sample denoted HNO3-CNT), the purity of the HNO_3-CNTs was investigated by TGA and TEM analysis. Figure 34a

provides the TGA profile of the HNO_3-CNTs. This profile displays behavior as expected with chemically functionalized HNO3-CNTs. Below temperatures ca. 600-700^{o}C the observed weight loss is attributed to oxidation of the surface functional groups and disordered carbon species present in the HNO3-CNT sample, where beyond this range the weight loss is due to oxidation of graphitic carbon species [205]. TGA analysis indicated that after heating to 900^{o}C, there was ca. 1 weight % residual attributed to metal remnants from the growth catalyst utilized for CNT synthesis. TEM images indicated that these residual particles were entrapped by several graphitic layers in the compartments of the HNO_3-CNTs as shown in Figure 34b. Several TEM images were obtained to ensure these metallic species were not present on, or near the surface or HNO_3-CNTs. The presence of entrapped metallic particles even after numerous purification treatments can be explained by their inaccessibility. Thus, the influence of these metal particles during cyanamide treatment of the CNT surfaces can be considered negligible, and any ORR activity observed on CNT-cy samples can be attributed to active site formation occurring in the absence of metal species.

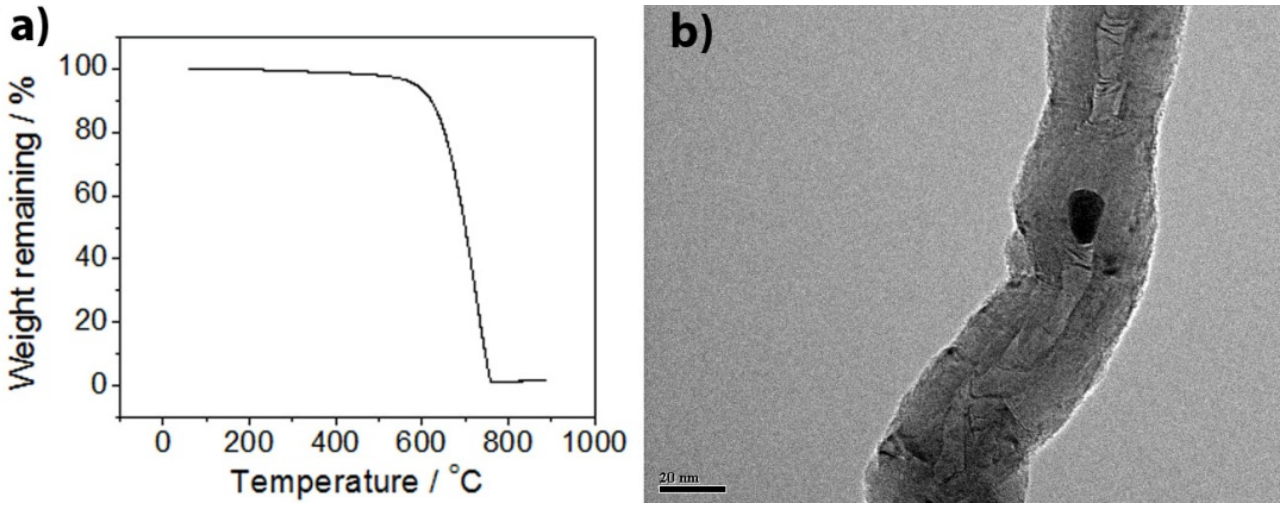

Figure 34: a) TGA profile of HNO3-CNTs and b) TEM image displaying metal catalyst remnant particle entrapped within the graphitic walls.

After treating HNO_3-CNTs with cyanamide using weight ratios of 1:1, 1:2 and 1:4 (HNO_3-CNT:cyanamide) followed by pyrolysis at 900^{o}C, the ORR activity of CNT-cy1, CNT-cy2 and CNT-cy4 were measured by electrochemical half cell testing, respectively. Figure 35a displays ORR polarization curves obtained for each of these samples, along with HNO_3-CNT for comparison. Clearly the metal-free post-treatment of HNO_3-CNTs with cyanamide results in significant ORR activity enhancements. A slight shift in the onset potential for ORR is observed with CNT-cy samples, along with significantly enhanced reaction kinetics at low overpotentials. Moreover, improved current densities and H_2O selectivities

(Figure 35b) determined from ring current data were observed with increased cyanamide weight ratios. The shift in onset potential and the transfer from a more predominant 2 electron reduction process for HNO_3-CNTs towards an overall 4 electron reduction process for CNT-cy4 gives positive indication of active site formation on the surface of CNTs resulting from cyanamide treatment.

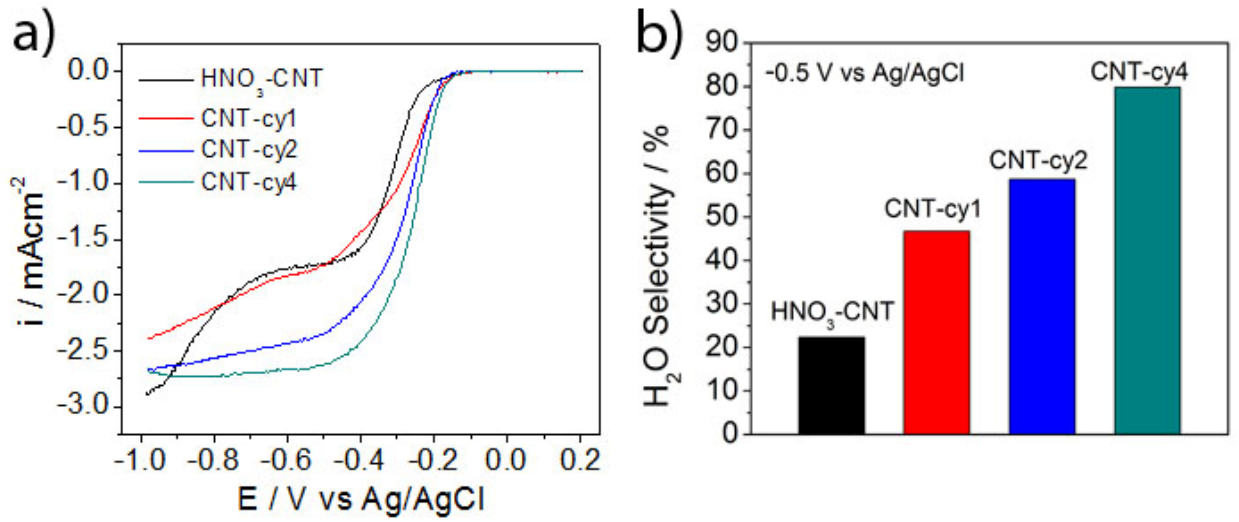

Figure 35: a) ORR polarization curves obtained in 0.1 M KOH at a scan rate of 10 mVs-1 and electrode rotation speed of 900rpm. b) H2O selectivity values for catalyst materials calculated at an electrode potential of -0.5 V vs Ag/AgCl.

The conglomeration of nitrogen, carbon and oxygen species on the surface of CNTs make it very difficult to decipher the specific structural transformations occurring during high temperature pyrolysis. The resulting effects and interactions of these species will be confounded, and in the case of CNT-cy, they have resulted in ORR active site formation. Based on observation of TEM images (Figure 36), the CNT-cy samples had a surface layer deposited on them without alteration of their bulk nanostructure, consistent with previous reports on post-treatment methods [206]. The presence of this thin film is a very interesting observation as it has previously been reported that cyanamide species are completely vapourized at temperatures exceeding 750^{o}C in an inert environment [190]. This provides confirmation that some sort of interaction is occurring between the cyanamide species and the surface of the functionalized HNO_3-CNTs, where upon heat treatment to 900^{o}C in Ar, a catalytically active residue remains. The most apparent difference between the three CNT-cy samples based on investigation of numerous TEM images was that increased cyanamide loadings led to deposition of a more uniform surface layer with a higher degree of CNT surface coverage. At low cyanamide loading, CNT-cy1 (Figure 37a and 37b) displayed agglomeration of this coating material in some regions (black arrows), whereas other regions of the CNT-cy1 surface were found to have no coating at all. CNT-cy2 (Figure 37c and 37d)

displayed a more uniform surface coverage, however there were still some portions of the CNT-cy2 surface with very thin, or even a lack of this surface layer. Upon doubling the cyanamide loading during synthesis, CNT-cy4 (Figure 37e and 37f) was found to have a relatively uniform coating layer, with a thickness between ca. 4-10 nm covering the majority of the CNT-cy4 surface.

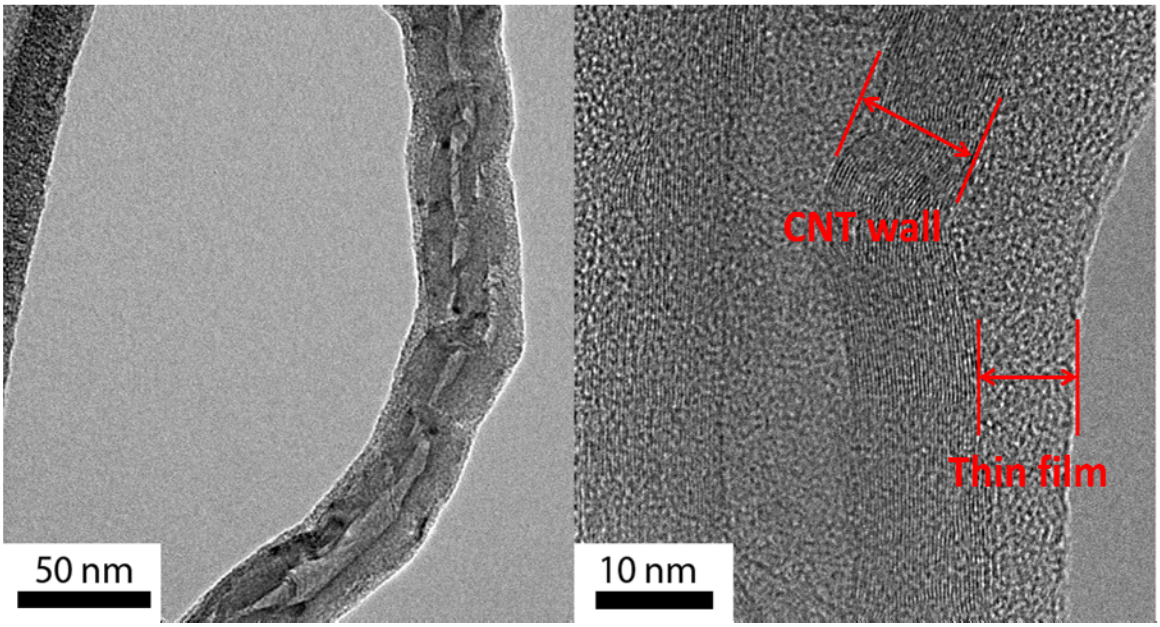

Figure 36: TEM images of CNT-cy4 displaying preserved CNT structure and deposition of a thin film on the surface.

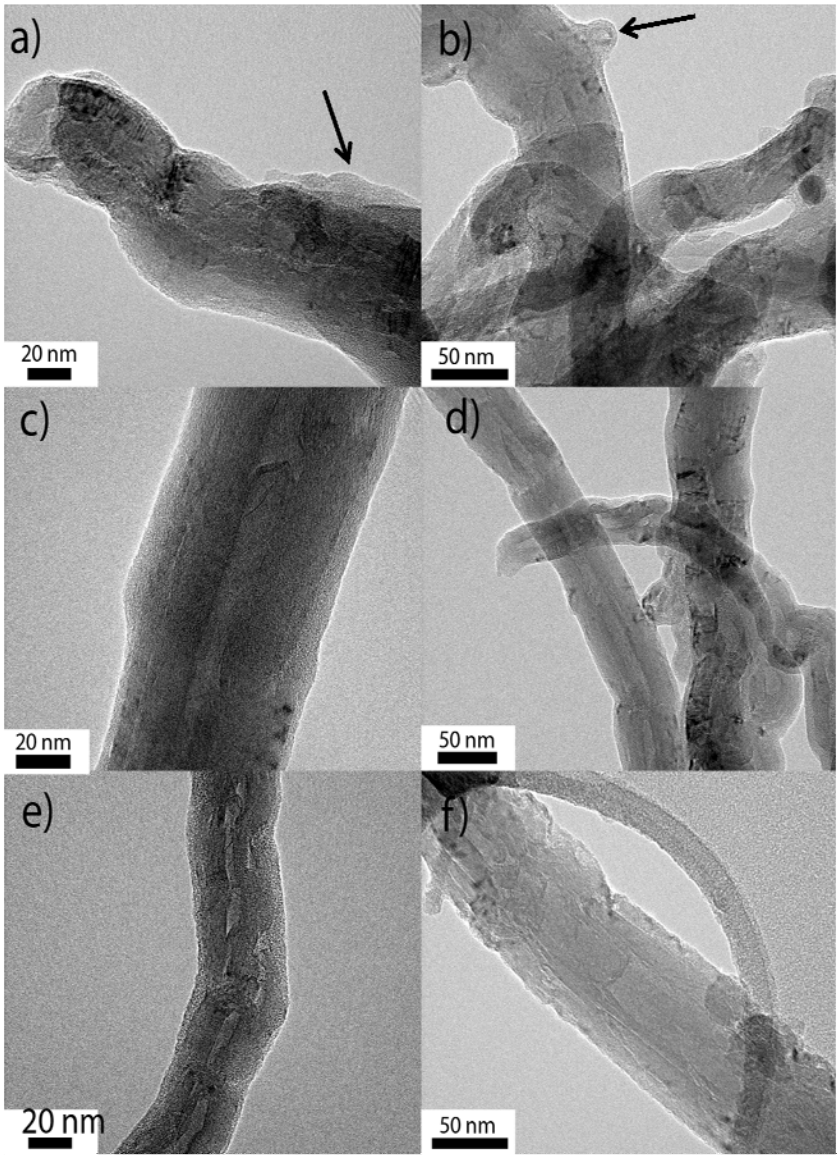

Figure 37: TEM images of a, b) CNT-cy1, c, d) CNT-cy2 and e, f) CNT-cy4.

To provide insight regarding the nature of the surface coating layer observed on CNT-cy catalysts, various characterization techniques were applied. Figure 38 displays the XRD patterns obtained for CNT-cy samples along with the signal obtained for the aluminum tray holder in order to distinguish background peaks. All three CNT-cy samples displayed peaks representative of graphitic CNT materials located at approximately 26, 43 and 53^{o}, which correspond to the (002), (100) and (004) structures, respectively. At increased cyanamide loadings, the observed peaks were found to shift to lower diffraction angles. This could be due to the distortion of crystallinity in the CNT samples, which could likely be due either to amorphous species present in the surface layer [83, 207] or through nitrogen incorporation into the graphitic lattice of the CNT structure [197, 203]. Presence of the (004)

peak confirms preservation of the bulk crystalline structure of the CNTs in this sample and is indicative of a large number of stacked graphitic walls [203].

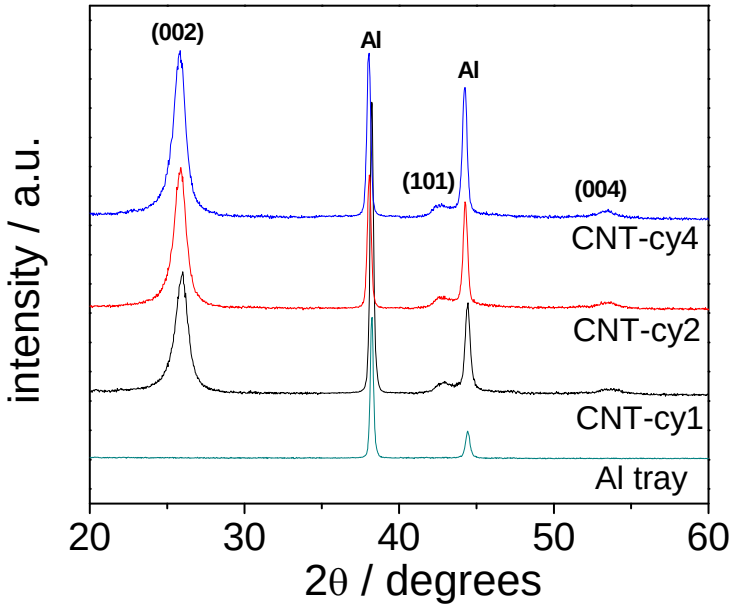

Figure 38: XRD pattern for CNT-cy samples and the Al sample holder.

Due to the simultaneous presence of carbon, nitrogen and oxygen species on the CNT surface during pyrolysis, combined with mixed reports delegating specific binding energies to various carbon-nitogen species [202, 208], discernment of catalytically active site structures must be carried out prudently in order to avoid any unsubstantiated claims. Interestingly, the overall surface concentration of nitrogen species in all three CNT-cy samples was found to be very similar. High resolution N1s signals obtained from XPS analysis are presented in Figure 39. The N1s spectrum was de-convoluted into 5 contributing peaks, each of which was attributed to differing nitrogen configurations displayed in Table 3 along with their respective peak locations. Commonly, catalytic activity towards the ORR can be associated with pyridinic and quaternary nitrogen species, located at binding energies of ca. 396.5 and 401.1 eV, respectively [8, 84, 203]. Through XPS analysis, both of these species are present in similar amounts for all three CNT-cy samples which could provide logical explanation of the ORR activity observed. The N5 peak observed at binding energies as high as 405.6 eV for CNT-cy samples can be attributed to NO_2 species [209]. This observation is particularly peculiar however, as NO_x species are relatively unstable and have been found to dissociate at temperatures exceeding ca. 500^{o}C in inert environments [209]. Moreover, CNT-cy1, CNT-cy2 and CNT-cy4 all displayed significant oxygen surface

contents of 5.11, 5.31 and 5.69 at. %, respectively, despite being exposed to a high temperature pyrolysis at 900^{o}C. This is contradictory to previous reports indicating the instability of surface oxygen species at elevated temperatures [209, 210], with minimal surface oxygen containing groups surviving temperatures up to 900^{o}C. The fact that a significant amount of surface NO_x and oxide groups remain after high temperature pyrolysis suggests that cyanamide may provide some sort of stabilizing interaction towards these functional groups. This is similar to a recent report by Chung et al. [188] attributing the stable incorporation of sulfur into heat treated iron based catalysts to cyanamide depressing the decomposition of sulfate groups. The oxygen content on the surface of the catalyst materials was found to increase with cyanamide loading where CNT-cy1, CNT-cy2 and CNT-cy3 had oxygen surface concentrations of 5.11, 5.31 and 5.69 at. %.

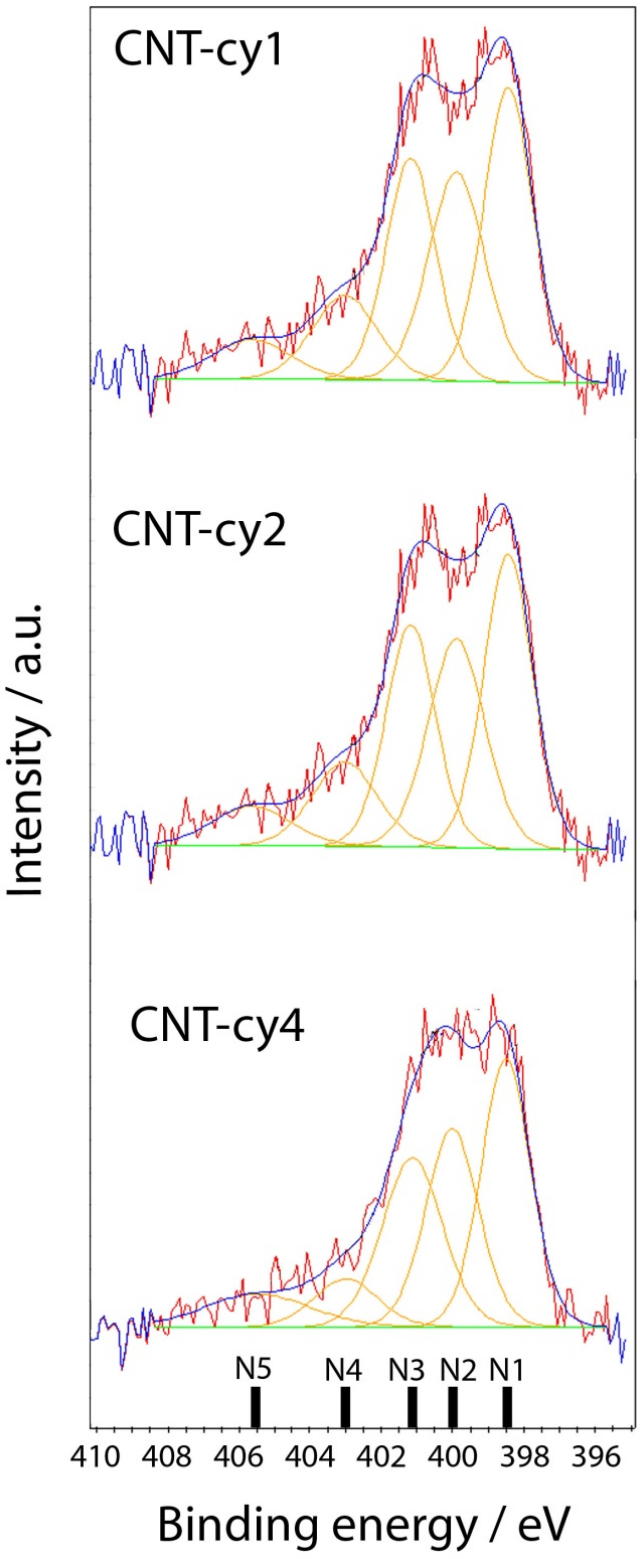

Figure 39: High resolution N1s spectra for CNT-cy samples deconvoluted into 5 contributing peaks.

Table 4: Deconvoluted N1s signal peak designations and locations.

		Peak location / eV		
Peak	Nitrogen species	CNT-cy1	CNT-cy2	CNT-cy4
N1	Pyridinic	398.45	398.47	398.51
N2	Pyrrolic	399.90	399.92	400.02
N3	Quaternary	401.18	401.13	401.14
N4	Oxidized pyridinic	403.03	402.96	403.00
N5	NO_2	405.56	405.59	405.49

With similar nitrogen contents and functional moieties determined by XPS for CNT-cy samples, the primary limiting factor towards ORR activity was dispersion of the surface layer remaining after pyrolysis. Improved ORR activity was found for samples with a more uniformly dispersed surface layer, favoured at higher cyanamide loadings. This surely results in a more homogeneous dispersion of catalytically active site structures (most likely pyridinic and quaternary nitrogen species). Moreover, increased CNT coverage by this surface layer was found to result in increased oxygen functional group retention, which may exert some effect on the ORR activity observed [199]. This work provides indication that catalytically active site structures can be formed by the pyrolysis of cyanamide coated onto CNT supports in the absence of any metal interaction. Improved ORR activity and product selectivity were observed for samples synthesized with higher cyanamide weight ratios in the precursors. Despite only marginal improvements in the ORR activity compared to Pt or other highly active catalysts, these materials represent an emerging class of metal-free ORR electrocatalysts that would provide immense economical and environmental benefits towards the commercialization of low temperature fuel cells. While the performance can most likely be improved by optimization of the synthesis parameters or utilization of a high surface area carbon support; this work provides insight into the development of metal free ORR catalysts based on cyanamide complexes.

6.4 Conclusions

Improved ORR activity and product selectivity were obtained by pyrolysis of HNO_3-CNTs in the presence of cyanamide. Cyanamide was initially coated onto the HNO_3-CNT surface by a reflux procedure in ethanol solvent. High temperature pyrolysis at 900^{o}C was found to result in the deposition of a thin coating on the surface of CNT-cy samples, with improved surface coverage and uniform coating observed at higher cyanamide loadings. Increased ORR performance was attributed to a more uniform surface coating containing active site structures formed in the absence of any metal species interaction. Specifically, CNT-cy4 displayed a slight improvement in on-set potential, improved ORR kinetics in the

full potential range investigated and a four fold improvement in H_2O selectivity compared with HNO_3-CNTs. Cyanamide was found to interact with the surface of HNO_3-CNTs in forming these ORR active moieties and furthermore resulted in the stabilized incorporation of oxide and nitride surface functional groups despite treatments at temperature beyond their stability range.

7.0 Summary and future direction

In summary, the application of N-CNTs towards the electrocatalysis of ORR in low temperature fuel cells has been demonstrated through four separate studies. The primary objective was to exploit the unique structural, surface and electronic properties of N-CNTs in the development of highly active catalyst materials with reduced or eliminated Pt dependence for PEMFCs and AFCs.

The first study entailed the utilization of N-CNTs synthesized from ethylenediamine and pyridine precursor solutions as Pt nanoparticle supports. These composites were investigated for their activity towards the ORR under PEMFC conditions (i.e. in acidic media) and the importance of nitrogen incorporation in the support material was elucidated upon comparison with undoped CNTs as Pt supports. Moreover, the importance of high nitrogen contents was demonstrated, where ED-CNTs with enhanced nitrogen contents were found to facilitate the deposition of more uniform sized, well dispersed Pt nanoparticles compared with Py-CNTs with a lower nitrogen content. Upon testing in a MEA, Pt/ED-CNTs displayed significantly higher performance than Pt/CNTs, highlighting the benefits of using N-CNTs as a catalyst support in fuel cell setups.

The second study was inspired by recent reports indicating the high ORR activity of N-CNTs in alkaline conditions, similar to those present in AFCs. The effect of utilizing different precursor materials was investigated, where three aliphatic diamines with varying carbon chain lengths (and by extension varying nitrogen-carbon ratios) were used as precursor solutions for N-CNTs growth. The importance of utilizing a nitrogen rich precursor solution was apparent, where this led to higher nitrogen concentrations in the N-CNTs, along with improved ORR activity determined through half-cell testing. Detailed material characterization techniques were carried out and the ORR activity observed was attributed to pyridinic and quaternary nitrogen species present on the surface of the N-CNT materials.

The third study investigated the applicability of the most promising N-CNT materials investigated in the second study as a cathode catalyst in an AEMFC setup. Highly active ED-CNTs were fabricated into a thin, free standing membrane which was tested as a standalone cathode in a single cell AEMFC. The performance of this cell was found to be superior to a similar AEMFC setup utilizing commercial Pt/C as the cathode catalyst material. Improved performance was attributed to the high inherent ORR activity of ED-CNTs and the distinct structure and morphology of the cathode layer including high surface aspect ratios and a highly porous nature.

The fourth study investigated CNTs coated with cyanamide and then exposed to a high temperature pyrolysis. This post treatment method was done in the absence of any metallic species on

the surface of the CNTs and thus any catalytic activity observed can be attributed to active site formation occurring *in lieu* of metal interactions. CNT-cy samples were found to have improved ORR activity resulting from the post treatment procedure utilizing cyanamide as the nitrogen precursor. It was observed that a thin surface layer was deposited on the CNT-cy samples following pyrolysis. At higher cyanamide loadings, improved uniformity and surface coverage of this thin film was favoured. This was also found to result in higher ORR activity for CNT-cy samples treated with increasing amounts of cyanamide.

The studies presented herein provide novel approaches to the utilization of N-CNTs or N-CNT composites as cathode electrocatalyst materials for fuel cell applications. Electrochemical studies were coupled with detailed structural and surface characterization techniques in order to provide insight regarding the factors affecting the ORR activity for this class of materials and potential approaches to improve their electrocatalytic performance. Future work can potentially encompass:

- Further MEA testing in order to investigate the stability of N-CNTs and their composites in fuel cell systems. This will provide further insight into their applicability as cathodic electrocatalysts and moreover will elucidate potential degradation mechanisms.
- Synthesis of N-CNTs from alternative precursor materials in order to potentially improve ORR activity by obtaining N-CNTs with higher nitrogen contents and pyridinic/quaternary surface groups. Focus should be on precursor materials with high nitrogen contents.
- Optimization of synthesis parameters. This will be in an effort to tailor the specific structural, electronic and atomic properties of the N-CNT materials in order to obtain higher ORR activity.
- Utilization of N-CNTs or their composites towards other applications. These could include metal-air batteries or fuel cells. The unique structural and electronic properties of N-CNTs are very appealing and still not well understood. The applicability of these materials towards many other technologies still remains to be investigated.

References

[1] S. Basu, Recent Trends in Fuel Cell Science and Technology,"Future Directions of Fuel Cell Science and Technology" (2007) 356.

[2] R. Borup, J. Meyers, B. Pivovar, Y.S. Kim, R. Mukundan, N. Garland, D. Myers, M. Wilson, F. Garzon, D. Wood, Chemical reviews,"Scientific aspects of polymer electrolyte fuel cell durability and degradation" 107 (2007) 3904.

[3] J. Larminie, A. Dicks, Knovel, Fuel cell systems explained: Second Edition, John Wiley and Sons, Inc., 2003.

[4] Y. Shao, G. Yin, Y. Gao, Journal of power sources,"Understanding and approaches for the durability issues of Pt-based catalysts for PEM fuel cell" 171 (2007) 558.

[5] E. Guilminot, A. Corcella, M. Chatenet, F. Maillard, F. Charlot, G. Berthome, C. Iojoiu, J.Y. Sanchez, E. Rossinot, E. Claude, Journal of the Electrochemical Society,"Membrane and active layer degradation upon PEMFC steady-state operation" 154 (2007) B1106.

[6] A. Taniguchi, T. Akita, K. Yasuda, Y. Miyazaki, Journal of power sources,"Analysis of electrocatalyst degradation in PEMFC caused by cell reversal during fuel starvation" 130 (2004) 42.

[7] D.C. Higgins, D. Meza, Z. Chen, The Journal of Physical Chemistry C,"Nitrogen-Doped Carbon Nanotubes as Platinum Catalyst Supports for Oxygen Reduction Reaction in Proton Exchange Membrane Fuel Cells" 114 (2010) 21982.

[8] D. Higgins, Z. Chen, Z. Chen, Electrochimica Acta,"Nitrogen doped carbon nanotubes synthesized from aliphatic diamines for oxygen reduction reaction" 56 (2011) 1570.

[9] D.C. Higgins, Z. Chen, ECS Transactions,"Nitrogen Doped Carbon Nanotube Thin Films as Efficient Oxygen Reduction Catalyst for Alkaline Anion Exchange Membrane Fuel Cell" 28 (2010) 63.

[10] K. Prater, Journal of power sources,"The renaissance of the solid polymer fuel cell" 29 (1990) 239.

[11] V. Mehta, J.S. Cooper, Journal of power sources,"Review and analysis of PEM fuel cell design and manufacturing" 114 (2003) 32.

[12] M.F. Mathias, R. Makharia, H.A. Gasteiger, J.J. Conley, T.J. Fuller, C.J. Gittleman, S.S. Kocha, D.P. Miller, C.K. Mittelsteadt, T. Xie, Electrochemical Society Interface,"Two fuel cell cars in every garage" 14 (2005) 24.

[13] J.M. Ogden, M.M. Steinbugler, T.G. Kreutz, Journal of power sources,"A comparison of hydrogen, methanol and gasoline as fuels for fuel cell vehicles: implications for vehicle design and infrastructure development" 79 (1999) 143.

[14] A.A. Gewirth, M.S. Thorum, Inorganic chemistry,"Electroreduction of dioxygen for fuel-cell applications: Materials and challenges" 49 (2010) 3557.

[15] H.A. Gasteiger, S.S. Kocha, B. Sompalli, F.T. Wagner, Applied Catalysis B: Environmental,"Activity benchmarks and requirements for Pt, Pt-alloy, and non-Pt oxygen reduction catalysts for PEMFCs" 56 (2005) 9.

[16] DOE, Types of Fuel Cells,"(http://www1.eere.energy.gov/hydrogenandfuelcells/fuelcells/fc_types.html).

[17] S. Litster, G. McLean, Journal of power sources,"PEM fuel cell electrodes" 130 (2004) 61.

[18] DOE, Comparison of Fuel Cell Technologies,"(http://www1.eere.energy.gov/hydrogenandfuelcells/fuelcells/pdfs/fc_comparison_chart.pdf).

[19] DOE, Technical Plan - Fuel Cells,"Technical Plan - Fuel Cells" (2007).

[20] B.D. James, J.A. Kalinoski, DOE Hydrogen Program Review,"Mass Production Cost Estimation for Direct H2 PEM Fuel Cell Systems for Automotive Applications" (2008).

[21] X. Yu, S. Ye, Journal of power sources,"Recent advances in activity and durability enhancement of Pt/C catalytic cathode in PEMFC:: Part II: Degradation mechanism and durability enhancement of carbon supported platinum catalyst" 172 (2007) 145.

[22] N. Yousfi-Steiner, P. Moçotéguy, D. Candusso, D. Hissel, Journal of power sources,"A review on polymer electrolyte membrane fuel cell catalyst degradation and starvation issues: Causes, consequences and diagnostic for mitigation" 194 (2009) 130.

[23] S. Zhang, X. Yuan, J. Hin, H. Wang, K. Friedrich, M. Schulze, Journal of power sources,"A review of platinum-based catalyst layer degradation in proton exchange membrane fuel cells" (2009).

[24] O. Baturina, S. Aubuchon, K. Wynne, Chemistry of Materials,"Thermal stability in air of Pt/C catalysts and PEM fuel cell catalyst layers" 18 (2006) 1498.

[25] V. Mazumder, M. Chi, K.L. More, S. Sun, Journal of the American Chemical Society,"Core/Shell Pd/FePt Nanoparticles as an Active and Durable Catalyst for the Oxygen Reduction Reaction" 132 (2010) 7848.

[26] Z. Peng, H. Yang, Journal of the American Chemical Society,"Synthesis and oxygen reduction electrocatalytic property of Pt-on-Pd bimetallic heteronanostructures" 131 (2009) 7542.

[27] Z. Chen, M. Waje, W. Li, Y. Yan, Angewandte Chemie,"Supportless Pt and PtPd Nanotubes as Electrocatalysts for Oxygen Reduction Reactions" 119 (2007) 4138.

[28] S. Sun, G. Zhang, D. Geng, Y. Chen, M.N. Banis, R. Li, M. Cai, X. Sun, Chemistry–A European Journal,"Direct Growth of Single Crystal Pt Nanowires on Sn@ CNT Nanocable: 3D Electrodes for Highly Active Electrocatalysts" 16 (2010) 829.

[29] M.K. Debe, A.K. Schmoeckel, G.D. Vernstrom, R. Atanasoski, Journal of power sources,"High voltage stability of nanostructured thin film catalysts for PEM fuel cells" 161 (2006) 1002.

[30] Y. Chen, J. Wang, H. Liu, R. Li, X. Sun, S. Ye, S. Knights, Electrochemistry Communications,"Enhanced stability of Pt electrocatalysts by nitrogen doping in CNTs for PEM fuel cells" 11 (2009) 2071.

[31] S.Y. Huang, P. Ganesan, S. Park, B.N. Popov, Journal of the American Chemical Society,"Development of a titanium dioxide-supported platinum catalyst with ultrahigh stability for polymer electrolyte membrane fuel cell applications" 131 (2009) 13898.

[32] S. Koh, J. Leisch, M. Toney, P. Strasser, Journal of Physical Chemistry C,"Structure-Activity-Stability Relationships of Pt- Co Alloy Electrocatalysts in Gas-Diffusion Electrode Layers" 111 (2007) 3744.

[33] V. Stamenkovic, B.S. Mun, K.J.J. Mayrhofer, P.N. Ross, N.M. Markovic, J. Rossmeisl, J. Greeley, J.K. Nørskov, Angewandte Chemie,"Changing the activity of electrocatalysts for oxygen reduction by tuning the surface electronic structure" 118 (2006) 2963.

[34] T. Moffat, J. Mallett, S. Hwang, Journal of the Electrochemical Society,"Oxygen Reduction Kinetics on Electrodeposited Pt, PtNi, and PtCo" 156 (2009) B238.

[35] S. Mukerjee, S. Srinivasan, Journal of Electroanalytical Chemistry,"Enhanced electrocatalysis of oxygen reduction on platinum alloys in proton exchange membrane fuel cells" 357 (1993) 201.

[36] V.R. Stamenkovic, B. Fowler, B.S. Mun, G. Wang, P.N. Ross, C.A. Lucas, N.M. Markovi Science,"Improved oxygen reduction activity on Pt3Ni (111) via increased surface site availability" 315 (2007) 493.

[37] M. Saha, Y. Chen, R. Li, X. Sun, Asia Pacific Journal of Chemical Engineering,"Enhancement of PEMFC performance by using carbon nanotubes supported Pt Co alloy catalysts" 4 (2009) 12.

[38] S. Sun, G. Zhang, D. Geng, Y. Chen, R. Li, M. Cai, X. Sun, Angewandte Chemie,"A Highly Durable Platinum Nanocatalyst for Proton Exchange Membrane Fuel Cells: Multiarmed Starlike Nanowire Single Crystal" 123 (2011) 442.

[39] Z. Zhang, M. Li, Z. Wu, W. Li, Nanotechnology,"Ultra-thin PtFe-nanowires as durable electrocatalysts for fuel cells" 22 (2011) 015602.

[40] R.R. Adzic, J. Zhang, K. Sasaki, M.B. Vukmirovic, M. Shao, J. Wang, A.U. Nilekar, M. Mavrikakis, J. Valerio, F. Uribe, Topics in Catalysis,"Platinum monolayer fuel cell electrocatalysts" 46 (2007) 249.

[41] J. Zhang, M.B. Vukmirovic, K. Sasaki, A.U. Nilekar, M. Mavrikakis, R.R. Adzic, Journal of the American Chemical Society,"Mixed-metal Pt monolayer electrocatalysts for enhanced oxygen reduction kinetics" 127 (2005) 12480.

[42] J. Zhang, M.B. Vukmirovic, Y. Xu, M. Mavrikakis, R.R. Adzic, Angewandte Chemie International Edition,"Controlling the Catalytic Activity of Platinum Monolayer Electrocatalysts for Oxygen Reduction with Different Substrates" 44 (2005) 2132.

[43] G. McLean, T. Niet, S. Prince-Richard, N. Djilali, International journal of hydrogen energy,"An assessment of alkaline fuel cell technology" 27 (2002) 507.

[44] S. Gu, R. Cai, T. Luo, Z. Chen, M. Sun, Y. Liu, G. He, Y. Yan, Angewandte Chemie International Edition,"A Soluble and Highly Conductive Ionomer for High Performance Hydroxide Exchange Membrane Fuel Cells" 48 (2009) 6499.

[45] K. Scott, E. Yu, G. Vlachogiannopoulos, M. Shivare, N. Duteanu, Journal of power sources,"Performance of a direct methanol alkaline membrane fuel cell" 175 (2008) 452.

[46] J.R. Varcoe, R.C.T. Slade, G.L. Wright, Y. Chen, The Journal of Physical Chemistry B,"Steady-state dc and impedance investigations of H2/O2 alkaline membrane fuel cells with commercial Pt/C, Ag/C, and Au/C cathodes" 110 (2006) 21041.

[47] N. Wagner, M. Schulze, E. Gülzow, Journal of power sources,"Long term investigations of silver cathodes for alkaline fuel cells" 127 (2004) 264.

[48] S. Maldonado, K. Stevenson, J. Phys. Chem. B,"Influence of nitrogen doping on oxygen reduction electrocatalysis at carbon nanofiber electrodes" 109 (2005) 4707.

[49] A. Appleby, Journal of power sources,"From Sir William Grove to today: fuel cells and the future" 29 (1990) 3.

[50] K. Strasser, Journal of power sources,"The design of alkaline fuel cells" 29 (1990) 149.

[51] E. Gülzow, Journal of power sources,"Alkaline fuel cells: a critical view" 61 (1996) 99.

[52] K. Kordesch, V. Hacker, K. Reichmann, M. Cifrain, T. Hejze, Electric Auto Conference Proceeding,"The Safe and Economic Revival of Alkaline Hydrogen/Air Fuel Cells with Circulating Electrolytes. Recommended for Vehicles using Battery Hybrid Systems and Hydrogen from Ammonia Crackers" (2008).

[53] A. Khalidi, B. Lafage, P. Taxil, G. Gave, M. Clifton, P. Cezac, International journal of hydrogen energy,"Electrolyte and water transfer through the porous electrodes of an immobilised-alkali hydrogen-oxygen fuel cell" 21 (1996) 25.

[54] C. Sollogoub, A. Guinault, C. Bonnebat, M. Bennjima, L. Akrour, J. Fauvarque, L. Ogier, Journal of Membrane Science,"Formation and characterization of crosslinked membranes for alkaline fuel cells" 335 (2009) 37.

[55] G. Wang, Y. Weng, D. Chu, D. Xie, R. Chen, Journal of Membrane Science,"Preparation of alkaline anion exchange membranes based on functional poly (ether-imide) polymers for potential fuel cell applications" 326 (2009) 4.

[56] X. Zhang, S.W. Tay, Z. Liu, L. Hong, Journal of power sources,"Alkaline anion-exchange polymer membrane with grid-plug microstructure for hydrogen fuel cell application" (2011).

[57] S. Iijima, nature,"Helical microtubules of graphitic carbon" 354 (1991) 56.

[58] R.H. Baughman, A.A. Zakhidov, W.A. De Heer, Science,"Carbon nanotubes--the route toward applications" 297 (2002) 787.

[59] C. Dekker, Physics Today,"Carbon nanotubes as molecular quantum wires" 52 (1999) 22.

[60] E.T. Thostenson, Z. Ren, T.W. Chou, Composites science and technology,"Advances in the science and technology of carbon nanotubes and their composites: a review" 61 (2001) 1899.

[61] P. Ajayan, Chemical reviews,"Nanotubes from carbon" 99 (1999) 1787.

[62] O. Stephan, P. Ajayan, C. Colliex, P. Redlich, J. Lambert, P. Bernier, P. Lefin, Science,"Doping graphitic and carbon nanotube structures with boron and nitrogen" 266 (1994) 1683.

[63] C. Ewels, M. Glerup, Journal of nanoscience and nanotechnology,"Nitrogen doping in carbon nanotubes" 5 (2005) 1345.

[64] M. Terrones, P. Ajayan, F. Banhart, X. Blase, D. Carroll, J. Charlier, R. Czerw, B. Foley, N. Grobert, R. Kamalakaran, Applied Physics A: Materials Science & Processing,"N-doping and coalescence of carbon nanotubes: synthesis and electronic properties" 74 (2002) 355.

[65] K. Jiang, L.S. Schadler, R.W. Siegel, X. Zhang, H. Zhang, M. Terrones, Journal of Materials Chemistry,"Protein immobilization on carbon nanotubes via a two-step process of diimide-activated amidation" 14 (2004) 37.

[66] A. Okotrub, N. Maksimova, T. Duda, A. Kudashov, Y.V. Shubin, D.S. Su, E. Pazhetnov, A. Boronin, L. Bulusheva, Fullerenes, nanotubes, and carbon nanostructures,"Fluorination of CNx nanotubes" 12 (2004) 99.

[67] Y.H. Li, T.H. Hung, C.W. Chen, Carbon,"A first-principles study of nitrogen-and boron-assisted platinum adsorption on carbon nanotubes" 47 (2009) 850.

[68] L. Panchakarla, A. Govindaraj, C. Rao, ACS nano,"Nitrogen-and Boron-Doped Double-Walled Carbon Nanotubes" 1 (2007) 494.

[69] J. Goldstein, D.E. Newbury, D.C. Joy, P. Echlin, C.E. Lyman, E. Lifshin, Scanning electron microscopy and X-ray microanalysis, Springer Us, 2003.

[70] L. Reimer, H. Kohl, Transmission electron microscopy: Physics of image formation, Springer Verlag, 2008.

[71] J.F. Shackelford, Introduction to materials science for engineers: Sixth Edition, Macmillan, 2005.

[72] E. Antolini, F. Cardellini, Journal of alloys and compounds,"Formation of carbon supported PtRu alloys: an XRD analysis" 315 (2001) 118.

[73] W. Li, C. Liang, W. Zhou, J. Qiu, Z. Zhou, G. Sun, Q. Xin, J. Phys. Chem. B,"Preparation and characterization of multiwalled carbon nanotube-supported platinum for cathode catalysts of direct methanol fuel cells" 107 (2003) 6292.

[74] V. Radmilovic, H. Gasteiger, P. Ross, Journal of Catalysis,"Structure and chemical composition of a supported Pt-Ru electrocatalyst for methanol oxidation" 154 (1995) 98.

[75] M.S. Dresselhaus, G. Dresselhaus, R. Saito, A. Jorio, Physics Reports,"Raman spectroscopy of carbon nanotubes" 409 (2005) 47.

[76] M. Dresselhaus, G. Dresselhaus, A. Jorio, A. Souza Filho, R. Saito, Carbon,"Raman spectroscopy on isolated single wall carbon nanotubes* 1" 40 (2002) 2043.

[77] E. Liang, P. Ding, H. Zhang, X. Guo, Z. Du, Diamond and Related Materials,"Synthesis and correlation study on the morphology and Raman spectra of CNx nanotubes by thermal decomposition of ferrocene/ethylenediamine" 13 (2004) 69.

[78] Y. Lin, Y. Hsu, C. Wu, S. Chen, K. Chen, L. Chen, Diamond and Related Materials,"Effects of nitrogen-doping on the microstructure, bonding and electrochemical activity of carbon nanotubes" 18 (2009) 433.

[79] P. Ding, E. Liang, M. Chao, X. Guo, J. Zhang, Physica E: Low-dimensional Systems and Nanostructures,"Synthesis, characterization and low field emission of CNx nanotubes" 25 (2005) 654.

[80] S. Maldonado, S. Morin, K. Stevenson, Carbon,"Structure, composition, and chemical reactivity of carbon nanotubes by selective nitrogen doping" 44 (2006) 1429.

[81] S. Maldonado, K. Stevenson, J. Phys. Chem. B,"Direct preparation of carbon nanofiber electrodes via pyrolysis of iron (II) phthalocyanine: electrocatalytic aspects for oxygen reduction" 108 (2004) 11375.

[82] G. Liu, X. Li, P. Ganesan, B. Popov, Applied Catalysis B: Environmental,"Development of non-precious metal oxygen-reduction catalysts for PEM fuel cells based on N-doped ordered porous carbon" 93 (2009) 156.

[83] P. Matter, L. Zhang, U. Ozkan, Journal of Catalysis,"The role of nanostructure in nitrogen-containing carbon catalysts for the oxygen reduction reaction" 239 (2006) 83.

[84] S. van Dommele, A. Romero-Izquirdo, R. Brydson, K. de Jong, J. Bitter, Carbon,"Tuning nitrogen functionalities in catalytically grown nitrogen-containing carbon nanotubes" (2007).

[85] Z. Chen, L. Xu, W. Li, M. Waje, Y. Yan, Nanotechnology,"Polyaniline nanofibre supported platinum nanoelectrocatalysts for direct methanol fuel cells" 17 (2006) 5254.

[86] A. Pozio, M. De Francesco, A. Cemmi, F. Cardellini, L. Giorgi, Journal of power sources,"Comparison of high surface Pt/C catalysts by cyclic voltammetry" 105 (2002) 13.

[87] J.W. Weidner, V.A. Sethuraman, J.W. Van Zee, Electrochemical Society Interface,"Membrane Electrode Assembly" (2003) 41.

[88] T. Frey, M. Linardi, Electrochimica Acta,"Effects of membrane electrode assembly preparation on the polymer electrolyte membrane fuel cell performance" 50 (2004) 99.

[89] K. Lee, J. Zhang, H. Wang, D.P. Wilkinson, Journal of applied electrochemistry,"Progress in the synthesis of carbon nanotube-and nanofiber-supported Pt electrocatalysts for PEM fuel cell catalysis" 36 (2006) 507.

[90] T. Maiyalagan, B. Viswanathan, U. Varadaraju, Electrochemistry Communications,"Nitrogen containing carbon nanotubes as supports for Pt–Alternate anodes for fuel cell applications" 7 (2005) 905.

[91] A. Kongkanand, S. Kuwabata, G. Girishkumar, P. Kamat, Langmuir,"Single-wall carbon nanotubes supported platinum nanoparticles with improved electrocatalytic activity for oxygen reduction reaction" 22 (2006) 2392.

[92] C. Wang, M. Waje, X. Wang, J. Tang, R. Haddon, Y. Yan, Nano letters,"Proton exchange membrane fuel cells with carbon nanotube based electrodes" 4 (2004) 345.

[93] S. Wang, S.P. Jiang, T.J. White, J. Guo, X. Wang, The Journal of Physical Chemistry C,"Electrocatalytic Activity and Interconnectivity of Pt Nanoparticles on Multiwalled Carbon Nanotubes for Fuel Cells" 113 (2009) 18935.

[94] G. Girishkumar, T. Hall, K. Vinodgopal, P. Kamat, J. Phys. Chem. B,"Single wall carbon nanotube supports for portable direct methanol fuel cells" 110 (2006) 107.

[95] W. Li, C. Liang, J. Qiu, W. Zhou, H. Han, Z. Wei, G. Sun, Q. Xin, Carbon,"Carbon nanotubes as support for cathode catalyst of a direct methanol fuel cell" 40 (2002) 791.

[96] M. Saha, R. Li, X. Sun, Journal of power sources,"High loading and monodispersed Pt nanoparticles on multiwalled carbon nanotubes for high performance proton exchange membrane fuel cells" 177 (2008) 314.

[97] M. Waje, X. Wang, W. Li, Y. Yan, Nanotechnology,"Deposition of platinum nanoparticles on organic functionalized carbon nanotubes grown in situ on carbon paper for fuel cells" 16 (2005) S395.

[98] J. Yang, G. Goenaga, A. Call, D. Liu, Electrochemical and Solid-State Letters,"Polymer Electrolyte Fuel Cell with Vertically Aligned Carbon Nanotubes as the Electrocatalyst Support" 13 (2010) B55.

[99] K. Gong, F. Du, Z. Xia, M. Durstock, L. Dai, Science,"Nitrogen-doped carbon nanotube arrays with high electrocatalytic activity for oxygen reduction" 323 (2009) 760.

[100] Z. Chen, D. Higgins, Electrochimica Acta,"Electrocatalytic activity of nitrogen doped carbon nanotubes with different morphologies for oxygen reduction reaction" 55 (2010) 4799.

[101] Z. Chen, D. Higgins, H. Tao, R.S. Hsu, The Journal of Physical Chemistry C,"Highly active nitrogen-doped carbon nanotubes for oxygen reduction reaction in fuel cell applications" 113 (2009) 21008.

[102] G. Vijayaraghavan, K. Stevenson, Langmuir,"Synergistic assembly of dendrimer-templated platinum catalysts on nitrogen-doped carbon nanotube electrodes for oxygen reduction" 23 (2007) 5279.

[103] M. Saha, R. Li, X. Sun, S. Ye, Electrochemistry Communications,"3-D composite electrodes for high performance PEM fuel cells composed of Pt supported on nitrogen-doped carbon nanotubes grown on carbon paper" 11 (2009) 438.

[104] M. Wilson, J. Valerio, S. Gottesfeld, Electrochimica Acta,"Low platinum loading electrodes for polymer electrolyte fuel cells fabricated using thermoplastic ionomers" 40 (1995) 355.

[105] S. van Dommele, A. Romero-Izquirdo, R. Brydson, K. de Jong, J. Bitter, Carbon,"Tuning nitrogen functionalities in catalytically grown nitrogen-containing carbon nanotubes" (2007) 138.

[106] P. Matter, L. Zhang, U. Ozkan, J. Catal.,"The role of nanostructure in nitrogen-containing carbon catalysts for the oxygen reduction reaction" 239 (2006) 83.

[107] S. van Dommele, K. Jong, J. Bitter, Chem. Commun.,"Nitrogen-containing carbon nanotubes as solid base catalysts" 2006 (2006) 4859.

[108] Z. Chen, D. Higgins, H. Tao, R.S. Hsu, Z. Chen, J. Phys. Chem. C,"Highly Active Nitrogen-Doped Carbon Nanotubes for Oxygen Reduction Reaction in Fuel Cell Applications" 113 (2009) 21008.

[109] M. Terrones, H. Terrones, N. Grobert, W. Hsu, Y. Zhu, J. Hare, H. Kroto, D. Walton, P. Kohler-Redlich, M. Rühle, Appl. Phys. Lett.,"Efficient route to large arrays of CN nanofibers by pyrolysis of ferrocene/melamine mixtures" 75 (1999) 3932.

[110] A. Gewirth, M. Thorum, Inorg. Chem.,"Electroreduction of Dioxygen for Fuel-Cell Applications: Materials and Challenges" 49 (2010) 3557.

[111] R. Czerw, M. Terrones, J. Charlier, X. Blase, B. Foley, R. Kamalakaran, N. Grobert, H. Terrones, P. Ajayan, W. Blau, Nano Lett.,"Identification of electron donor states in N-doped carbon nanotubes" 1 (2001) 457.

[112] Y. Shao, J. Sui, G. Yin, Y. Gao, Appl. Catal. B-Environ.,"Nitrogen-doped carbon nanostructures and their composites as catalytic materials for proton exchange membrane fuel cell" 79 (2008) 89.

[113] Y. Li, T. Hung, C. Chen, Carbon,"A first-principles study of nitrogen-and boron-assisted platinum adsorption on carbon nanotubes" 47 (2009) 850.

[114] M. Saha, R. Li, X. Sun, S. Ye, Electrochem. Commun.,"3-D composite electrodes for high performance PEM fuel cells composed of Pt supported on nitrogen-doped carbon nanotubes grown on carbon paper" 11 (2009) 438.

[115] P. Matter, E. Wang, M. Arias, E. Biddinger, U. Ozkan, J. Phys. Chem. B,"Oxygen reduction reaction catalysts prepared from acetonitrile pyrolysis over alumina-supported metal particles" 110 (2006) 18374.

[116] H. Du, C. Wang, H. Hsu, S. Chang, U. Chen, S. Yen, L. Chen, H. Shih, K. Chen, Diam. Relat. Mater.,"Controlled platinum nanoparticles uniformly dispersed on nitrogen-doped carbon nanotubes for methanol oxidation" 17 (2008) 535.

[117] C. Sun, L. Chen, M. Su, L. Hong, O. Chyan, C. Hsu, K. Chen, T. Chang, L. Chang, Chem. Mater,"Ultrafine Platinum Nanoparticles Uniformly Dispersed on Arrayed CNx Nanotubes with High Electrochemical Activity" 17 (2005) 3749.

[118] S. Bian, Z. Ma, W. Song, J. Phys. Chem. C,"Preparation and Characterization of Carbon Nitride Nanotubes and Their Applications as Catalyst Supporter" 113 (2009) 8668.

[119] J. Yang, T. Deivaraj, H. Too, J. Lee, Langmuir,"Acetate stabilization of metal nanoparticles and its role in the preparation of metal nanoparticles in ethylene glycol" 20 (2004) 4241.

[120] A. Zamudio, A. Elías, J. Rodríguez-Manzo, F. López-Urías, G. Rodríguez-Gattorno, F. Lupo, M. Rühle, D. Smith, H. Terrones, D. Díaz, Small,"Efficient anchoring of silver nanoparticles on N-doped carbon nanotubes" 2 (2006) 346.

[121] X. Wang, M. Waje, Y. Yan, Electrochem. Solid St.,"CNT-based electrodes with high efficiency for PEMFCs" 8 (2005) A42.

[122] S. Wang, S. Jiang, X. Wang, Nanotechnology,"Polyelectrolyte functionalized carbon nanotubes as a support for noble metal electrocatalysts and their activity for methanol oxidation" 19 (2008) 265601.

[123] M. Waje, X. Wang, W. Li, Y. Yan, Nanotechnology,"Deposition of platinum nanoparticles on organic functionalized carbon nanotubes grown in situ on carbon paper for fuel cells" 16 (2005) S395.

[124] K. Lee, J. Zhang, H. Wang, D. Wilkinson, J. Appl. Electrochem.,"Progress in the synthesis of carbon nanotube-and nanofiber-supported Pt electrocatalysts for PEM fuel cell catalysis" 36 (2006) 507.

[125] E. Liang, P. Ding, H. Zhang, X. Guo, Z. Du, Diam. Relat. Mater.,"Synthesis and correlation study on the morphology and Raman spectra of CNx nanotubes by thermal decomposition of ferrocene/ethylenediamine" 13 (2004) 69.

[126] B. Sumpter, V. Meunier, J. Romo-Herrera, E. Cruz-Silva, D. Cullen, H. Terrones, D. Smith, M. Terrones, ACS nano,"Nitrogen-mediated carbon nanotube growth: diameter reduction, metallicity, bundle dispersability, and bamboo-like structure formation" 1 (2007) 369.

[127] S. Yang, G. Zhao, E. Khosravi, J. Phys Chem. C,"First Principles Studies of Nitrogen Doped Carbon Nanotubes for Dioxygen Reduction" 114 (2010) 3371.

[128] Y. Chen, J. Wang, H. Liu, R. Li, X. Sun, S. Ye, S. Knights, Electrochem. Commmun.,"Enhanced stability of Pt electrocatalysts by nitrogen doping in CNTs for PEM fuel cells" 11 (2009) 2071.

[129] N. Elezovic , B. Babic , L. Vracar, N. Krstaji J. Serb. Chem. Soc,"Oxygen reduction at platinum nanoparticles supported on carbon cryogel in alkaline solution" 72 (2007) 699.

[130] N. Alonso-Vante, H. Tributsch, O. Solorza-Feria, Electrochim. Acta,"Kinetics studies of oxygen reduction in acid medium on novel semiconducting transition metal chalcogenides" 40 (1995) 567.

[131] O. Solorza-Feria, K. Ellmer, M. Giersig, N. Alonso-Vante, Electrochim. Acta,"Novel low-temperature synthesis of semiconducting transition metal chalcogenide electrocatalyst for multielectron charge transfer: molecular oxygen reduction" 39 (1994) 1647.

[132] Y. Feng, T. He, N. Alonso-Vante, Electrochim. Acta,"Oxygen reduction reaction on carbon-supported CoSe2 nanoparticles in an acidic medium" 54 (2009) 5252.

[133] J. Yang, D. Liu, N. Kariuki, L. Chen, Chem. Commun.,"Aligned carbon nanotubes with built-in FeN 4 active sites for electrocatalytic reduction of oxygen" 2008 (2008) 329.

[134] N. Mano, V. Soukharev, A. Heller, J. Phys. Chem. B,"A laccase-wiring redox hydrogel for efficient catalysis of O2 electroreduction" 110 (2006) 11180.

[135] E. Biddinger, D. von Deak, U. Ozkan, Top. Catal.,"Nitrogen-Containing Carbon Nanostructures as Oxygen-Reduction Catalysts" 52 (2009) 1566.

[136] P. Gouerec, M. Savy, J. Riga, Electrochim. Acta,"Oxygen reduction in acidic media catalyzed by pyrolyzed cobalt macrocycles dispersed on an active carbon: The importance of the content of oxygen surface groups on the evolution of the chelate structure during the heat treatment" 43 (1997) 743.

[137] A. Widelöv, R. Larsson, Electrochim. Acta,"ESCA and electrochemical studies on pyrolysed iron and cobalt tetraphenylporphyrins" 37 (1992) 187.

[138] M. Lefèvre, J. Dodelet, Electrochim. Acta,"Fe-based catalysts for the reduction of oxygen in polymer electrolyte membrane fuel cell conditions: determination of the amount of peroxide released during electroreduction and its influence on the stability of the catalysts" 48 (2003) 2749.

[139] M. Lefevre, E. Proietti, F. Jaouen, J. Dodelet, Science,"Iron-based catalysts with improved oxygen reduction activity in polymer electrolyte fuel cells" 324 (2009) 71.

[140] A. Titov, P. Zapol, P. Kral, D. Liu, H. Iddir, K. Baishya, L. Curtiss, J. Phys. Chem. C,"Catalytic Fe-xN Sites in Carbon Nanotubes" 113 (2009) 21629.

[141] F. Charreteur, F. Jaouen, S. Ruggeri, J. Dodelet, Electrochim. Acta,"Fe/N/C non-precious catalysts for PEM fuel cells: Influence of the structural parameters of pristine commercial carbon blacks on their activity for oxygen reduction" 53 (2008) 2925.

[142] G. Liu, X. Li, P. Ganesan, B. Popov, Appl. Catal. B-Environ.,"Development of non-precious metal oxygen-reduction catalysts for PEM fuel cells based on N-doped ordered porous carbon" 93 (2009) 156.

[143] V. Nallathambi, J. Lee, S. Kumaraguru, G. Wu, B. Popov, J. Power Sources,"Development of high performance carbon composite catalyst for oxygen reduction reaction in PEM Proton Exchange Membrane fuel cells" 183 (2008) 34.

[144] Z. Chen, D. Higgins, Carbon,"Nitrogen doped carbon nanotubes and their impact on the oxygen reduction reaction in fuel cells" 48 (2010) 3057.

[145] Z. Chen, D. Higgins, H. Tao, R. Hsu, J. Phys. Chem. C,"Highly Active Nitrogen-Doped Carbon Nanotubes for Oxygen Reduction Reaction in Fuel Cell Applications" 113 (2009) 21008.

[146] M. Nath, B. Satishkumar, A. Govindaraj, C. Vinod, C. Rao, Chem. Phys. Lett.,"Production of bundles of aligned carbon and carbon-nitrogen nanotubes by the pyrolysis of precursors on silica-supported iron and cobalt catalysts" 322 (2000) 333.

[147] Z. Chen, D. Higgins, Electrochim. Acta,"Electrocatalytic Activity of Nitrogen Doped Carbon Nanotubes with Different Morphologies for Oxygen Reduction Reaction" 55 (2010) 4799.

[148] J. Feng, Y. Li, F. Hou, X. Zhong, Mater. Sci. Eng.,"Controlled growth of high quality bamboo carbon nanotube arrays by the double injection chemical vapor deposition process" 473 (2008) 238.

[149] Y. Chen, J. Wang, H. Liu, R. Li, X. Sun, S. Ye, S. Knights, Electrochem. Commun.,"Enhanced stability of Pt electrocatalysts by nitrogen doping in CNTs for PEM fuel cells" 11 (2009) 2071.

[150] J. Liu, S. Webster, D. Carroll, J. Phys. Chem. B,"Temperature and flow rate of NH3 effects on nitrogen content and doping environments of carbon nanotubes grown by injection CVD method" 109 (2005) 15769.

[151] S. van Dommele, A. Romero-Izquirdo, R. Brydson, K. de Jong, J. Bitter, Carbon,"Tuning nitrogen functionalities in catalytically grown nitrogen-containing carbon nanotubes" 46 (2007) 138.

[152] M. Terrones, P. Redlich, N. Grobert, S. Trasobares, W. Hsu, H. Terrones, Y. Zhu, J. Hare, C. Reeves, A. Cheetham, Adv. Mater.,"Carbon nitride nanocomposites: Formation of aligned CxNy nanofibers" 11 (1999) 655.

[153] M. Terrones, P. Ajayan, F. Banhart, X. Blase, D. Carroll, J. Charlier, R. Czerw, B. Foley, N. Grobert, R. Kamalakaran, Appl. Phys. A-Mater.,"N-doping and coalescence of carbon nanotubes: synthesis and electronic properties" 74 (2002) 355.

[154] P. Ding, E. Liang, M. Chao, X. Guo, J. Zhang, Physica E,"Synthesis, characterization and low field emission of CNx nanotubes" 25 (2005) 654.

[155] B. Sumpter, J. Huang, V. Meunier, J. Romo-Herrera, E. Cruz-Silva, H. Terrones, M. Terrones, Int. J. Quantum Chem.,"A theoretical and experimental study on manipulating the structure and properties of carbon nanotubes using substitutional dopants" 109 (2008) 97.

[156] M. Terrones, H. Terrones, N. Grobert, W. Hsu, Y. Zhu, J. Hare, H. Kroto, D. Walton, P. Kohler-Redlich, M. Rühle, Appl. Phys. Lett.,"Efficient route to large arrays of CN nanofibers by pyrolysis of ferrocene/melamine mixtures" 75 (1999) 3932.

[157] P. Ghosh, T. Soga, K. Ghosh, R. Afre, T. Jimbo, Y. Ando, J. Non-Cryst. Solids,"Vertically aligned N-doped carbon nanotubes by spray pyrolysis of turpentine oil and pyridine derivative with dissolved ferrocene" 354 (2008) 4101.

[158] Q. Yang, P. Hou, M. Unno, S. Yamauchi, R. Saito, T. Kyotani, Nano Lett.,"Dual Raman features of double coaxial carbon nanotubes with N-doped and B-doped multiwalls" 5 (2005) 2465.

[159] S. Dommele, K. Jong, J. Bitter, Chem. Commun.,"Nitrogen-containing carbon nanotubes as solid base catalysts" 2006 (2006) 4859.

[160] N. Subramanian, X. Li, V. Nallathambi, S. Kumaraguru, H. Colon-Mercado, G. Wu, J. Lee, B. Popov, J. Power Sources,"Nitrogen-modified carbon-based catalysts for oxygen reduction reaction in polymer electrolyte membrane fuel cells" 188 (2009) 38.

[161] V. Strelko, N. Kartel, I. Dukhno, V. Kuts, R. Clarkson, B. Odintsov, Surf. Sci.,"Mechanism of reductive oxygen adsorption on active carbons with various surface chemistry" 548 (2004) 281.

[162] R. Czerw, M. Terrones, J. Charlier, X. Blase, B. Foley, R. Kamalakaran, N. Grobert, H. Terrones, P. Ajayan, W. Blau, Nano Lett.,"Identification of electron donor states in N-doped carbon nanotubes" 1 (2000) 457.

[163] B. Stöhr, H. Boehm, R. Schlögl, Carbon,"Enhancement of the catalytic activity of activated carbons in oxidation reactions by thermal treatment with ammonia or hydrogen cyanide and observation of a superoxide species as a possible intermediate" 29 (1991) 707.

[164] M. Lefevre, J. Dodelet, P. Bertrand, J. Phys. Chem. B,"Molecular oxygen reduction in PEM fuel cells: Evidence for the simultaneous presence of two active sites in Fe-based catalysts" 106 (2002) 8705.

[165] N. Elezovic , B. Babic , L. Vracar, N. Krstajic J. Serb. Chem. Soc,"Oxygen reduction at platinum nanoparticles supported on carbon cryogel in alkaline solution" 72 (2007) 699.

[166] K. Scott, E. Yu, G. Vlachogiannopoulos, M. Shivare, N. Duteanu, J. Power Sources,"Performance of a direct methanol alkaline membrane fuel cell" 175 (2007) 452.

[167] J. Varcoe, R. Slade, G. Wright, Y. Chen, J. Phys. Chem. B,"Steady-State dc and Impedance Investigations of H2/O2 Alkaline Membrane Fuel Cells with Commercial Pt/C, Ag/C, and Au/C Cathodes" 110 (2006) 21041.

[168] C. Coutanceau, L. Demarconnay, C. Lamy, J. Léger, J. Power Sources,"Development of electrocatalysts for solid alkaline fuel cell (SAFC)" 156 (2006) 14.

[169] G. McLean, T. Niet, S. Prince-Richard, N. Djilali, Int. J. Hydrogen Energ.,"An assessment of alkaline fuel cell technology" 27 (2002) 507.

[170] Z. Chen, D. Higgins, H. Tao, R.S. Hsu, Z. Chen, J. Phys. Chem. C,"Highly Active Nitrogen-Doped Carbon Nanotubes for Oxygen Reduction Reaction in Fuel Cell Applications" 113 (2009) 21008.

[171] M. Saha, R. Li, X. Sun, S. Ye, Electrochem. Comm.,"3-D composite electrodes for high performance PEM fuel cells composed of Pt supported on nitrogen-doped carbon nanotubes grown on carbon paper" 11 (2009) 438.

[172] F. Jaouen, E. Proietti, M. Lefèvre, R. Chenitz, J. Dodelet, G. Wu, H. Chung, C. Johnston, P. Zelenay, Energy Environ. Sci.,"Recent advances in non-precious metal catalysis for oxygen-reduction reaction in polymer electrolyte fuel cells" (2010).

[173] G. Faubert, R. Côté, J. Dodelet, M. Lefevre, P. Bertrand, Electrochimica Acta,"Oxygen reduction catalysts for polymer electrolyte fuel cells from the pyrolysis of FeII acetate adsorbed on 3, 4, 9, 10-perylenetetracarboxylic dianhydride" 44 (1999) 2589.

[174] I. Galbiati, C.L. Bianchi, M. Longhi, A. Carrà, L. Formaro, Fuel Cells,"Iron and Copper Containing Oxygen Reduction Catalysts From Templated Glucose–Histidine" 10 (2010) 251.

[175] S. Gupta, D. Tryk, I. Bae, W. Aldred, E. Yeager, Journal of applied electrochemistry,"Heat-treated polyacrylonitrile-based catalysts for oxygen electroreduction" 19 (1989) 19.

[176] J. Ozaki, S. Tanifuji, A. Furuichi, K. Yabutsuka, Electrochimica Acta,"Enhancement of oxygen reduction activity of nanoshell carbons by introducing nitrogen atoms from metal phthalocyanines" 55 (2010) 1864.

[177] G.Q. Sun, J.T. Wang, S. Gupta, R. Savinell, Journal of applied electrochemistry,"Iron (III) tetramethoxyphenylporphyrin (FeTMPP-C1) as electrocatalyst for oxygen reduction in direct methanol fuel cells" 31 (2001) 1025.

[178] F. Zhao, F. Harnisch, U. Schroder, F. Scholz, P. Bogdanoff, I. Herrmann, Electrochemistry Communications,"Application of pyrolysed iron (II) phthalocyanine and CoTMPP based oxygen reduction catalysts as cathode materials in microbial fuel cells" 7 (2005) 1405.

[179] J.-Y. Choi, R.S. Hsu, Z. Chen, The Journal of Physical Chemistry C,"Highly Active Porous Carbon-Supported Nonprecious Metal−N Electrocatalyst for Oxygen Reduction Reaction in PEM Fuel Cells" 114 (2010) 8048.

[180] G. Liu, X. Li, P. Ganesan, B.N. Popov, Electrochimica Acta,"Studies of oxygen reduction reaction active sites and stability of nitrogen-modified carbon composite catalysts for PEM fuel cells" 55 (2010) 2853.

[181] M. Bron, S. Fiechter, M. Hilgendorff, P. Bogdanoff, Journal of applied electrochemistry,"Catalysts for oxygen reduction from heat-treated carbon-supported iron phenantroline complexes" 32 (2002) 211.

[182] M. Lefèvre, E. Proietti, F. Jaouen, J.P. Dodelet, Science,"Iron-based catalysts with improved oxygen reduction activity in polymer electrolyte fuel cells" 324 (2009) 71.

[183] H. Wang, R. Cote, G. Faubert, D. Guay, J. Dodelet, The Journal of Physical Chemistry B,"Effect of the pre-treatment of carbon black supports on the activity of Fe-based electrocatalysts for the reduction of oxygen" 103 (1999) 2042.

[184] Z. Chen, D. Higgins, Carbon,"Nitrogen doped carbon nanotubes and their impact on the oxygen reduction reaction in fuel cells" 48 (2010) 3057.

[185] R. Cote, G. Lalande, D. Guay, J. Dodelet, G. Denes, Journal of the Electrochemical Society,"Influence of Nitrogen Containing Precursors on the Electrocatalytic Activity of Heat Treated Fe (OH) on Carbon Black for O Reduction" 145 (1998) 2411.

[186] D. Ohms, S. Herzog, R. Franke, V. Neumann, K. Wiesener, S. Gamburcev, A. Kaisheva, I. Iliev, Journal of power sources,"Influence of metal ions on the electrocatalytic oxygen reduction of carbon materials prepared from pyrolyzed polyacrylonitrile" 38 (1992) 327.

[187] M. Groenewolt, M. Antonietti, Advanced materials,"Synthesis of g C3N4 Nanoparticles in Mesoporous Silica Host Matrices" 17 (2005) 1789.

[188] H.T. Chung, C.M. Johnston, K. Artyushkova, M. Ferrandon, D.J. Myers, P. Zelenay, Electrochemistry Communications,"Cyanamide-derived non-precious metal catalyst for oxygen reduction" (2010).

[189] H.T. Chung, C.M. Johnston, P. Zelenay, ECS Transactions,"Synthesis and Evaluation of Heat-treated, Cyanamide-derived Non-precious Catalysts for Oxygen Reduction" (2009).

[190] J. Tian, L. Birry, F. Jaouen, J. Dodelet, Electrochimica Acta,"Fe-based catalysts for oxygen reduction in proton exchange membrane fuel cells with cyanamide as nitrogen precursor and/or pore-filler" (2011).

[191] L. Birry, J.H. Zagal, J.P. Dodelet, Electrochemistry Communications,"Does CO poison Fe-based catalysts for ORR?" 12 (2010) 628.

[192] D.S. Su, J. Zhang, B. Frank, A. Thomas, X. Wang, J. Paraknowitsch, R. Schlögl, ChemSusChem,"Metal Free Heterogeneous Catalysis for Sustainable Chemistry" 3 (2010) 169.

[193] W. Li, A. Yu, D.C. Higgins, B.G. Llanos, Z. Chen, Journal of the American Chemical Society,"Biologically Inspired Highly Durable Iron Phthalocyanine Catalysts for Oxygen Reduction Reaction in Polymer Electrolyte Membrane Fuel Cells" (2010) 707.

[194] C.W.B. Bezerra, L. Zhang, K. Lee, H. Liu, A.L.B. Marques, E.P. Marques, H. Wang, J. Zhang, Electrochimica Acta,"A review of Fe-N/C and Co-N/C catalysts for the oxygen reduction reaction" 53 (2008) 4937.

[195] P.H. Matter, E. Wang, M. Arias, E.J. Biddinger, U.S. Ozkan, Journal of Molecular Catalysis A: Chemical,"Oxygen reduction reaction activity and surface properties of nanostructured nitrogen-containing carbon" 264 (2007) 73.

[196] S. Kundu, T.C. Nagaiah, W. Xia, Y. Wang, S.V. Dommele, J.H. Bitter, M. Santa, G. Grundmeier, M. Bron, W. Schuhmann, The Journal of Physical Chemistry C,"Electrocatalytic Activity and Stability of Nitrogen-Containing Carbon Nanotubes in the Oxygen Reduction Reaction" 113 (2009) 14302.

[197] L. Qu, Y. Liu, J.B. Baek, L. Dai, ACS nano,"Nitrogen-Doped Graphene as Efficient Metal-Free Electrocatalyst for Oxygen Reduction in Fuel Cells" 4 (2010) 1321.

[198] Y. Tang, B.L. Allen, D.R. Kauffman, A. Star, Journal of the American Chemical Society,"Electrocatalytic activity of nitrogen-doped carbon nanotube cups" 131 (2009) 13200.

[199] E.J. Biddinger, D. von Deak, U.S. Ozkan, Topics in Catalysis,"Nitrogen-Containing Carbon Nanostructures as Oxygen-Reduction Catalysts" 52 (2009) 1566.

[200] T. Iwazaki, R. Obinata, W. Sugimoto, Y. Takasu, Electrochemistry Communications,"High oxygen-reduction activity of silk-derived activated carbon" 11 (2009) 376.

[201] R. Liu, D. Wu, X. Feng, K. Müllen, Angewandte Chemie,"Nitrogen Doped Ordered Mesoporous Graphitic Arrays with High Electrocatalytic Activity for Oxygen Reduction" 122 (2010) 2619.

[202] S.M. Lyth, Y. Nabae, S. Moriya, S. Kuroki, M. Kakimoto, J. Ozaki, S. Miyata, The Journal of Physical Chemistry C,"Carbon Nitride as a Nonprecious Catalyst for Electrochemical Oxygen Reduction" 113 (2009) 20148.

[203] C.V. Rao, C.R. Cabrera, Y. Ishikawa, The Journal of Physical Chemistry Letters,"In Search of the Active Site in Nitrogen-Doped Carbon Nanotube Electrodes for the Oxygen Reduction Reaction" 18 (2010) 2622.

[204] X. Wang, J.S. Lee, Q. Zhu, J. Liu, Y. Wang, S. Dai, Chemistry of Materials,"Ammonia-treated ordered mesoporous carbons as catalytic materials for oxygen reduction reaction" 22 (2010) 2178.

[205] V. Datsyuk, M. Kalyva, K. Papagelis, J. Parthenios, D. Tasis, A. Siokou, I. Kallitsis, C. Galiotis, Carbon,"Chemical oxidation of multiwalled carbon nanotubes" 46 (2008) 833.

[206] D. Yu, E. Nagelli, F. Du, L. Dai, The Journal of Physical Chemistry Letters,"Metal-Free Carbon Nanomaterials Become More Active than Metal Catalysts and Last Longer" 1 2165.

[207] Y. Xia, R. Mokaya, Advanced materials,"Synthesis of Ordered Mesoporous Carbon and Nitrogen Doped Carbon Materials with Graphitic Pore Walls via a Simple Chemical Vapor Deposition Method" 16 (2004) 1553.

[208] W. Gammon, O. Kraft, A. Reilly, B. Holloway, Carbon,"Experimental comparison of N (1s) X-ray photoelectron spectroscopy binding energies of hard and elastic amorphous carbon nitride films with reference organic compounds" 41 (2003) 1917.

[209] W. Xia, Y. Wang, R. Bergsträßer, S. Kundu, M. Muhler, Applied Surface Science,"Surface characterization of oxygen-functionalized multi-walled carbon nanotubes by high-resolution X-ray photoelectron spectroscopy and temperature-programmed desorption" 254 (2007) 247.

[210] M.L. Toebes, J.M.P. van Heeswijk, J.H. Bitter, A. Jos van Dillen, K.P. de Jong, Carbon,"The influence of oxidation on the texture and the number of oxygen-containing surface groups of carbon nanofibers" 42 (2004) 307.